Dissertation zur Erlangung des Doktorgrades

der Fakultät für Chemie und Pharmazie
der Ludwig-Maximilians-Universität München

Functional insights of *ZYX* and *LY96* sequence variants identified in patients with Inflammatory Bowel Disease

Madlin Schenk

aus Zwickau, Deutschland

2024

Erklärung

Diese Dissertation wurde im Sinne von § 7 der Promotionsordnung vom 28. November 2011 von Herrn Prof. Dr. med. Dr. sci. nat. Christoph Klein betreut und von Herrn Prof. Dr. rer. nat. Karl-Peter Hopfner von der Fakultät für Chemie und Pharmazie vertreten.

Eidesstattliche Versicherung

Diese Dissertation wurde eigenständig und ohne unerlaubte Hilfe erarbeitet.

München, den 29.07.2024

Madlin Schenk

Dissertation eingereicht am: 29.07.2024

1. Gutachter: Prof. Dr. rer. nat. Karl-Peter Hopfner
2. Gutachter: Prof. Dr. med. Dr. sci. nat. Christoph Klein

Mündliche Prüfung am: 18.09.2024

Acknowledgements

This laboratory research was only possible through the great opportunity and support from various involved persons that I would like to sincerely thank.

First, I want to thank my supervisor Prof. Dr. med. Dr. sci. nat. Christoph Klein for giving me the generous opportunity to be a part of his multifaceted, inspiring department and group, supporting my work with his broad scientific and medical experience by fruitful discussions and his precious time.

I would kindly thank Prof. Dr. rer. nat. Karl-Peter Hopfner to be my internal thesis supervisor and his precious time and valuable guidance.

I would also like to especially thank PD Dr.med. Daniel Kotlarz, PhD, who gave me the tremendous support to conduct my laboratory work. His scientific expertise, pioneering research experience in inflammatory bowel disease as well as his patience and trust supported this work remarkably.

A special thanks to all the participating patients, family members and physicians, who were essential in making this research project possible.

Furthermore, I would like to acknowledge Prof. Dr. med. Veit Hornung for the kind gift of BLaER1 cells and the Helmholtz Zentrum München who kindly provided iPSCs.

I am very grateful to all members of AG Klein and AG Kotlarz, who provided helpful scientific support and ideas on the project in a pleasant lab atmosphere.

Finally, I want to thank my parents, friends and especially Peter and Lina for their unconditional support and inspiration.

A DFG Fellowship from the Graduate School of Quantitative Biosciences Munich (QBM) and the Research Consortium SFB1054 supported this research financially.

Summary

Inflammatory bowel disease (IBD) is a complex and multifactorial disease, constituted of intersecting environmental factors, immunological dysfunctions, epithelial barrier defects, imbalances of the microbial flora and genetic susceptibility. Incidences of patients with an onset below six years of age, defined as very early-onset IBD (VEO-IBD), have increased dramatically within the last decades. These patients often present with a more severe and progressive disease course. Consequently, conventional therapies often remain unsuccessful. For these patients we see a major need, to improve clinical management strategies, to better understand the pathomechanisms of VEO-IBD and to find possible treatment targets for therapeutic approaches. Genome analyses were pioneering improvements by shedding light on the role of monogenic variants in IBD pathogenesis.

Our WES analysis of IBD patients and their families revealed different biallelic monogenic variants, affecting *ZYX* or *LY96*, following an autosomal recessive mendelian inheritance pattern. With this work, we investigate the relevance and underlying pathomechanisms of these identified sequence variants, linking their impact to their molecular functions in target epithelial and immune cells. In my PhD thesis, we elucidate that *ZYX* variants from two independent IBD patients seemed to have a normal function on the Zyxin protein distribution, colocalization, association to the actin skeleton and ability to proliferate and build a non-permeable monolayer in a heterologous HCT116 cell model with reconstituted monogenic variants. However, we were able to show that ZYX deficiency impacts interferon I responses in epithelial HCT116 and monocytoid BLaER1 cells and further, identify an impairment in pro-inflammatory cytokine induction and secretion. On the contrary, the reconstitution of the patient variants in our heterologous cell models did not reveal an impact on these findings.

In a second project, my PhD thesis provides insights to a biallelic 3 bp in-frame deletion in *LY96* (coding for MD2) that has been detected in a VEO-IBD patient. Patient-derived monocytes and MD2-deficient iPSC-derived macrophages revealed

a LPS-mediated diminished TLR4 response, impaired MYD88-dependent signaling of NF-κB and MAPK pathways, and decreased pro-inflammatory cytokine secretion. This work provides another functional insight of Zyxin's role in association with the inflammasome, although the patient variants were shown not to be likely disease causing. On the other hand, we could demonstrate that MD2 is a crucial mediator leading to severe functional impairments in macrophages upon deficiency and shedding light on the complex understanding of IBD.

Zusammenfassung

Chronisch-entzündliche Darmerkrankungen (engl. *inflammatory bowel disease*, IBD) sind komplex und multifaktoriell. Diese können durch Umweltfaktoren, immunologische Funktionsstörungen, Defekte der epithelialen Barriere, einem Ungleichgewicht der mikrobiellen Flora und einer genetischen Suszeptibilität beeinflusst werden. Patienten, bei denen IBD unter sechs Jahren diagnostiziert wird, wird dies als frühkindlich (engl. *very early onset* IBD, VEO-IBD) bezeichnet. Dessen Inzidenz ist in den letzten Jahrzehnten dramatisch angestiegen. Bei diesen Patienten ist der Krankheitsverlauf oftmals schwerwiegender, komplexer und progressiver. Folglich bleiben herkömmliche Therapien bei VEO-IBD-Patienten oft erfolglos. Besonders für diese Patienten sehen wir einen großen Bedarf, das klinische Management zu verbessern, die Pathomechanismen der Erkrankung besser zu verstehen und therapeutische Ansätze zu finden. Genomanalysen ermöglichten hierbei maßgeblich, ein besseres Verständnis über die Rolle monogener Varianten bei der Pathogenese von IBD zu entwickeln.

Unsere Exom-Sequenzierungen von IBD-Patienten und deren Familien identifizierten neue biallelische monogene Varianten, in *ZYX* (Zyxin) und *LY96* (MD2), die einem autosomal-rezessiven Mendelschen Vererbungsmuster folgten. Diese Arbeit untersucht die zugrunde liegenden Pathomechanismen unserer neu identifizierten Varianten und verknüpft deren Auswirkungen mit den molekularen Funktionen in Epithel- und Immunzellen. Wir fanden heraus, dass die *ZYX*-Varianten von zwei unabhängigen IBD-Patienten im heterologen HCT116 Zellmodell eine normale Verteilung des Zyxinproteins in Epithelzellen und unveränderte Kolokalisierung mit Interaktionsproteinen haben, eine normale

Assoziation mit dem Aktinskelett und proliferative Fähigkeiten aufweisen. Wir konnten jedoch feststellen, dass eine Zyxin-Defizienz die Interferon I Antwort in epithelialen HCT116 und monozytoiden BLaER1 Zellmodellen beeinflusst und auch die pro-inflammatorische Zytokininduktion und -sekretion mindert. Die Rekonstitution der Patientenvarianten konnten diese Ergebnisse in den Zellmodellen jedoch nicht bestätigen.

Darüber hinaus liefert diese Arbeit Einblicke in eine biallelische 3 bp in-frame Deletion in *LY96*, die das Protein MD2 kodiert. Monozyten des VEO-IBD Patienten und MD2-defiziente iPSC-abstammende Makrophagen zeigten eine verminderte TLR4 Aktivierung durch LPS-Stimulation, eine beeinträchtigte MYD88-abhängige Signalübertragung im NF-κB- und MAPK-Signalweg, sowie eine verringerte proinflammatorische Zytokinsekretion.

Diese Arbeit liefert damit funktionelle Einblicke in die Rolle von Zyxin und dessen Assoziation zur Inflammasomaktivität, wobei die rekonstituierten Patientenvarianten in den heterologen Zellmodellen keinen Unterschied aufweisen konnten. Zudem konnte gezeigt werden, dass MD2 ein entscheidender immunologischer Mediator ist. MD2-Defizienz kann hierbei zu schweren, funktionellen Beeinträchtigungen in Makrophagen führen. Diese Einblicke werden uns weiterhelfen, frühkindliche chronisch-entzündliche Darmerkrankungen noch besser zu verstehen.

Table of contents

List of figures

List of tables

List of abbreviations

Abbreviations	Descriptions
%	Percent
°C	Degree Celcius
5-ASAs	5-Aminosalycilic acids
ADAM17	ADAM metallopeptidase domain 17
AIM2	Absent in melanoma 2
AK2	Adenylate kinase 2
Akt	AKT serine/threonine kinase
ALPI	Alkaline phosphatase intestinal
AMP	Antimicrobial peptides
AP1	Activator protein 1
APC	Allophycocyanin
APS	Ammoniumpersulfate
ASC	Apoptosis-associated speck-like protein containing a CARD
ATG16L1	Autophagy related 16 like 1
BJ	Human skin fibroblast cell line
BLaER1	Human B-cell precursor leukemia cell line
BMP4	Bone morphogenetic protein 4
bp	Base pairs
BSA	Bovine serum albumin
BV	Brilliant violet
c.	cDNA variant
CaCO2	Human colorectal adenocarcinoma cells
CARD9	Caspase recruitment domain family member 9
Cas	CRIPSR associated protein
CASP-	Caspase
CCAR1	Cell cycle and apoptosis regulator protein-1
CCDS	Consensus coding sequence
CCL	C-C motif chemokine ligand
CCR-	C-C motif chemokine receptor
CD	Crohn’s disease

CD-	Cluster of differentiation
CD284/TLR4	Toll like receptor 4
CDH1	Cadherin 1
cDNA	Complementary DNA
CDS	Coding sequence
cl. CASP1	Cleaved Caspase 1
CO2	Carbon dioxide
COL7A1	Collagen type VII alpha 1 chain
CRISPR	Clustered regularly interspaced short palindromic repeats
crRNA	CRISPR RNA
CTLA4	Cytotoxic T lymphocyte associated protein 4
CTSD	Cathepsin D
CXCL-	C-X-C motif chemokine ligand
CXCR-	C-X-C chemokine receptor type
Cy	Cyanine dye
CYBB	Cytochrome B-245 beta chain
DAMPs	Danger-associated molecular patterns
DAPI	4′,6-Diamidino-2-phenylindole dihydrochloride
DC	Dendritic cell
del	Deletion
DENND1B	DENN domain containing 1B
dH2O	Destilled H2O
DLG5	Discs large MAGUK scaffold protein 5
DMEM	Dulbecco's modified eagle medium
DNA	Deoxyribonucleic acid
DNase	Deoxyribonuclease
DNMT3A	DNA methyltransferase 3 alpha
dNTP	Deoxynucleotide triphosphates
DSS	Dextran sodium sulfate
E, L, S	Extent, location, severity in Montreal disease classification
E. coli	*Escherichia coli*
ECM1	Extracellular marix protein 1
EDTA	Ethylenediaminetetraacetic acid

ELISA	Enzyme-linked immunosorbent assay
ENAH	ENAH actin regulator
ENV	Gene encoding for viral envelope protein vesicular stomatitis virus-G Protein
EPCAM	Epithelial cell adhesion molecule
ER	Endoplasmic reticulum
Ex	Exon
FACS	Fluorescence-activated cell sorting
FADD	FAS-associated death domain protein
FAK	Focal adhesion kinase
FBS	Fetal bovine serum
FERMT1	Fermitin family protein 1
FGF	Fibroblast growth factor
FITC	Fluorescein isothiocyanate
FLT3	Fms like tyrosine kinase 3
FOXP3	Forkhead box P3
FUT2	Fucosyltransferase 2
fwd	Forward
g	Gram
G-CSF	Granulocyte colony-stimulating factor
G6PC3	Glucose-6-phosphatase catalytic subunit 3
GAG	HIV-1 gene encoding for virion proteins
GALT	Gut-associated lymphoid tissue
GAPDH	Glyceraldehyde-3-phosphate dehydrogenase
GC	Guanine-cytosine
gDNA	Genomic DNA
GFP	Green fluorescent protein from *Aequorea victoria*
GI	Gastrointestinal
GM-CSF	Granulocyte-macrophage colony-stimulating factor
gnomAD	Genome aggregation database
GUCY2C	Guanylate cyclase 2C
GWAS	Genome wide association studies
h	Hour

HeLa	Cervical cancer cell line
HEPES	4-(2-hydroxyethyl)-1-piperazineethanesulfonic acid
HMGU1	Human reprogrammed induced pluripotent stem cell line
HRP	Horseradish peroxidase
HSCT	Hematopoietic stem cell transplantation
IBD	Inflammatory bowel disease
IBDU	Inflammatory bowel disease unclassified
IEC	Intestinal epithelial cells
IEL	Intraepithelial lymphocyte
IFN-	Interferon
IFNB	Interferon beta
IFNG	Interferon gamma
Ig-	Immuneglobuline
IKBKG	Nuclear factor kappa B kinase regulatory subunit gamma
IL-	Interleukin
IL10	Interleukin 10
IL10RA/B	Interleukin 10 receptor alpha/beta
IL18RAP	Interleukin 18 receptor accessory protein
IL1B	Interleukin 1 beta
IL1R2	Interleukin 1 receptor type 2
IL23R	Interleukin 23 receptor
IL2RA	Interleukin 2 receptor subunit alpha
IL6	Interleukin 6
ILC	Innate lymphoid cell
iNOS	Inducible nitric oxide synthase
iPSC	Induced pluripotent stem cell
IRAKs	IL 1 receptor kinases
IRES	Internal ribosome entry site
IRF3	Interferon regulatory factor 3
IRGM	Immunity related GTPase M
JAK	Janus kinase
kDa	Kilodalton
KI	Knock-in

KIF26B	Kinesin family member 26B
KO	Knockout
lacZ	β-galactosidase
LAMB1	Laminin subunit beta 1
LB	Lysogeny broth
LIM	LIN-11, Isl-1 and MEC-3
LPS	Lipopolysaccharide
LRBA	LPS responsive beige-like anchor protein
LRR	Leucine-rich repeat domain
LTA	Lipoteichoic acid
LY96/MD2	Lymphocyte antigen 96/Myeloid differentiation 2
M	Molar
M-CSF	Macrophage colony-stimulating factor
M1/M2	Polarization of macrophages
mA	Milliampere
MadCAM-1	Mucosal addressin cell adhesion molecule-1
MAPK	Mitogen-activated protein kinases
MAVS	Mitochondrial antiviral-signaling protein
mCD14	Membrane-bound CD14
MDA-5	Melanoma differentiation–associated protein-5
MDCK	Madin-Darby canine kidney
mg	Milligram
MHC II HLA-DR	Major histocompatibility complex, class II, DR
min	Minute
miR-155	Micro RNA-155
mL	Milliliter
MMP	Matrix metalloproteases
mRNA	Messenger RNA
MST1	Macrophage stimulating 1
MUC	Mucin
MYD88	Myeloid differentiation primary response 88
N/A	Not available
NA	Numerical aperture

NaOH	Sodium hydroxide
NCF	Neutrophil cytosolic factor
NF-κB	Nuclear factor kappa B
NK	Natural killer
NLR	NOD-like receptor
NLRP	NLR family pyrin domain containing
NLRP3	NLR family pyrin domain containing 3
nm	Nanometer
NOD1/2	Nucleotide binding oligomerization domain containing 1/2
NSAID	Non-steroidal anti-inflammatory drug
oligo(dT)	Oligonucleotide primer with deoxythymidine residues
oligos	Oligonucleotides
p-	Phospho-
p.	Protein sequence
PAMPs	Pathogen-associated molecular patterns
Pat	Patient
PBMCs	Peripheral blood mononuclear cells
PBS	Phosphate buffered solution
PCR	Polymerase chain reaction
P	Plasmacytoid dendritic cell
PE	Phycoerythrin
PEI	Polyethylenimine
PFA	Paraformaldehyde
pg	Picogram
PIC	Protease inhibitor cocktail
PMSF	Phenylmethylsulfonyl fluoride
POL	HIV-1 gene encoding for virus-specific enzymes
Poly I:C	Polyinosinic:polycytidylic acid
PolyPhen	Polymorphism phenotyping
PRR	Pattern recognition receptor
PTK2	Protein tyrosine kinase 2
PVDF	Polyvinylidene fluoride
Pyk2	Pyruvate kinase 2

qPCR	Quantitative real-time polymerase chain reaction
RASGRP	RAS guanyl nucleotide-releasing protein
REL	REL proto-oncogene NF-κB subunit
rev	Reverse
RFP	Red fluorescent protein
RhoB	Ras homolog family member
RIG-I	Retinoic acid-inducible gene I
RIPK1	Receptor interacting serine/threonine kinase 1
RNA	Ribonucleic acid
ROS	Reactive oxygen species
rpm	Rounds per minute
RPMI	Roswell park memorial institute
RT	Room temperature
SB431542	TGF-β receptor kinase inhibitor
SCF	Stem cell factor
SCR7	DNA ligase IV inhibitor
SDS	Sodium dodecyl sulfate
sCD14	Soluble CD14
SDS-PAGE	Sodium dodecyl sulfate–polyacrylamide gel electrophoresis
sec	Seconds
sgRNA	Single-guide RNA
SIFT	Sorting intolerant from tolerant
sIgA	Secretory IgA
SIRT1	Sirtuin 1
SLC11A1	Solute carrier family 11 member 1
SLC37A4	Solute carrier family 37 member 4
SMAD3	SMAD family member 3
SNP	Single nucleotide polymorphism
SNT	Supernatant
ssDNA	Single-stranded DNA
ssODN	Single-stranded oligodeoxynucleotides
STAT-	Signal transducer and activator of transcription
STING	Stimulator of interferon genes

sTLR4-MD2	Soluble TLR4-MD2
T116del	Deletion of amino acid Threonine on position 116
T4	Escherichia virus T4
T84	Human colorectal adenocarcinoma cells
Taq	*Thermus aquaticus*
TBS	Tris buffered saline
TC	Travel conrol
TCR	T cell receptor
TEER	Transepithelial resistance
TEMED	Tetramethylethylenediamine
Tfh	T follicular helper
TGF-β	Transforming growth factor beta
Th	T helper type
THP-1	Human monocytic cell
TIR	Toll-interleukin-1 receptor
TIRAP	TIR domain containing adaptor protein
TLR	Toll-like receptor
TMB	3,3',5,5'-Tetramethylbenzidin
TNF	Tumor necrosis factor
TNFSF	TNF superfamily related
TPO	Thrombopoietin
tracrRNA	Trans-activating crRNA
TRAF6	TNF receptor associated factor 6
TRAM	Toll/IL-1R domain-containing adaptor-inducing IFN-β-related adaptor molecule
Tregs	Regulatory T cells
TRIF	TIR-domain-containing adapter-inducing interferon-β
TRIS	Tris-(hydroxymethyl)-aminomethan
TSLP	Thymic stromal lymphopoietin
TTC7A	Tetratricopeptide repeat domain 7A
TYK2	Tyrosine kinase 2
U	Unit
UC	Ulcerative colitis

UV	Ultra violet
V	Volt
VASP	Vasodilator stimulated phosphoprotein
VEGF	Vascular endothelial growth factor
VEO-IBD	Very early onset inflammatory bowel disease
Vinc	Vinculin
vol %	Percent by volume
WES	Whole exome sequencing
WGS	Whole genome sequencing
WT	Wild-type
x g	Relative centrifugal force
XBP1	X-Box binding protein 1
XIAP	X-Linked inhibitor of apoptosis
Y-27632	Rho kinase inhibitor
ZYX	Zyxin
µg	Microgram
µl	Microliter
µm	Micrometer
µM	Micromolar

1. Introduction

1.1. Inflammatory bowel disease

Inflammatory bowel disease (IBD) is a complex, heterogeneous, inflammatory disease of the gastrointestinal tract driven by multiple intrinsic and extrinsic factors [1-3]. The disease is characterized by relapses and remission over time, which result in a significant burden on patient quality of life. The average age of onset is between 20 to 40 years of age, while the incidence of disease has greatly increased over the last 30 years, especially in western and newly industrialized countries [4-7]. In 2017, 6.8 million people were affected by IBD, while it was estimated that over 3 million of these people were from Europe and North America [5]. Underlining the growing impact of the disease to the western population, a predictive IBD prevalence model forecasted a 4 to 6 times higher rate in 2030 based on data from 2003-2007 [8].

The major distinguishable manifestations of IBD are Ulcerative Colitis (UC) and Crohn's Disease (CD) [9]. While CD has two peaks of onset, one between 20 to 30 years of age and the other between 60 to 70, UC mainly manifests at the age of 20 to 30 [10-12]. Both diseases have unique clinical features and manifestations of the gastrointestinal tract but commonly include fever, diarrhea and abdominal pain [13, 14]. The clinical phenotype of UC is mostly characterized by a continuous mucosal inflammation of the colon and rectum [15, 16]. In contrast, CD typically manifests as a segmental, transmural inflammation throughout the gastrointestinal tract, especially in the terminal ileum, and includes fistula formation, bowel strictures and the development of abscesses [13, 17-19].

1.1.1. Ulcerative colitis

The highest annual incidence rates for UC are found in Europe (0.6 to 24.3 per 100,000) and North America (0 to 19.2 per 100,000) [20]. The disease course is substantially different from adults to children, displaying mostly a proximal inflammatory extension from the rectum in adults, whereas children mainly present with pancolitis or an inflammatory extension throughout the whole colon [21]. Endoscopic investigations in UC patients show a continuous inflammation of the mucosa and submucosa, altered

vascularization patterns, and histological examinations reveal crypt abscesses and cryptitis [22]. The Montreal classification differentiates UC by the disease extent (E), specifying ulcerative proctitis (E1), left-sided/distal UC (E2) and extensive UC/pancolitis (E3), while disease severity is characterized as mild (S1), moderate (S2), severe (S3) and clinical remission (S0), (Figure 1A) [23].

At the time of diagnosis, patients have either a left-sided colitis (40.1 %), extensive colitis (30.5 %) or proctitis (29.4 %) [24]. About two thirds of patients with UC can be treated with sulfasalazine and 5-aminosalycilic acids (5-ASAs) mainly in mild to moderate disease activities [25]. The current therapeutic landscape for UC includes the use of: 5-ASAs, corticosteroids, as well as antibodies that selectively inhibit TNF, IL-12/23, α4β7-integrin, and JAKs [26]. Upon low responsiveness with therapeutic agents, surgery is considered.

The disease burden of UC is high, with one third of patients suffering from disease even after ten years of treatment, while around one fifth of those patients have to undergo colectomy [27]. One study that monitored UC patients for 25 years revealed that around 50 % of the patients are in remission at any time but have a 90 % relapse probability [27].

1.1.2. Crohn's disease

While more patients worldwide suffer from UC than CD, the highest annual incidence rates for CD are found in Europe (0.3 to 12.7 per 100,000) and North America (0 to 20.2 per 100,000) [20]. CD is characterized by patchy inflammation that penetrates the bowel wall through all layers along the gastrointestinal tract [28, 29]. This inflammation results in fistulas and stenosis, in addition to other extraintestinal manifestations [28, 29]. CD can also be associated with a spectrum of other autoimmune diseases driven by similar inflammatory processes [28, 29]. Using the Montreal classification, it differs by the age of diagnosis, disease behavior, and locations (L). CD manifests in the terminal ileum (L1, 45 %) of the time, the colon (L2, 32 %) of the time, the ileocolon (L3, 19 %) of the time, and the upper gastrointestinal tract (L4, 4 %) of the time (Figure 1B) [30]. It can occur also simultaneously in the upper and lower gastrointestinal tract [30]. CD has a similar current therapeutic landscape to UC, including treatments such as: 5-ASAs,

corticosteroids, as well as antibodies that selectively inhibit TNF, IL-12/23, α4β7-integrin, and JAKs [26]. CD can require a surgery of gut patches, although it is often not as effective as in UC.

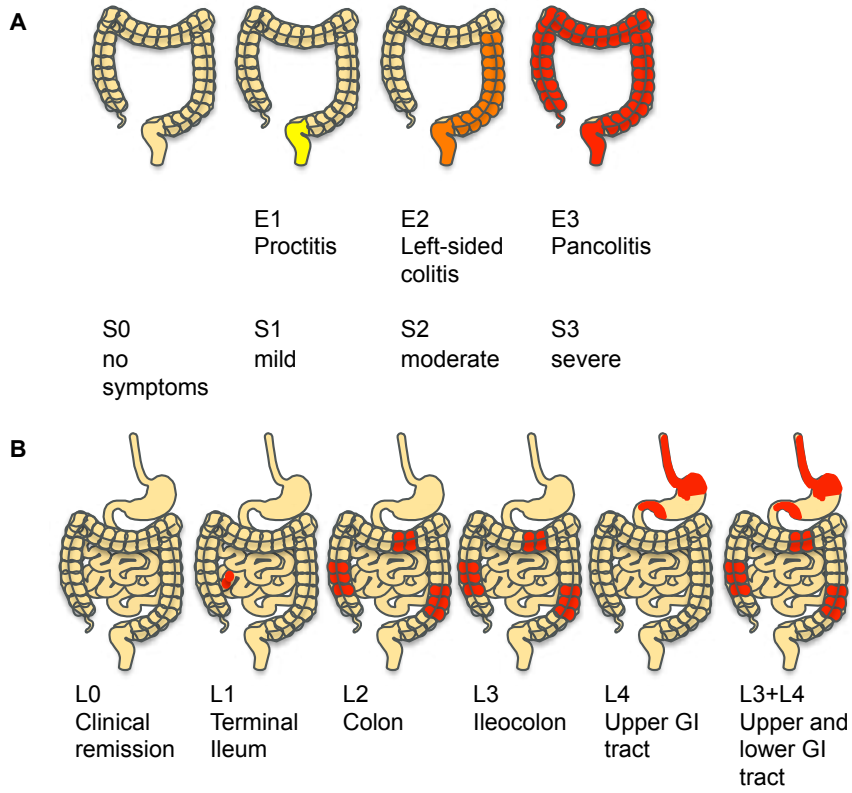

Figure 1 Phenotypes in Ulcerative colitis (A) and Crohn‘s disease (B) based on the Montreal classification.
UC is described by its extent (E1-3) and severity (S). Yellow indicates mild, orange indicates moderate and red indicates severe symptoms in the colon. Crohn‘s disease differentiates the age of diagnosis, disease behavior and is defined by location (L) L0 to L4. Modified from Satsangi et al. [23].

In the IBD disease landscape there are increasing numbers of indistinguishable manifestations, which are defined as indeterminate colitis or IBD unclassified (IBDU) [31, 32]. This form emerges in around 6-10 % of the adult population, while in children the number is up to 50 % higher, dependent on the observed study [33, 34]. Furthermore, an age-dependent classification analysis that took place over 20 years showed that the earlier the age of disease onset, the higher the prevalence of IBD unclassified [35, 36].

1.1.3. IBD in children

Around 25 % of all IBD cases are diagnosed within the first twenty years of life, while the rates of IBD increase with the age from the first year of life until teenage age [37, 38]. The Paris classification was created as a modification of the Montreal classification to further classify pediatric IBD, as children frequently have more severe, complex disease phenotypes that are distinct from adults, and higher reliance on corticosteroid therapies [39-44]. The Montreal classification has its diagnostic cut off for pediatric-onset IBD at the age of 17, which was refined by the Paris classification in 2011 [39, 40]. The Paris classification further classifies onset at 10-17 years of age as pediatric-onset IBD, below 10 years of age as early-onset IBD (EO-IBD), below 6 years of age as very early-onset IBD (VEO-IBD), below 2 years of age as infantile-onset IBD and below 28 days of age as neonatal IBD, while also accounting for disease progression, location, and possible monogenetic factors [45-47].

1.2. IBD Etiology

IBD is a complex, heterogeneous disease driven by multiple factors. This can involve different components of environmental factors, the microbial flora, a defective epithelial barrier, an immunological dysfunction and genetic susceptibility, which all can intersect in multiple ways among patients and drive IBD pathogenesis (Figure 2) [48]. Specific pathomechanisms and interplays still remain unsolved and are part of current research.

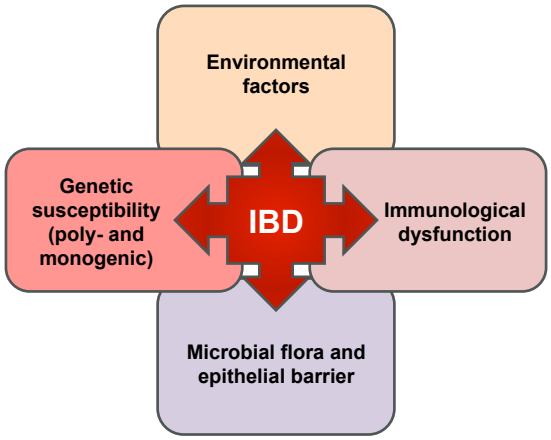

Figure 2 Pathogenesis of IBD.
Multiple factors drive disease onset and progression including environmental factors, immunological dysfunction, microbial flora and epithelial barrier and poly- or monogenetic susceptibility. Modified from Sartor [48].

1.2.1. Environmental factors

The amount of IBD patients has greatly increased since the 1950's [4, 49]. The exposure to environmental triggers plays an important role in the IBD disease onset and progression, which cannot be explained by a genetic selection or drift [4, 49]. This remarkably affects the regions of Europe, North America, and developing countries among Africa, Asia and South America.

The heterogenic, influential and external factors, that one is exposed to during a lifetime is known as the exposome [50]. The exposome changes continuously and triggers can be variously present or absent among a patient's life.

In IBD, commonly studied environmental factors shaping disease emergence are lifestyle, smoking, stress, diet, hygiene, pharmacological substances, vaccinations, air

and water pollution, and infectious diseases [51]. Exposure in early life to antibiotics, infections or tobacco smoke is associated with IBD emergence, while breastfeeding seems protective against the development of IBD [52]. A recent study has revealed that in adults urban living, antibiotic use, oral contraceptives, enterohepatic *Helicobacter* species (non-*H. pylori*-like), and vitamin D deficiency increase the risk for IBD [53]. Specific risk factors for CD are smoking, appendectomy, and tonsillectomy, whereas soft drink consumption is a specific risk factor for UC [53]. According to another study, adhering to a specific lifestyle can prevent IBD [54]. A prevention of over 40 % of CD or UC cases was predicted, taking smoking status, physical activity, non-steroidal anti-inflammatory drug (NSAID) use, and body mass index into consideration [54]. The highest impact was predicted by a healthy diet, which could prevent up to 61 % of CD and 42 % of UC cases [54].

1.2.2. Microbial flora and epithelial barrier

The microbiome and its metabolic products play a key role in IBD pathogenesis. A reduced diversity of the human gut microbiome, imbalanced gut homeostasis, a deregulated immunological response and a defective epithelial barrier can promote the development of IBD in susceptible individuals [55-58]. In the postnatal state, the microbial flora is established and essential to drive immune system maturation, although breastfeeding and birth mode of the infant contribute likewise [59, 60].

The human gut microbiome consists in total of over 100 trillion microorganisms, while the highest density of cells (10^{11}-10^{12} cells/mL) appears in the colon and regions of fecal stasis, like the terminal ileum and rectum, which are the most prominently affected sites in IBD [61-64]. In addition to fungi, viruses, phages, yeast and archaea, the gut microbiome is mostly comprised of bacteria, with at least 150 but up to 1150 different species found in human gut samples [65, 66]. *Firmicutes* and *Bacteroidetes* are among the predominant phyla in the human gastrointestinal tract along with *Proteo*- and *Actinobacteria* [67]. While commensal bacteria are responsible for the production of essential metabolites such as vitamins, amino acids or short fatty acids as nutrient sources, the host must maintain a tightly regulated immune tolerance towards them and prevent pathogenic invasion and infections. The epithelial barrier in the gut is the first surface of interaction between the host and the environment. The complex regulation of the host adaptive and innate immune system through their immune cells, cytokines, and

effector cells on the mucosal barrier against commensal microbes, pathogens or food antigens is crucial for the maintenance of a healthy gut homeostasis (Figure 3).

A defective epithelial barrier and specific external factors such as antibiotics, diet or smoking can increase the risk for IBD, shaping the abundance, composition and perception for commensal bacteria in the gut and ultimately driving inflammatory processes [68].

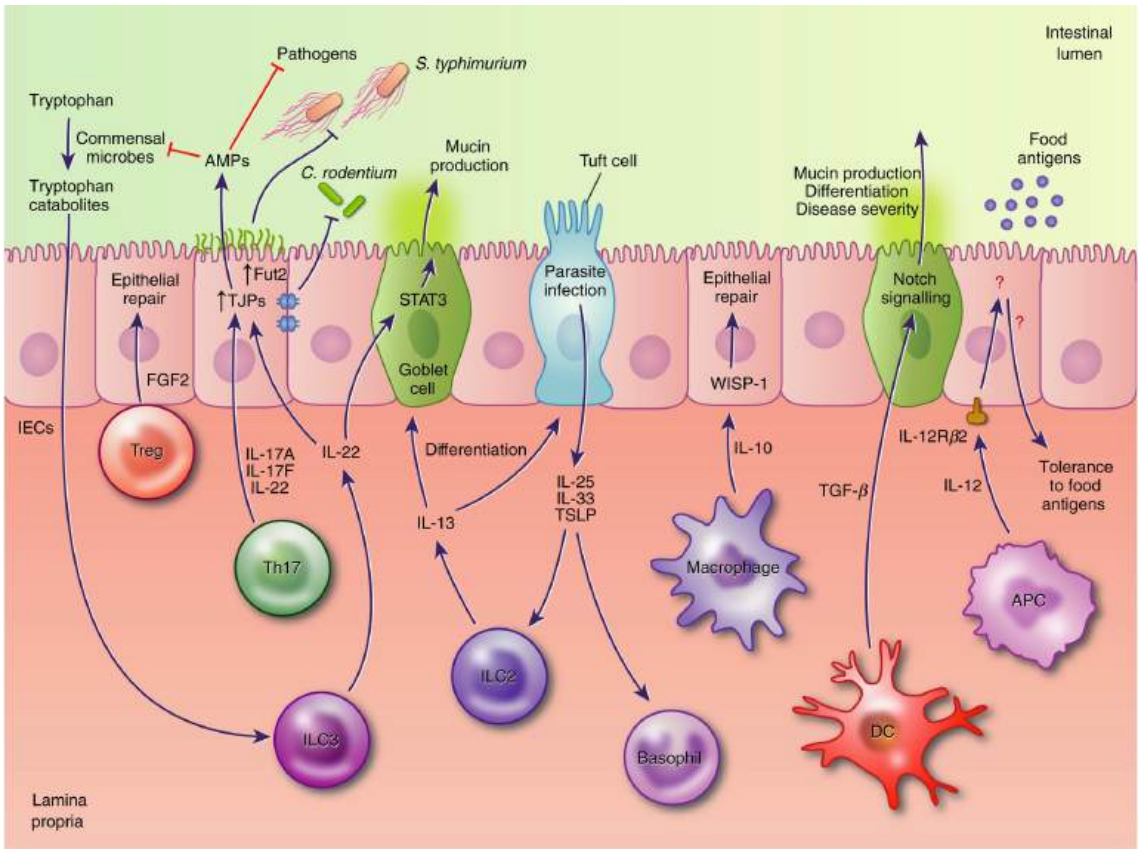

Figure 3 Intestinal homeostasis and involved immune cells.
To prevent the invasion of microbes to the lamina propria, the intestinal epithelial cells (IECs) are linked by tight junctions, which provide the first physical barrier in the intestinal tissue. The apical layer of IECs consists of high amounts of mucus, produced by goblet cells, cytokines (IL-25, IL-33, TSLP) against parasitic infections from tuft cells, and AMPs (antimicrobial peptides) secreted by IECs (paneth cells) against commensal and pathogenic microbes towards the gut lumen. IECs can induce immune responses to specific pathogen-associated molecular patterns (PAMPs) by their Toll-like receptors (TLRs) and NOD-like receptors (NLRs). The lamina propria contains of innate and adaptive immune cells in a complex network of cytokines, regulating inflammatory and anti-viral responses distal of IECs. The immune network of the lamina propria exists in the mucosa-associated lymphoid tissue, blood and lymph vessels. Modified from Soderholm and Pedicord [69].

1.2.3. Immunological features in IBD

The epithelial barrier is composed of intestinal epithelial cells (IECs) connected through tight junctions, which prevent microbial infiltration into the lamina propria. The mucus layer is mainly provided by mucin secreting goblet cells and is located apically of IECs. Mucins are linked, glycosylated proteins of the mucus (e.g. MUC2, 5B, and 6) secreted into the lumen to prevent microbial contact to IECs, while membrane-bound mucins (e.g. MUC1, 3A/B, 4, 12, 15, 17, 20, 21) form the glycocalyx and sense microbial-host interactions [70]. Mucins are differentially expressed among the several sections (duodenum, jejunum, colon) of the intestine. The mucin secretion and expression is rapidly adapted upon stimulation with cytokines as type I interferons, TNF, IL-1, -4, -5, -9, -13, -22 or pathogen-associated molecular pattern (PAMPs) (e.g. lipopolysaccharides (LPS), lipoteichoic acid or flagellin) [71].

Paneth cells, located at the crypt base, secrete antimicrobial peptides (AMPs) such as antimicrobial α-defensins and β-defensins, which lead to an elimination of microbes. Misfolded α-defensins can promote CD, while impaired secretion of another AMP Regenerating islet-derived protein 3 was shown to be significantly upregulated in IBD patients [72-74].

Secretory IgA (sIgA) serve as a further protective layer of the epithelial barrier, produced by plasma B cells in the Payers's patches of the gut-associated lymphoid tissue (GALT) in response to intestinal antigen presenting dendritic cells (DCs) and follicular T helper cells [75, 76]. It has been shown in IBD that levels of sIgA are positively correlated with the disease activity status [77, 78].

The immune system in the gut is characterized by innate and adaptive immune responses, which promote homeostasis and become activated whenever microbes or their components are sensed. Cells of the innate immune system in the gut include neutrophils, monocytes, macrophages and dendritic cells. These cells express pattern recognition receptors (PRRs), in particular NOD-like receptors (NLR) including Nucleotide binding oligomerization domain containing 1/2 (NOD1/2) in the cytosol, or cytosolic sensors of the NLR family pyrin domain containing proteins (NLRP1-14), forming the inflammasome [79, 80]. Additionally they can express PRRs like Toll-like

receptors (TLRs 1-9), which are membrane-bound (TLR1, 2, 4, 5, 6) or intracellular (TLR3, 7, 8, 9), as well as cytosolic Retinoic acid-inducible gene I (RIG-I)-like receptors, sensing viral RNA [81, 82]. PRRs can also be cytosolic DNA sensors, e.g. Absent in melanoma 2 (AIM2) or Stimulator of interferon genes (STING)-associated sensor [83]. All PRRs sense PAMPs such as microbial molecules, cell wall peptidoglycans as well as DNA or RNA, while damage-associated molecular patterns (DAMPs) are set free from perforated or dying cells [84]. Besides immune cells, IECs as non-immune cells harbor PRRs to recognize PAMPs and DAMPs to provide another layer of defense mechanism [85]. Several IBD susceptibility genes have been identified which are involved in innate mucosal defense (e.g. *NOD2, CARD9, SLC11A1*) [86].

Phagocytic cells such as dendritic cells, neutrophils and macrophages are part of the innate immunity in the gut. Chemotactic gradients of cytokines (e.g. IL-1β, IL-6, TNF), chemokines (e.g. CXCL2, CXCL10) or growth factors (e.g. G-CSF, GM-CSF) from inflammatory sites of the epithelium lead to the mobilization of neutrophils, eliminating phagocytized microbes by reactive oxygen species (ROS) production, degranulation and neutrophil extracellular trap formation (Figure 4) [87]. Neutrophils can release pro-inflammatory IL-1β, IL-8 and TNF attracting other immune cells. Dysfunctional ROS production has been shown in IBD [88]. IBD patients, lacking CARD9, neutrophils have an increased ROS production leading to a promoted intestinal inflammation and epithelial barrier damage through inducible nitric oxide synthase (iNOS) and matrix metalloproteases (MMP) [88].

Monocyte-derived and tissue-resident macrophages are responsible for tolerating commensal bacteria and sensing pathogens by their PRRs. M1 macrophages secrete pro-inflammatory cytokines such as IL-1β or IL-6, upon activation [89]. M2 macrophages can release large amounts of anti-inflammatory IL-10 as a regulatory function [89]. A dysbalance of M1 and M2 macrophages in IBD patients have been shown to impair homeostasis and maintain inflammation [90]. Activated macrophages can also prime subsets of T cells and promote Th17 cell differentiation (Figure 4). In CD in particular, large infiltrations of macrophages can appear in granulomas of the intestinal wall [91].
Innate lymphoid cells (ILCs) are involved in bidirectional mucosal crosstalk and secrete effector cytokines such as TNF, IFN-γ from ILC1s; IL-4, -5, -6, -9, and -13 from ILC2s; and IL-17, IL-22 from ILC3s, maintaining epithelial barrier integrity and T cell activation

[92]. ILC3s produce IL-17 and IL-22, similar to Th17 cells, enhancing mucus and defensine production, IgA secretion into the lumen as well as promoting tight junctions to maintain the epithelial barrier (Figure 4).

Dendritic cells extend their dendrites through IECs, to sample antigens and present them to T cells within GALT structures like Payer's patches [93]. These lymphoid follicular structures contain B lymphocytes, follicular T helper cells, dendritic cells and macrophages, while microfold cells absorb and pass transcellular antigens to the GALT [94]. The GALT represents the assembly of intestine-draining mesenteric lymph nodes, which are located under the basement membrane of the gut epithelium [95]. Immunological induction sites for adaptive immune cells to undergo priming and differentiation are located in the GALT tissues, whereas the lamina propria and IECs represent the effector sites for homeostasis and immunity [96].

Homing of B and T cells is achieved mainly through their expression of integrin α4β7, binding Mucosal addressin cell adhesion molecule-1 (MadCAM-1) on endothelial cells of the lamina propria. Selective anti-integrin α4β7 therapy can serve as a targeted approach in UC and CD to reduce intestinal inflammation [97].

It was previously assumed that CD was mainly associated with pro-inflammatory cytokines, like TNF and IFN-γ of the Th1 (T helper type 1) response, while UC was more associated with a cytokine profile of a Th2 (T helper type 2) response, including IL-5/-13 [98, 99]. It is now hypothesized that that the imbalance of Th1 and Th2 responses can determine onset and intensity of both conditions (UC, CD), whereas the distinct cytokines are not mutually exclusively responsible for one or the other [100].

There are several distinct T cells populations in the gut, including T helper subsets of Th1, Th2, Th9, Th17, Th22 cells, regulatory T cells (Tregs), T follicular helper cells, and intraepithelial lymphocytes (IELs). In homeostatic conditions, the abundance of CD4+ cells is relatively low in the lamina propria, while IBD is associated with a dysregulation or increased activation of CD4+ T cells [101]. In IBD, there is often a shift towards pro-inflammatory cytokines (TNF, IFN-γ, IL-1β, IL-6, IL-13, IL-23) instead of a presence of anti-inflammatory cytokine IL-10 or normal regulatory T cell function [102].

Upon microbial stimulation, DCs and macrophages release key cytokines IL-6, IL-12, IL-18, IL-23, IL-1β and TNF, stimulating T helper subsets, which release a cascade of cytokines, driving immune phenotypes of CD and UC (e.g. IL-2, IL-6, IL-9, TNF, IL-17, IL-21, IL-22), respectively (Figure 4) [86, 103].

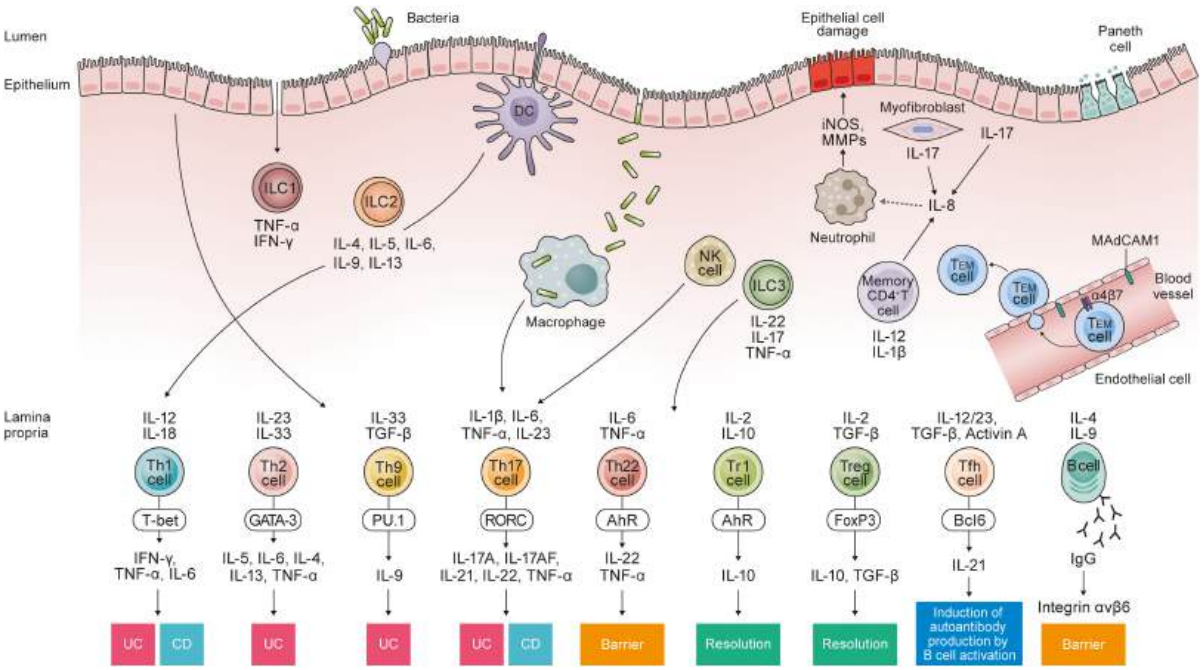

Figure 4 Overview of involved immune cells in CD und UC pathology.
Phagocytic cells (neutrophils, dendritic cells and macrophages) are part of the innate immunity in the gut. Dendritic cells extend dendrites through the epithelium, sampling antigens, processing and presenting them to T cells. Upon microbial stimulation, DCs and macrophages release key cytokines IL-6, IL-12, IL-18, IL-23, IL-1β and TNF, stimulating T helper subsets in the lamina propria. Distinct T cells populations home in the gut, including T helper subsets of Th1, Th2, Th9, Th17, Th22 cells, regulatory T cells (Tregs), T follicular helper cells (Tfh) with their unique cytokine profiles, contributing to specific signatures of UC, CD or both. A dysregulation or increased activation of CD4+ T cells, promotes a shift towards more pro-inflammatory cytokines, instead of anti-inflammatory cytokine IL-10 or normal Treg function, which usually leads to a resolution of the inflammation in UC and CD patients. Innate lymphoid cells 1-3 (ILCs) are involved in the bidirectional mucosal crosstalk, while IL-8, induces neutrophils migration and infiltration leading through to migrate to and infiltrate the intestines, contributing to the release of iNOS and MMPs that induce epithelial cell damage. Modified from Nakase et al. [103].

Another large, heterogeneous mucosal subset of cells are intraepithelial lymphocytes, which patrol between epithelial cells and basement membranes. IELs promote fast Th1 responses towards infected or stressed epithelium and maintain the mucosal barrier function. Dependent on their expression profiles, IELs can express different T cell receptor (TCR) subsets (e.g. TCRαβ+, TCRγδ+) or lack TCR (TCR−) [104]. Most IELs

are TCR+ and can either infiltrate the epithelial layer after antigen exposition in the periphery, which are called ‘induced IELs’ such as TCRαβ+ or reside after development in the epithelium, named ‘natural IELs’ like TCRγδ+ [105]. TCR-IELs comprise of ILC1-like, ILC3-like and intracellular iCD3+ and iCD8α cells, which are referred to as ‘natural IELs’ [106]. IELs may play a role in IBD progression, since it was shown that increased IL-23 levels can enhance the cytotoxic functions of IELs towards enterocytes in IBD [107]. Further, the factor Apoptosis inhibitor 5, secreted from TCRγδ+ IELs, was recently identified to promote Paneth cell viability in a Atg16l1-mutant murine model, proposing Apoptosis inhibitor 5 as a therapeutic target in patients with CD with a susceptibility gene variant of *ATG16L1* [108, 109].

In IBD, the lamina propria is not only heavily infiltrated by T cells, but also by plasma cells and IgG+ B cells. Besides the extensive production of anti-inflammatory secretory IgA from plasma cells against commensal bacteria, B cells express more pro-inflammatory IL-8 and mucosal IgG in IBD patients [110]. UC samples showed that naïve B and IgG-producing plasma cell numbers are increased and circulating IgG1 antibodies as well as auto-reactive clones against integrin αvβ6 are present [111]. In CD, granulomatous tissue is infiltrated by B-lymphocytes and was shown to harbor increased reactive IgG2 autoantibodies [112]. A recent murine study of dextran sodium sulfate (DSS)-induced intestinal damage postulated that the increased number of B cells on the damaged intestinal epithelium prevents stromal cell and IEC interactions, which are necessary for mucosal healing, suggesting B cell depletion as a beneficial option for IBD patients [113].

1.2.4. Genetics in IBD

Genetics play an important role in IBD susceptibility, since a positive family history is a risk factor for up to 12 % of IBD cases [114, 115]. The risk for first-degree-relatives is higher in CD patients (0.35 %-4.5 %) than in UC patients (0.3-2.7 %), describing an up to 8-fold higher risk compared to individuals without an IBD history [116]. Monozygotic twin studies underline the impact of genetics, while the concordance rate for CD is around 20-50 %, yet for dizygotic twins it is less than 10 % [117]. A cumulative effect of an increased risk for IBD was demonstrated based on the number of relatives that were affected, meanwhile the age of onset of IBD was then shifted towards a younger age

[118]. Ethnic background also plays a role in IBD susceptibility, since the Jewish Ashkenazi community has a two to four times higher prevalence for CD, with enriched rare genetic risk alleles, caused by a founder effect [119, 120].

Genome wide association studies (GWAS) have identified more than 240 different genetic loci that are linked to IBD over the last two decades [121-123]. Single nucleotide polymorphisms (SNPs) or the combination of SNPs are associated with IBD pathogenesis, reflecting a monogenic or polygenic disease phenotype. In general, not only coding variants of genes can be affected, but also untranslated 3' or 5' regions or microRNAs, as well as epigenetic modifications can be associated with IBD [124-127]. GWAS assumed that more than a single gene is involved in IBD etiology. These risk loci suggested functional defects in autophagy, epithelial barrier function, ER stress response or dysfunctional immune responses.

First, only designated regions of chromosomes were linked to IBD, named IBD 1-9 [128]. The first discovered susceptibility locus was *NOD2*, mapped to chromosome 16 of CD patients [129]. NOD2-deficient DCs show an impaired autophagic capacity and bacterial handling [130]. Further associated risk alleles involved in autophagy are Immunity related GTPase M (*IRGM*) and *ATG16L1* [131, 132]. Interleukin 23 receptor (*IL23R*) was first identified in CD but also later in UC, linking loci of the Th17 pathway directly to IBD pathogenesis [133, 134]. The overlap of genetic variants in UC and CD can be found at loci related to Th17-related signaling (*STAT3, IL12B, AK2, FUT2, TYK2)* or immune mediator loci (*IL10 (R), IL1R2, MST1, CARD9*, *REL, TNFSF15, TNFRSF6B, SMAD3)* [135]. Loci of both UC and CD include also *KIF26B,* cell adhesion-associated *DLG5* or ER stress-associated *XBP1* [136-138].

Previous GWAS studies postulated UC variants impairing the epithelial barrier function (e.g. *CDH1*, *ECM1*, *LAMB1*), immune regulatory functions of the TNF pathway (*TNFRSF9, TNFRSF14*), interferon gamma signaling (*IFNG)*, interleukin and interleukin receptor functions (*IL2, IL21, IL26*, *IL7R*, *CXCR1*, *CXCR2*), apoptosis pathway (*DAP*) or janus kinase activity (*JAK2*) [139, 140]. GWAS previously identified *IL2RA, IL18RAP, IL27, CCR6, MUC1, DNMT3A* or *DENND1B* among other variants, as unique loci for CD [138]. Recently, many presumed unique GWAS loci were identified in both entities of UC and CD. The progression to more precise sequencing techniques via whole

exome sequencing (WES), whole genome sequencing (WGS) and fine-mapping refined the identification of very rare SNPs as causal disease variants in IBD (Figure 5) [141, 142].

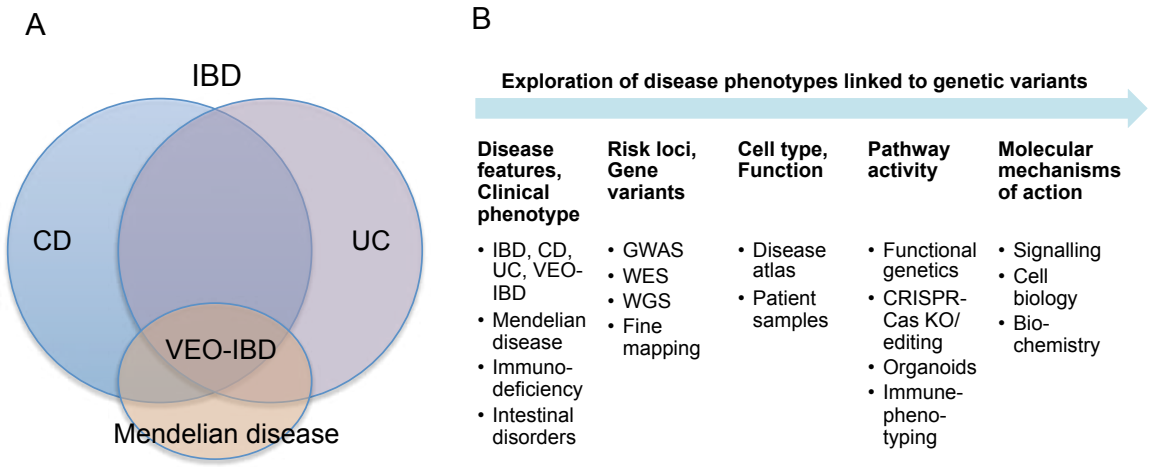

Figure 5 Overview of strategic genetics in IBD and exploration of causative variants.
A) IBD is featured through genetic variants overlapping in UC and CD or represented with unique genetic variants for UC or CD. Very early onset (VEO)-IBD features rare genetic variants, following a mendelian inheritance pattern, which is also found in primary immunodeficiencies. B) Exploration of disease phenotypes to genotypes. Linking genetic examination by genome wide association studies (GWAS), whole exome (WES) or whole genome sequencing (WGS) of genetic variants to affected cell types and a functional testing (e.g. by Clustered Regularly Interspaced Short Palindromic Repeats (CRISPR), CRISPR associated protein (Cas), Knockout (KO)) to identify underlying molecular mechanisms of action. Modified from Graham and Xavier [143].

1.2.5. Genetics in VEO-IBD

In VEO-IBD patients, who have an onset of disease below the age of 6 years and a higher frequency of monogenic variants, following a Mendelian inheritance pattern, Interleukin 10 receptor alpha *IL10RA* was identified as the first causative gene, impairing IL-10 signaling [144]. A recent systematic review described the most common monogenic genes in IBD with 124 cases with *IL10RA* variants, 69 cases of variants in X-linked inhibitor of apoptosis (*XIAP)*, 68 cases of Cytochrome B-245 beta chain (*CYBB)* variants, 33 cases of Interleukin 10 receptor beta (*IL10RB)* variants, 31 cases of LPS responsive beige-like anchor protein (*LRBA)* variants as well as 31 cases of Tetratricopeptide repeat domain 7A (*TTC7A)* [145]. Notably, nearly two thirds (63.5 %) of patients develop IBD before the age of six, while the age of onset differs among the IBD-associated disorders, e.g. TTC7A deficiency, IL-10 and IL-10 receptor associated colitis and Receptor interacting serine/threonine kinase 1 (*RIPK1*) deficiency manifest within the first six months after birth; as on the contrary, Guanylate cyclase 2 diarrhea syndrome (*GUCY2C*) has an average onset at over 30 years [145]. Genetic variants can appear in autosomal dominant, autosomal recessive, X-linked recessive or compound heterozygous inheritance patterns. A WES cohort study of 1000 pediatric IBD patients revealed most variant types to be a missense (67 %), stop gained (15 %), splice site (8 %), frameshift (7 %) or in-frame deletion (3 %), however intronic variants or copy number variations are also possible [146].

Based on the functional impact of genetic variants, one functional cluster represents variants playing a role in T cell immune tolerance. Variants causing defective IL-2 signaling (*IL2RA*) lead to a lower abundance of peripheral T cells, while specifically *FOXP3,* S*TAT1, 3, 5A* and *5B* or *CTL4A* variants lead to a decreased amount, quality and appropriate autoimmune response of Tregs [147-150]. Immune modulation by regulating inflammation can be found in *IL10/R* variants, as deficiency and impaired IL-10 signaling lead to excessive IL-1β secretion of pro-inflammatory macrophages and continuous inflammation of the gut [151]. Another cluster is found to affect neutrophil function specifically in chronic granulomatous disease, impacting phagocytic activity of neutrophils, ROS generation and a higher susceptibility for recurrent infections by variants of *CYBB*, *NCF1/2/4*, *SLC37A4* and *G6PC3,* which can not only drive IBD but also neutropenia in these patients [152-155]. Variants causing an impaired apoptosis

pathway like Caspase 8 (*CASP8)* deficiency, lead to an impaired inflammasome response to LPS and altered TNF induced cell death response [156]. Similarly, RIPK1 deficiency was recently demonstrated to be causative in VEO-IBD, reducing NF-κB activity upon TNF treatment and increased inflammasome activity upon LPS priming [157]. Alkaline phosphatase intestinal deficiency is found in IBD patients, which results in a failure to detoxify LPS, promotes TLR-4 signaling and a disproportionate pro-inflammatory IL-8 release, disturbing of the gut homeostasis and intestinal epithelial cell activation and signaling [158]. On the contrary, ADAM metallopeptidase domain 17 (*ADAM17*) deficiency leads to a dysfunctional response to TNF and variants of Inhibitor of nuclear factor kappa B kinase regulatory subunit gamma (*IKBKG)* show reduced NF-κB signaling, a master regulator of inflammatory responses, in IECs [159, 160]. TTC7A deficiency is one of the most frequent variants found in IBD driving IEC adhesion and polarization along with Epithelial cell adhesion molecule (*EPCAM*) supporting intraepithelial junction function, Collagen type VII alpha 1 chain (*COL7A1*) driving the anchorage to the basement membrane, and Fermitin family protein 1 (*FERMT1*) involved in focal adhesion stability of IECs [161].

Effective treatments for monogenic IBD disorders can include bowel surgery (27.1 %) and biologic treatments (8.4 %), whereas allogenic hematopoietic stem cell transplantation (HSCT) can lead also to IBD improvement (16.6 %) [145]. Significant improvement through HSCT can be achieved in patient with inborn errors of immunity such as IL-10, IL-10R or XIAP deficiency, while patients affected by variants in epithelial polarity and barrier function like TTC7A or IKBKG showed very low effectiveness [162-164]. Therefore, new nanoparticle-mediated gene therapies targeting the gut epithelium might give a future perspective in personalized treatment options for IBD patients [165]. Recently, Uhlig et al. gave valuable insights to monogenic IBD treatment options to correlate precision medicine in a genotype-phenotype approach, since randomized controlled studies are lacking [166].

1.3. Zyxin

Proteins involved in epithelial integrity and barrier function have been shown to drive inflammatory processes in IBD patients, like those harboring variants in *EPCAM* or *FERMT1* [167, 168]. Murine models underline the lack of focal adhesion proteins, like Protein tyrosine kinase 2 (PTK2) or Pyruvate kinase 2 (PYK2), promoting susceptibility to DSS-induced colitis, while lacking both proteins lead to spontaneous colitis with a full penetrance [169, 170].

Multiprotein integrin-based assemblies, called focal adhesions, connect the actin cytoskeleton with the extracellular matrix, and play a critical role in cellular morphogenesis, stability, polarity, proliferation, signaling, cell adhesion, wound healing, and cell motility [171]. As of now, more than 230 components of the focal adhesion network have been identified, with dynamic assembly and reassembly properties, and primarily divided into either structural or signaling functions [172, 173]. Focal adhesions are organized in three parallel layers to the plasma membrane. This includes the integrin signaling layer, closest to the plasma membrane, harboring proteins like Paxillin, Phospho-paxillin and Protein tyrosine kinase 2. The force transduction layer is spanned with Vinculin and Talin, whereas the most proximal actin regulatory layer, connects actin fibers with α-Actinin, Zyxin and Vasodilator stimulated phosphoprotein (VASP) (Figure 6).

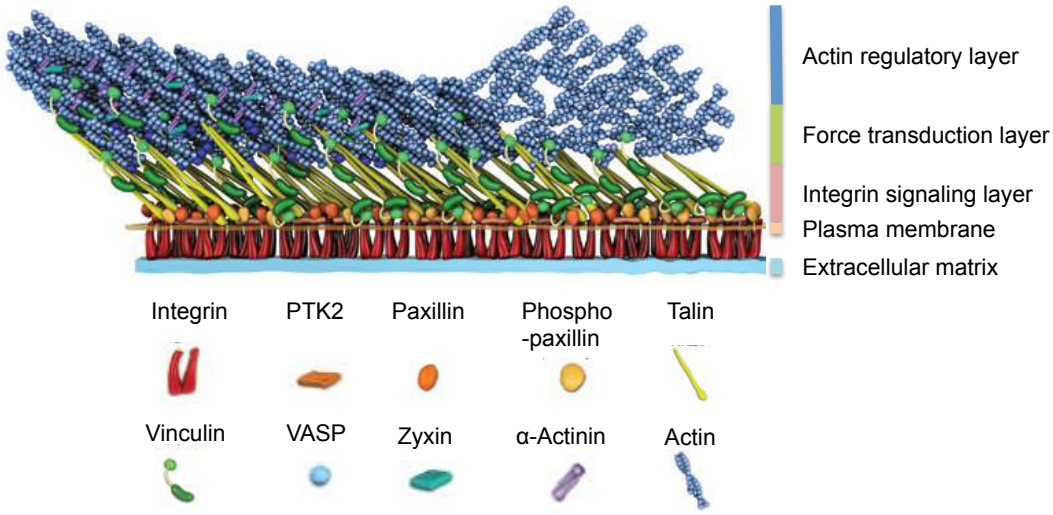

Figure 6 Selected nanostructure components of focal adhesions.
Integrins are bound to the extracellular matrix, spanning through the plasma membrane, connecting the integrin signaling layer with Protein tyrosine kinase 2 (PTK2), Paxillin, Phospho-paxillin and Talin heads. The force transduction layer spans through Talin and Vinculin, while the proximal tip of the actin regulatory layer connects the actin stress fibers with α-Actinin, Zyxin, and Vasodilator stimulated phosphoprotein (VASP). Modified from Case and Waterman [174].

Zyxin (ZYX) is an evolutionary conserved protein and a regulator of actin assembly, which is mainly located at focal adhesions, and can be also detected at spindle poles during mitosis, leading edges of lamellipodia, and transiently in nuclei [175-178]. It belongs to the LIM protein family, characterized by a proline-rich N-terminal domain and three C-terminal cysteine- and histidine-rich motifs, called LIM domain (Figure 7) [179]. The proline-rich N-terminal domain has been proven to interact with distinct proteins of the Ena/VASP family such as VASP or ENAH actin regulator (ENAH) and actin assembly proteins (e.g. α-Actinin), whereas the C-terminal LIM domain is critical for localization at focal adhesion and has a tandem zinc-finger structure that might be implicated in the regulation of mechanosensitive gene expression [180-182]. It was also shown that Zyxin can be involved in innate immunity, stabilizing cytoplasmic viral RNA sensor RIG-I and its interaction with MAVS (Mitochondrial antiviral signaling protein) leading to IFN-β release in cellular models [183]. The role of Zyxin in migration and invasion by promoting cancer was supported by its overexpression in human colorectal cancer samples and definition as a novel prognostic marker [184, 185]. Zyxin has been identified as an oncogene in colorectal cancer as well as several other cancer entities, such as hepatocellular carcinoma, breast, ovarian cancer and non-Hodgkin lymphoma, while demonstrating tumor suppressor activity in gastric, prostate, bladder and testicular cancer [186]. The first connection of Zyxin to IBD was in a recent single cell RNA sequencing analysis of peripheral blood cells, in which it was identified along with Ras homolog family member (*RHOB*) and Cathepsin D (*CTSD*) to be highly expressed in UC patients monocytes, T cells, B cells, NK cells and granulocyte-monocyte progenitors [187].

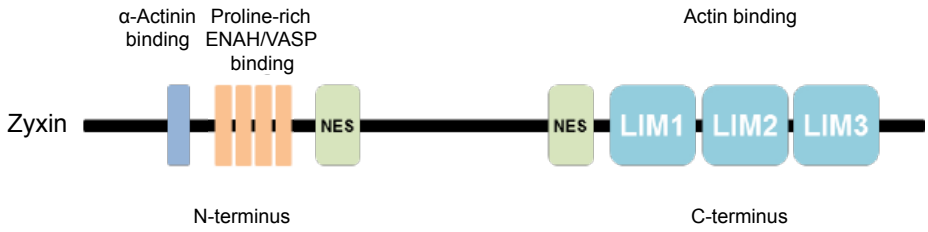

Figure 7 Domain structure of Zyxin, a member of the LIM protein family.
Schematic N-terminus of Zyxin contains a domain for α-Actinin binding and four prolin-rich repeats. In the middle are two nuclear export signals (NES) located as well as three C-terminal LIM domains for Actin binding. Modified from Hoffman et al. and Oldenburg et al. [188, 189].

1.4. MD2 and TLR4 signaling

Innate immunity and Toll-like receptor 4 (TLR4) are indispensible for pattern recognition and first line defense, initiating pro-inflammatory cascades responding to bacterial compounds [190]. LPS consists of outer membrane components of gram-negative bacteria such as *E. coli* or *Salmonella* and is the agonist for the membrane-bound TLR4 [191]. Myeloid differentiation 2 (MD2), encoded by gene *LY96,* was discovered to associate extracellularly with TLR4, and is crucial for its responsiveness to LPS, along with the accessory protein of Cluster of differentiation 14 (CD14) [192]. Both TLR4-MD2 and TLR2-MD2 can respond to LPS and lipoteichoic acid, exclusively to gram-positive bacteria and peptidoglycan [193]. Expression levels of *TLR2* and *TLR4* in human peripheral blood mononuclear cells (PBMCs) are highest in monocytes, and moderately present in B cells; while *TLR4* expression is very low in other subtypes such as pDCs, NK cells, and T cells [194].

MD2-deficient mice are hyporesponsive to LPS, identical to $TLR4^{-/-}$ mice, which has also been confirmed in humans with *TLR4* mutations [195, 196]. Overall, aberrant activation of TLR4-MD2 signaling is associated with the worsening of inflammation in epithelial cancers like ovarian, breast cancer or prostate cancer [197-199]. TLR4 and MD2 are overexpressed in colorectal cancer samples and soluble complexes of sTLR4-MD2 were shown to successfully inhibit colorectal cancer progression in mice, by competing LPS binding with membrane-bound TLR4 [200]. While IBD patients have an up to 60 % higher risk for colorectal cancer development, it was shown that TLR4 activation promotes colitis-associated tumor genesis by synergistically inducing *miR-155* expression [201, 202]. Human monocytes were recently found displaying an alternative inflammasome pathway, via TLR4-TRIF-RIPK1-FADD-CASP8 upstream of NLRP3, enabling IL-1β secretion without pyroptosis [203]. Highlighting MD2's role in inflammation, it was demonstrated in alveolar macrophages that MD2 regulates LPS-induced NLRP3 inflammasome activation and IL-1β secretion via Myeloid differentiation primary response 88 (MYD88)-/ nuclear factor-κB (NF-κB)-dependent pathway [204].

TLR4 signaling is facilitated by several extra- and intracellular components. The interaction of these key molecules leads to pro-inflammatory cytokine production such as TNF, IL-1β, IL-6, IL-8 or IFN-β [205]. LPS micelles from bacteria are recognized in serum by the LPS-binding protein and transferred to CD14, which breaks down micelles to monomers, and presents them to TLR4-MD2 [206, 207]. CD14 can then be soluble (sCD14) or anchored to the surface by glycosylphosphatidylinositol, referred as membrane-bound CD14 (mCD14) [208]. MD2 is stable associated in a complex with TLR4 and essential for functional downstream signaling (Figure 8). Upon LPS binding, TLR4-MD2 complexes oligomerize and undergo conformational change, resulting in an interaction of their extracellular Leucine-rich repeat domain (LRR) and intracellular Toll-interleukin-1 receptor (TIR) domains. This activates the MYD88 pathway, through TIR domain containing adaptor protein (TIRAP) [209]. MYD88 signaling is transmitted to IL-1 receptor kinases (IRAKs), while further components like TNF receptor associated factor 6 (TRAF6) are recruited. This cascade induces the transcription factors, Activator protein 1 (AP1) and NF-κB, as well as Mitogen-activated protein kinases (MAPK), leading to pro-inflammatory cytokine production of TNF and IL-6 [210]. While NF-κB signaling can additionally induce IL-1β, IL-18 and NLRP3 inflammasome formation [211].

mCD14 can also facilitate LPS binding to the TLR4-MD2 complex, leading to endocytosis of the TLR4-MD2 complex and activation of a second pathway, mutually exclusive and independent of MYD88 [212]. This pathway is less inflammatory, while the TIR domain of TLR4 uses TRAM (Toll/IL-1R domain-containing adaptor-inducing IFN-β-related adaptor molecule) to recruit TRIF (TIR domain-containing adaptor inducing IFN-β) inducing a downstream signaling cascade leading to type I interferon production (e.g. IFN-β) and subsequently to activation of IFN-inducible genes as C-X-C motif chemokine ligand 10 (*CXCL10*), C-C motif chemokine ligand 2 and 5 (*CCL2, CCL5*) [213-216].

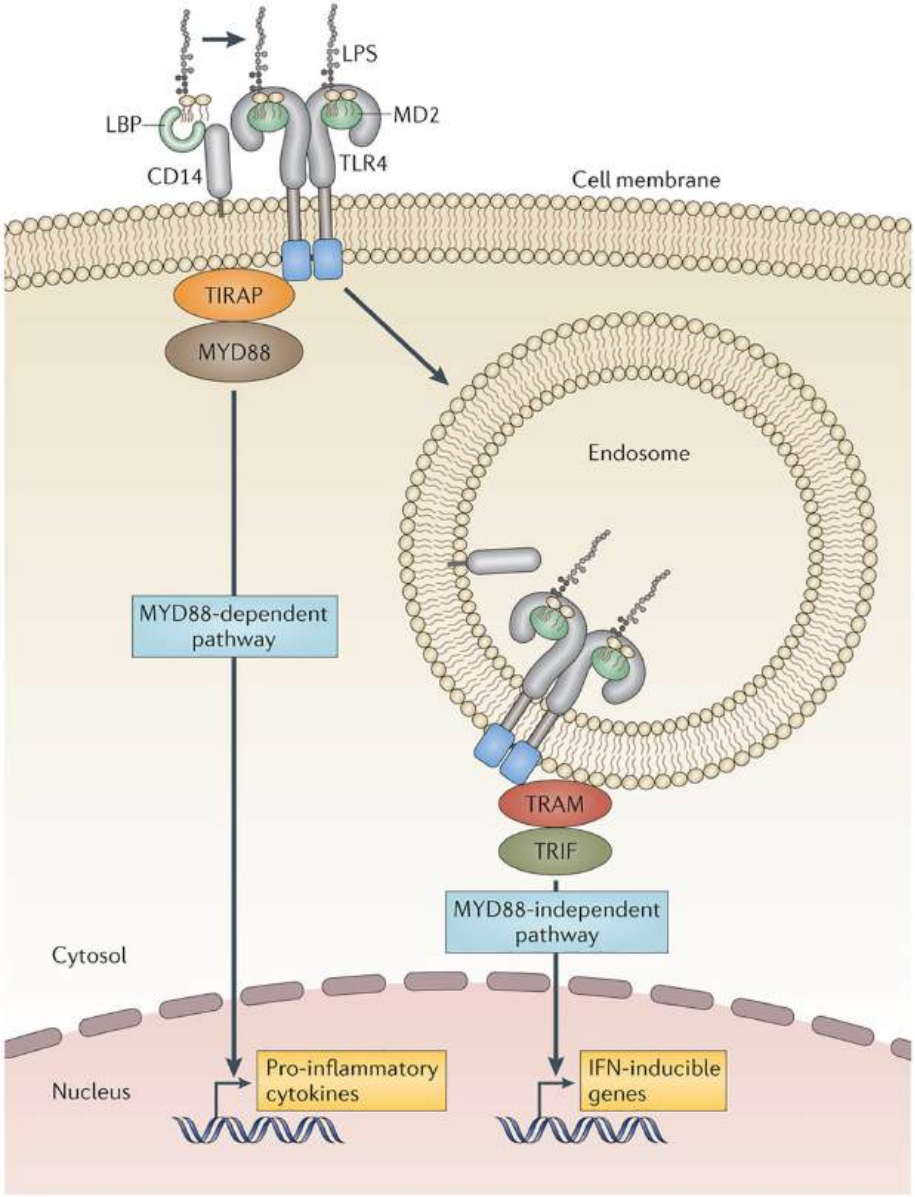

Figure 8 TLR4-MD2 signaling pathway upon LPS stimulation.
TLR4 is a membrane-bound receptor, which is associated with the accessory protein MD2 and activated by LPS. LPS binding protein (LBP) facilitates the display of LPS to TLR4-MD2, by the help of mCD14. Upon LPS binding, TLR4-MD2 oligomerizes, undergoes conformational change, recruits downstream adaptors of the Myeloid differentiation primary response 88 (MYD88) pathway and induces Nuclear factor-κB (NF-κB), Mitogen-activated protein kinases (MAPK) and Activator protein 1 (AP1), subsequently inducing pro-inflammatory cytokines like TNF, IL-1β, IL-6 or IL-8. Independent of MYD88, mCD14 facilitates LPS binding to the TLR4-MD2 complex, leading to its endocytosis and activation of a less inflammatory pathway via TRAM (Toll/IL-1R domain-containing adaptor-inducing IFN-β-related adaptor molecule) and TRIF (TIR domain-containing adaptor inducing IFN-β). TRAM/TRIF activation leads to type I interferon production, like IFN-β and activation of IFN-inducible genes as C-X-C motif chemokine ligand 10 (*CXCL10*), C-C motif chemokine ligand 2 and 5 (*CCL2, CCL5*). Modified from Needham and Trent [217].

2. Objectives and aims of the PhD thesis

Inflammatory bowel disease is a complex and multifactorial disease. Patients, suffering from VEO-IBD often present with a more severe, complex and progressive disease course. Consequently, conventional therapies often remain unsuccessful in VEO-IBD patients and underlying mechanisms are an important topic of current research to improve patients' disease burden and their clinical disease management. Since genomic susceptibility plays a pivotal role in VEO-IBD, we identified biallelic variants, affecting either *ZYX* or *LY96*, following both an autosomal recessive mendelian inheritance pattern, although *LY96* shows an incomplete penetrance of the VEO-IBD phenotype.

With this PhD thesis work, we validate the functional relevance of the identified variants and to shed light on potential mechanisms.

Specific aims of the study:

1) Zyxin
   a. Functional validation of *ZYX* variants in genetically engineered HCT116 cells by studying the i) proliferative capacity ii) cellular distribution, iii) colocalization with interacting proteins, and iiii) association with the actin skeleton.
   b. Investigation of ZYX deficiency in i) stable monolayer of HCT116 cells, ii) type I IFN responses, iii) inflammasome activation in BLaER1 and iPSC-derived macrophages.

2) MD2
   a. Analysis of a biallelic mutation in patient-derived monocytes for i) protein expression, ii) inflammasome activation, and iii) pro-inflammatory cytokine secretion.
   b. Assessment of genetically engineered iPSC-derived macrophages with KO or expression of the patient mutation regarding i) TLR4 responsiveness in signal transduction, ii) inflammasome activation, iii) pro-inflammatory cytokine production, and iiii) M1/M2 macrophage polarization.

3. Materials and methods

3.1. Materials

Table 1 List of all materials.

Material	Supplier	Catalogue number
General materials, media and supplements		
15 mL Falcon tubes	Sarstedt	62.554.502
50 mL Falcon tubes	Sarstedt	62.547.254
SafeSeal 1.5mL tube	Sarstedt	72.706
Serological pipette 2 mL	Sarstedt	861.252.025
Serological pipette 5 mL	Sarstedt	861.253.001
Serological pipette 10 mL	Sarstedt	861.254.001
Serological pipette 25 mL	Sarstedt	861.685.001
6-well plates	Sarstedt	833.920.005
12-well plates	Sarstedt	83,3921
24-well plates	Sarstedt	833.922.005
48-well plates	Sarstedt	833.923.005
96-well plates, flat bottom	Sarstedt	833.924.005
Nunc MaxiSorp™ flat bottom	ThermoFisher	44-2404-21
T-25 Cell culture flask 25 cm^2, filter cap	Sarstedt	833.911.002
T-75 Cell culture flask 75 cm^2, filter cap	Sarstedt	833.911.502
T-175 Cell culture flask 175 cm^2, filter cap	Sarstedt	833.912.002
25 culture-inserts for self-insertion	Ibidi	80209
Advanced DMEM/F12	ThermoFisher	12634
Bambanker freezing medium	Niippon Genetics	BB01
CellClip for cellspin cellclip rotor	Tharmac	302-1
Cellfunnel, reusable	Tharmac	304-12
Cellspin filtercards	Tharmac	305-200
Corning® Costar® transwell® permeable supports	ThermoFisher	10147291
Corning® Costar® transwell® cell culture inserts, diam. 6.5 mm, pore size 8.0 µm	Sigma Aldrich	CLS3464
Cryo tubes 2 mL	Greiner Bio-One	121263
DMEM	ThermoFisher	11960085
Essential 6 medium	ThermoFisher	A1516401
FACS tubes	Corning	352008
Filter FACS tubes	Corning	352235
mTeSR plus	StemCell	5825
Neubauer counting chamber	Marienfeld	640110
RPMI 1640 medium	ThermoFisher	61870036
StemPro-34 SFM	ThermoFisher	10639011
Accutase cell detachment solution	Sigma Aldrich	SCR005
Brilliant stain buffer	BD Biosciences	563794
Cell lysis buffer (10x)	Cell Signaling	9803S

	Technology	
Collagenase type IV (1 mg/mL)	StemCell	7909
Corning® Matrigel® for cultivation	Corning	356231
Corning® Matrigel® for differentiation	Corning	354234
FBS	ThermoFisher	10270106
Ficoll® paque plus	Merck Millipore	GE17-1440-03
Gentamycin	ThermoFisher	15750060
HEK-Blue™ detection	InvivoGen	hb-det3
HEPES (1M)	ThermoFisher	15630-056
L-Glutamine (200 mM)	ThermoFisher	25030123
Lipofectamine 3000 transfection reagent	Invitrogen	L3000001
PBS	ThermoFisher	14190-094
PEI	Polysciences	23966
Penicillin-streptomycin (5,000 U/mL)	ThermoFisher	15070-063
PIC	Sigma Aldrich	P8340
PlasmoTest™ - mycoplasma detection kit	InvivoGen	rep-pt1
PMSF	Alpha Diagnostic Intl	PMSF16-S-50
Sodium pyruvate	ThermoFisher	2026H-001
Trypan blue solution, 0.4 %	ThermoFisher	15250061
Trypsine-EDTA solution	Merck Millipore	T3924-100ML
Cytokines/reagents		
β-estradiol	Sigma Aldrich	E8875
CHIR9902 (25 mM)	Merck Millipore	361571
LPS O26:B6 from *E.coli*	Sigma Aldrich	L2654-1MG
Polyinosinic:polycytidylic acid	Sigma Aldrich	P9582
Recombinant human BMP4	Peprotech	120-05
Recombinant human FGF-basic	Peprotech	100-18B
Recombinant human Flt3-Ligand	Peprotech	300-19
Recombinant human GM-CSF	Peprotech	315-03
Recombinant human IFN-γ	Peprotech	300-02
Recombinant human IL-10	Peprotech	200-10B
Recombinant human IL-3	Peprotech	200-03
Recombinant human IL-4	Peprotech	200-04
Recombinant human M-CSF	Peprotech	300-25
Recombinant human SCF	Peprotech	300-07
Recombinant human TGF-β	Peprotech	100-21
Recombinant human TPO	Peprotech	300-18
Recombinant human VEGF	Peprotech	100-20
SB431542	Selleckchem	S1067
SCR7	StemCell	74102
Y-27632	Biotrend	Y-5301-10 mg

Genetic engineering and RNA analysis		
6x loading dye	ThermoFisher	R0611
5-alpha competent *E. coli* (subcloning efficiency)	New England BioLabs GmbH	C2988J
Alt-R™CRISPR/Cas9 system (sgRNAs, tracrRNA Cas9 nuclease)	IDT	/
dNTP mix 10 mM	Biozym	331520
Ethidium bromide solution 1 %	AppliChem GmbH	A1152,0010
ExoSAP-IT™	ThermoFisher	78200.200
FastAP thermosensitive alkaline phosphatase (1 U/µL)	ThermoFisher	EF0651
FastDigest *AgeI* (*BshTI*)	ThermoFisher	FD1464
FastDigest *BamHI*	ThermoFisher	FD0054
FastDigest *BpiI* (*BbsI*)	ThermoFisher	FD1014
FastDigest Buffer(10x)	ThermoFisher	supplement of enzymes
FastDigest *SalI*	ThermoFisher	FD0644
FastDigest *SpeI* (*BcuI*)	ThermoFisher	FD1254
High range DNA ladder	JenaBioscience	M-204L
Illustra™ ExoProStar™	Sigma Aldrich	GEUS78211
Mid range DNA ladder	Jena Bioscience	M-203L
MuLV reverse transcriptase	NEB	M0253S
Oligo(dT)18 primer	ThermoFisher	SO132
One*Taq* polymerase	NEB	M0482L
pGEM®-T easy vector systems	Promega	A1360
Powrup SYBR mastermix 10x5 mL	ThermoFisher	A25778
Primers	Eurofins Genomics	/
pSpCas9(BB)-2A-GFP (PX458)	Addgene	48138
PureLink™ DNase set	ThermoFisher	12185010
PureLink™ RNA mini kits	ThermoFisher	12183020
Q5® High-fidelity DNA polymerase	NEB	M0491L
RiboLock RNase inhibitor (40 U/µL)	ThermoFisher	EO0382
Rnase-free DNase set (50)	Qiagen	79254
T4 DNA ligase	ThermoFisher	EL0011
T4 DNA ligase buffer (10x)	ThermoFisher	EL0011
T4 polynucleotide kinase	NEB	M0201S

Kits		
CD14 microbeads human	Miltenyi Biotec GmbH	130050201
Cell line nucleofactor kit V	Lonza	VCA-1003
EasySep™ human CD14 positive selection kit II	Stemcell Technologies	17858
High-capacity cDNA reverse transcription kit	ThermoFisher	4368813
Human stem cell nucleofector kit 2	Lonza	VPH-5022
QIAGEN plasmid plus maxi kit (100)	Qiagen	12965
QIAmp DNA blood mini kit	Qiagen	61104
QIAquick gel extraction kit (250)	Qiagen	28706
RNEasy plus mini kit (250)	Qiagen	74136
Zyppy plasmid mini prep kit	Zymo Research	D4020
Immunoblotting		
12 % Criterion TGX stain-free gel26W 15 µL	BioRad	5678045
PageRuler prestained protein ladder, 10 to 180 kDa	ThermoFisher	26616
Restore western blot stripping buffer	ThermoFisher	21059
SuperSignal west dura extended duration substrate	ThermoFisher	34076
Whatman® gel blotting paper	Merck	WHA10426892
Roti nanoquant 5x	Millipore	101424
Amersham hybond P 0.45 PVDF	Merck Millipore	GE10600023
Immunoblotting supply		
Criterion cell and single-row any gel Stand	BioRad	1656020
Mini-PROTEAN® tetra vertical electrophoresis cell for mini precast gels	BioRad	1658005
PowerPac™ basic power supply	BioRad	1645050
Trans-Blot® Turbo™ transfer system	BioRad	1704150EDU
ELISA		
eBioscience™ TMB solution (1x)	ThermoFisher	00-4201-56
Human TNF ELISA set	BD Biosciences	555212
Human IL-1 beta/IL-1F2 DuoSet ELISA	R&D/ biotechne	DY201
Microscopy		
Coverslips, round, Stärke 1, CE, 12 mm	Hecht	41001112
Cytoslides slide, coated, a circle	Tharmac	JC311
Fluorescence mounting medium	Dako	S3023
Giemsa's azur eosin methylene blue solution	Merck Millipore	109204
May-Grünwald's eosine-methylene blue solution modified	Merck Millipore	101424

Microscope slides	Marienfeld	1000200
Paraformaldehyde solution 4 % in PBS	Santa Cruz Biotechnology	sc-281692
Other chemicals		
Agarose basic	AppliChem	A8963
Acryl-bisacrylamide	Carl Roth	A121.1
Ammonium chloride	Sigma Aldrich	A9434-500G
Ammonium persulfate	Serva	13375.02
Bovine serum albumine	AppliChem	A6588,0100
Bromphenolblue	Carl Roth	A512.1
Crystal violet	Carl Roth	T123.1
Ethanol absolut ≥99.5%	VWR	83813-440
Ethidium bromide	AppliChem	A1152
Glycerol	Carl Roth	3783.1
Glycine	Carl Roth	3908.3
Methanol	Carl Roth	T909.1
Milk powder	Carl Roth	T145.3
Saponin	Sigma Aldrich	SAE0073
SDS	Carl Roth	183.1
SDS (20%)	Carl Roth	1057.1
TEMED	Carl Roth	2367.3
Tris	Carl Roth	5429.2
Tween® 20	AppliChem	142312.1611

Table 2 List of all devices.

Devices	Software	Supplier	Catalogue number
autoMACS	none	Milteny Biotec	/
AxioVert 40C microscope	Axio Vision software	Zeiss	/
BD FACSAria II cell sorter	BD FACSDiva™ software, FlowJo v10 software	BD Biosciences	/
BD LSRFortessa	BD FACSDiva™ software, FlowJo v10 software	BD Biosciences	/
Cellspin I	none	Tharmac	/
ChemiDoc XRS+ system	Image lab software	BioRad	1708265
Confocal microscope LSM 800	Zen blue software	Zeiss	/
EasyEights™ EasySep™ magnet	none	Stemcell Technologies	18103
Epithelial Volt/Ohmmeter	none	World Precision Instruments Inc.	EVOM2
Eppendorf thermomixer R	none	Eppendorf	5355
Gel Doc XR+	Image lab software	BioRad	/
NanoDrop 2000	Operating software, v1.6	ThermoFisher	/
NucleofectorTM 2b device	none	Lonza	AAB-1001
PeqSTAR 96X universal gradient	none	VWR	732-2887
StepOne™ real-time PCR system	ABI StepOne plus Real-time PCR software	ThermoFisher	4376357
Synergy H1 hybrid reader	Gen5.11 software	BioTek	/
General computer software	AmplifX software		1.7.0.-2.1.0.
	ApE sofware		2.0.47-3.0.8
	GraphPad PRISM	Dotmatics	v.6.0.
	Microsoft Office	Microsoft	diverse

3.2. Cell culture methods

3.2.1. Cell lines and conditions

Table 3 Cell lines.

Cell lines	Cell type	Supplier
Human HEK 293T	Embryonic kidney cell line	DSMZ, Germany
Human HCT116 (ATCC® CCL-247™)	Colorectal carcinoma cell line, male	ATCC
Human BLaER1	Human B-cell precursor leukemia cell line	Gift of Prof. Dr. Veit Hornung [203]
Human iPSCs	Reprogrammed BJ fibroblast (ATCC #CRL-2522) to iPSCs (HMGU1)	Generated by Human Induced Pluripotent Stem Cell Core Facility, Helmholtz Center Munich

HEK293 T cells were maintained in DMEM with 10 % FBS, 1 % penicillin-streptomycin, 1 % L-glutamine and 1 % HEPES (DMEM complete). HCT116 cells were kept under the same conditions. Passaging of both adherent cell lines was initiated after cells were grown to 80 % confluency. Cells were washed with PBS, detached with trypsin-EDTA for 5-10 min at 37°C, flushed from flask with medium and pelleted at 1200 rpm, 5 min. Cells were resuspended in and an aliquot was stained with trypan blue, to determine single live cell numbers by neubauers counting chamber. Cells were either diluted to a determined flask volume or frozen. Dependent on confluency, cells were split every 2-3 days.

If cells were kept for long-term storage, pelleted cells were resuspended in 1 mL freezing solution, containing FBS and 10 % DMSO and transferred to cryovials. These cryopreserved cells were first stored in freezing containers, cooling down samples controlled -1 °C/min at -80 °C, while long-term storage occurred in liquid nitrogen tanks at -196 °C.

BLaER1 cells are suspension cells, which were cultured in RPMI-1640 with 10 % FBS, 1 % penicillin-streptomycin and 1 % L-glutamine (RPMI complete). For splitting, suspension cells were pelleted at 1200 rpm for 5 min, washed with PBS, pelleted again at 1200 rpm for 5 min and diluted to a desired volume and flask. Freezing for long and

short-term storage was the same as for adherent cell lines with 1 mL FBS and 10 % DMSO solution. BLaER1 cells can be trans-differentiated to monocytoid-/ macrophage-like cells, which then become adherent [203]. Trans-differentiation was induced after fresh splitting by adding 100 nM β-estradiol, 10 ng/mL M-CSF and 10 ng/mL IL-3 for 6 days, while changing media every 2 days with added supplements.
Thawing of HEK293T, HCT116 and BLaER1 cells occurred quickly after taking the cells out of liquid nitrogen tank. Cells were kept at room temperature until thawed, were resuspended in pre-warmed medium, pelleted at 1200 rpm for 5 min, and diluted in according medium to start culturing the cells in flasks.

Human iPSCs are more sensitive when handling than other cell lines and occur in smaller aggregates than in single cells. They were cultivated on a basement membrane matrix, called matrigel, which needed to be coated on cell culture dishes in advance. Matrigel was thawed on ice and diluted in DMEM/F12 1:100. 6-well plates were coated with 1 mL of this solution and incubated 1 h at 37 °C. Plates were washed with PBS and 1.5 mL pre-warmed mTeSR plus medium was added. Medium was additionally supplemented with 10 µM rho kinase inhibitor Y-27632, if cryopreserved iPSCs were thawed. Frozen iPSCs were thawed in the waterbath for 2 min, transferred to 10 mL pre-warmed DMEM/F12 and pelleted at 200 x g for 3 min at RT. The cell pellet was gently resuspended in 500 µL mTeSR plus and dropwise added to the pre-warmed 6-well plates. Gentle shaking ensured even distribution of iPSCs. The next day, media was changed to mTeSR plus medium, without Rho kinase inhibitor Y-27632. Medium was changed on a daily basis until splitting.
For passaging of iPSCs, cells were mainly cultured in 6-well plates. In advance, 6-well plates were coated with 1 mL of 1:100 matrigel dilution in DMEM/F12 and incubated 1 h at 37 °C. Plates were washed once with PBS and added up with 1.5 mL pre-warmed mTeSR plus medium. For detachment of iPSCs, cells were first washed with PBS, followed by 0.5 mL of collagenase type VI (1 mg/mL) treatment per well. Plates were incubated for 30-45 min at 37 °C. 0.5 mL mTeSR plus was added and colonies were detached by gentle pipetting (usually using 2 mL serological pipette). Cells were transferred to a 15 mL falcon tube and the procedure was repeated with 1 mL PBS for all wells of the same genotype, collected in the same falcon tube. Cells were centrifuged 200 x g RT for 3 min, resuspended gently in the desired dilution of pre-warmed mTeSR

plus medium, e.g. in 3 mL for a ratio of 1:6, by adding 500 µL to each well of the prepared matrigel-covered plate with mTeSR plus medium.
For cryopreservation of iPSCs, colonies were treated as described for passaging iPSCs. Cells were resuspended after centrifugation in 1 mL Bambanker, transferred to cryo tubes and directly placed in the freezer of -80 °C. Due to their sensitivity, frozen iPSCs were transferred to liquid nitrogen (-196 °C) the next day.
All cells were cultured in humidified incubators at 5 % CO_2 at 37 °C and tested weekly for *Mycoplasma* contamination by using PlasmoTest including HEK-Blue cells and HEK-Blue detection.

3.2.2. Patient samples

Patients, their regarding families and healthy donors provided a written informed consent to use their samples for research and clinical data evaluation. Patient 1 was cared for at the Hopital Bologhine in Hammamet, Alger, Algeria, Patient 2 originated from Syria and was treated in the Pediatric Immunology Unit, Ankara Children's Hematology and Oncology Education and Research Hospital, Clinic of Pediatric Hematology, Ankara, Turkey. Both independent families were analyzed for two homozygous variants of the *ZYX* gene. The index patient found for the homozygous rare variant of *LY96,* coding for MD2, was from the department of Pediatrics B at Schneider Children's Medical Center of Israel, Tel Aviv, Israel. Patient samples were sent and processed at the Dr. von Hauner Children's Hospital at Ludwig-Maximilians-Universität, Munich in Germany.

3.2.3. Isolation of human PBMCs from peripheral blood

Heparinized or EDTA-anticoagulated blood samples from healthy donors, patients and family members were processed within 24-48 h after drawing and kept at RT. Processed amounts of blood samples were mainly dependent on age, usually between 3-20 mL. Isolation of PBMCs occurred by the ficoll-paque system, separating mononuclear human cells by density gradient centrifugation at RT. 12 mL ficoll-paque solution were transferred at the bottom of a 50 mL falcon tube. Blood samples were diluted with PBS, at least 1:1 to a maximal volume of 40 mL in a separate 50 mL falcon tube. The blood-PBS mixture was slowly layered to the ficoll-paque solution and

centrifuged at RT with a swing-rotor with breaks off (acceleration 2, deceleration 0) at 1600 rpm for 25 min. The upper layer containing plasma was aspirated, while leaving a residual amount of 2 mL. The second, cloudy layer, containing the mononuclear cells of interest, was collected with a 1 mL pipette without disturbing the layering and transferred to a 50 mL falcon tube on ice. Collected mononuclear cells were washed with pre-cooled PBS and centrifuged 1200 rpm for 10 min at 4 °C. If cells were used for experiments, the pellet was resuspended in RPMI-1640 (with 10 % FBS, 1 % penicillin-streptomycin, with or without 1 % L-glutamine), aliquots were stained with trypan blue, live cell number was determined by neubauer counting chamber and the according experiment was started.

If cells had to be cryopreserved for long-term storage, the pellet was resuspended in FBS and 10 % DMSO solution. Cryovials were stored in freezing containers, cooling down samples controlled -1 °C/min at -80 °C. The next day, vials were transferred to liquid nitrogen tanks at -196 °C.

3.3. Molecular biology and genetic engineering techniques

3.3.1. Whole exome sequencing (WES)

Whole exome sequencing of patient and family member samples was conducted from gDNA, isolated from blood samples by the Next-Generation Sequencing facility at the Dr. von Hauner Children's Hospital of the Ludwig-Maximilians-Universität, Munich (Germany) under supervision of Meino Rohlfs. Jacek Puchalka and Sebastian Hollizeck performed bioinformatic analyses of sequencing data. Patient variants were filtered through a self-established pipeline.

3.3.2. Polymerase chain reaction (PCR) and Sanger sequencing

Novel identified genetic signatures from WES needed to be confirmed by Sanger Sequencing. According gDNA sequences were downloaded from ensembl.org, human genome GRCh37.p13, for Zyxin (transcript ENST 00000322764.5) and MD2/LY96 (transcript ENST00000284818.2). Primer design was conducted with ApE Sofware (2.0.47-3.0.8) and AmplifX Software (1.7.0.-2.1.0.). UCSC In-Silico PCR tool was used for unique amplicon confirmation.

gDNA was isolated according to the protocol of the QIAmp DNA blood mini kit and DNA was content measured by NanoDrop. Polymerase chain reaction (PCR) was performed with the following PCR mastermix (Table 4), corresponding program (Table 5) and primers (Table 6) in the thermocycler. Annealing temperatures for PCR varied due to the different melting temperatures of primers. PCR products were either separated by agarose gel electrophoresis and recovered by QIAquick gel extraction kit (3.3.3) or treated with ExoSAP-IT. To remove residual primers and dNTPs by enzymatic hydrolysis, 2 µL ExoSAP-IT were added to 10 µL PCR product. The mixture was incubated for 30 min at 37 °C and inactivated for 15 min at 80 °C.

Purified PCR products were sent to Eurofins Genomics Germany GmbH, Ebersberg or GENEWIZ Germany GmbH, Leipzig with corresponding fw or rev primer. For genetic segregation analysis, files were analyzed by ApE Software and aligned with DNASTAR lasergene software (Seqman Pro).

Table 4 PCR mastermix.

Reagent	For 25 µL
5x Q5 polymerase buffer	5 µL
Primer forward (10 µM)	1.25 µL
Primer reverse (10 µM)	1.25 µL
dNTPs (2.5 mM)	2.5 µL
Q5 polymerase	0.5 µL
DNA	0.5-3 µL (30-80 ng)
DMSO (for GC-rich amplicons)	1.25 µL
dH_2O (nuclease-free)	Fill up to 25 µL

Table 5 PCR amplification program for gDNA for 30-45 cycles.

PCR program	Temperature °C	Time
Lid	100	hold
Initialization	95	5 min
Denaturation	98	30 sec
Annealing	Primer specific	30 sec
Elongation	72	30 sec
Final elongation	72	10 min
Store	4	infinite

Table 6 List of primers for Sanger sequencing.

Primers	Primer sequence 5'-3'
ZYX P1 fw	GAGTGGGGGTCACCAAGG
ZYX P1 rev	GTGCAGCTCCCGTTACACTT
ZYX P2 fw	CAGAATGTGGCTGTCAACG
ZYX P2 rev	AGCATGCGGTCAGTGATG
MD2 P1 fw	GCATATTAGCACTAGCTTGTTCATCG
MD2 P1 rev	ACCGCGTCTCTTCCAAAAGTACAAAACATTAGC

3.3.3. Agarose gel electrophoresis and DNA purification

PCR products, restriction enzyme digested vector backbones and PCR products were separated via agarose gel electrophoresis on a 1-3 % agarose gel (dependent on fragment size), supplemented with 1:10000 ethidium bromide solution (1 %). Gel was prepared with Tris buffered saline (TBS) solution (6.05 g Tris, 8.76 g NaCl filled up to 1 L with H2O and pH adjusted 7.5). Samples were mixed with 6x loading dye and loaded onto the gel together with 5 µL of mid-range (100 bp-3000 bp) or high range (500 bp-

10000 bp) DNA ladder. Gels were run at 100 V for 45 min. Agarose gels were imaged under UV light by Gel Doc XR+ with image lab software. DNA bands of interest were cut out, collected in 1.5 mL Eppendorf tubes and purified according to manufacturer's protocol of QIAquick gel extraction kit. Purified DNA was eluted in 8-30 µL nuclease free dH_2O.

3.3.4. RNA extraction and cDNA synthesis

To capture protein transcription profiles, RNA was isolated as described in the manufacturer's protocol of the RNEasy plus mini kit. RLT Plus buffer had to be substituted with 10 % ß-mercaptoethanol. Samples were mixed with 70 % Ethanol after gDNA elimination on a column and additionally treated with RNase-free DNase set, before washing steps. Elution of RNA occurred in nuclease-free dH_2O substituted with ribolock (1 µL/15 µL dH_2O), twice from the column in 10-30 µL. RNA concentrations were determined by UV light absorbance with NanoDrop and purity checked by 260/280 nm and 260/230 nm ratios.

Reverse transcription of RNA to cDNA was conducted with the high-capacity cDNA reverse transcription kit. Up to 1000 ng RNA per sample was reverse transcribed. Per sample, 2 µL buffer (10x), 5 µL dNTPs (10 mM), 1 µL oligo(dT)18 primer, 1 µL random primer, 1 µL MuLV reverse transcriptase and 50-1000 ng RNA in a total volume of 10 µL with nuclease free dH_2O and (200 U/µl) were mixed and incubated for 2 h 37 °C in the thermocycler.

3.3.5. Quantitative real-time PCR for mRNA expression

Expression patterns of cells were analyzed by quantitative real-time PCR (qPCR), using 0.5 µL fw primer, 0.5 µL rev primer, 0.5-1 µL cDNA, 5 µL Powrup SYBR mastermix and 3-3.5 µL nuclease free dH_2O per sample (Table 7). A 96-well plate was prepared with corresponding target primers in duplicates on ice, the plate was sealed with adhesive qPCR plate seals, short spun and placed in the StepOne™ teal-time PCR system.

The program started with 2 holding stages of 50 °C for 2 min and 95 °C for 2 min, entering the 40 cycles with 15 sec 95 °C and 1 min 60 °C, followed by final melting

curve acquisition from 60 °C to 95 °C in 0.3 °C steps. Comparative CT (ΔΔCT) method was used for analysis by first calculating the duplicates average. ΔCT was calculated by subtraction of housekeeping gene expression (e.g. GAPDH) from the gene of interest expression. For relative expression calculation, ΔΔCT was normalized to control or reference of the setup (e.g. untreated control) and fold change calculated by $2^{\Delta\Delta CT}$. Data were analyzed by ABI StepOne plus real-time PCR software and Excel.

Table 7 Primers for qPCR.

qPCR primers	Primer sequence 5'-3'
qZYX Ex 3-4 fw	CCCAGGGAGAAGGTGAGCAGTATTG
qZYX Ex 3-4 rev	TGGGGGCACATATCCAGATGACAC
qZYX Ex 7-8 fw	CCGTACTGCGAGGGCTGTT
qZYX Ex 7-8 rev	CAGACCACACAGGTGAAGCAGT
qZYX Ex 8-10 fw	CGACTACCACAAGCAGTACG
qZYX Ex 8-10 fw	TCATCTGCCTCAATCGACAG
qIL1B fw	GAAGCAGCCATGGCAGAAGTA
qIL1B rev	TCCTGGAAGGAGCACTTCATCT
qIL6 fw	TCCACAAGCGCCTTCGGTC
qIL6 fw	GTGAGTGGCTGTCTGTGTGG
qIFNB fw	CATTACCTGAAGGCCAAGGAGT
qIFNB rev	CACAGGCTAGGAGATCTTCAGTTTCGGA
qCXCL8 fw	CACTGCGCCAACACAGAAAT
qCXCL8 rev	TTCTCAGCCCTCTTCAAAAACTTC
qCXCL10 fw	TGCTTCCAAGGATGGACCACACAGA
qCXCL10 rev	ACCTTCCTACAGGAGTAGTAGCAGC
qTNF fw	GCTGCACTTTGGAGTGATCG
qTNF rev	GGGTTTGCTACAACATGGGC
qGAPDH fw	TGCTGGGGAGTCCCTGCCACA
qGAPDH rev	GGTACATGACAAGGTGCGGCTC

3.3.6. Cloning and overexpression vectors for *ZYX*

To obtain overexpression vectors for patient variants and genes of interest in cell models, plasmid backbones were used, which were formerly sequenced (Table 8). Template for genomic amplification of *ZYX* was a verified cDNA clone. P1 is stated as c.188 variant, P2 as c.1258 variant.

ZYX overexpression plasmids, with either a C-terminal tagged GFP or a construct with an *IRES* element, co-expressing a *RFP* reporter were cloned.

Table 8 Backbones for cloning.

Backbone (plasmid)	Restriction sites	Marker, resistance	Provided by
pRRL-RASGRP-IRES-GFP	*BamHI, SalI*	GFP, ampicilin	Benjamin Marquardt, Dr. von Hauner Children's Hospital of the Ludwig-Maximilians-Universität, Munich (Germany)
pRRL-IL3RAwt-IRES-RFP	*AgeI, SpeI*	RFP, ampicilin	Lina Wendeler, Dr. von Hauner Children's Hospital of the Ludwig-Maximilians-Universität, Munich (Germany)
pGEM-T Easy Vector	Several and introduced by PCR product	*lacZ*, ampicilin	Promega

To amplify specific parts of *ZYX* by PCR, several primers were designed (Table 9).

Table 9 Primers used for *ZYX* constructs.

Primers	Primer sequence 5'-3'
BamHI AgeI ZYX fw	ACTTGCGGATCCACCGGTGCCACCATGGCGGCCCCCCG
ZYX c188 fw	GGGTGGGCGAGAGTCCC
ZYX c188 rev	GGGACTCTCGCCCACCC
ZYX c1258 fw	AGCAGCTCAAGGGCCAGCAGT
ZYX c1258 rev	ACTGCTGGCCCTTGAGCTGC
ZYX-GFP fw	TGCTAGAGCCCAGACCGTGAGCAAGGGCGAGGAGCT
ZYX-GFP rev	AGCTCCTCGCCCTTGCTCACGGTCTGGGCTCTAGCA
GFP SalI rev	GTCGACGTCGACTTACTTGTACAGC
AgeI ZYX fw	ACCGGTACCGGTGCCACCATGGCGGCCCCCCGC
SpeI ZYX rev	ACTAGTACTAGTTCAGGTCTGGGCTCTA

Due to the size of the *ZYX* fusion construct and introduction of the patient specific variants (c.188, c.1258), PCRs were conducted for several parts each (Figure 9). Single parts were amplified by an overlap PCR by adding both cleaned up PCR products and flanking primers. This was repeated after the full *ZYX* (WT c.188, c.1258) PCR product was obtained, adding the C-terminal GFP part at final amplification step. All PCRs were

run with Q5 polymerase with corresponding mastermix (Table 4) and program (Table 5). Elongation time was adapted to product size, calculating 1 min per 1000 bp (Table 10). PCR products were separated by agarose gel electrophoresis and recovered by QIAquick gel extraction kit (3.3.11).

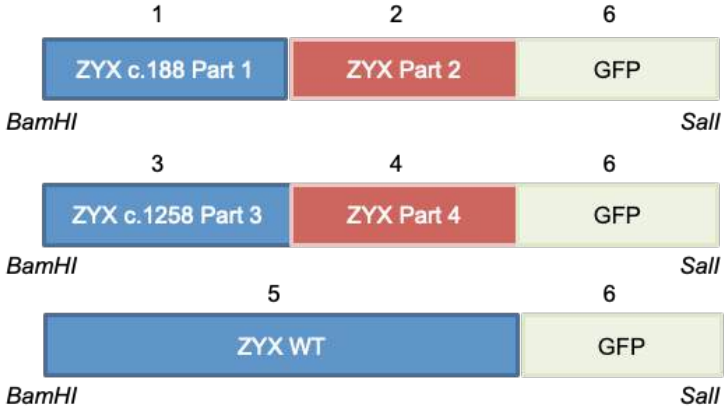

Figure 9 Overview of *ZYX* fusion constructs.
From top to bottom: ZYX c.188, ZYX c.1258, ZYX WT with flanking restriction sites 5' *BamHI*, 3' *SalI*

Table 10 Amplicons for *ZYX WT, c.188* and *c.1258* constructs.

Part	Primer pairs	Template	Size in bp
1	BamHI AgeI ZYX fw and ZYX c188 rev	ZYX cDNA clone	216
2	ZYX c188 fw and ZYX-GFP rev	ZYX cDNA clone	1561
3	BamHI AgeI ZYX fw and ZYX c1258 rev	ZYX cDNA clone	1294
4	ZYX c1258 fw and ZYX-GFP rev	ZYX cDNA clone	487
5	BamHI AgeI ZYX fw and ZYX-GFP rev	ZYX cDNA clone	1760
6	ZYX-GFP fw and GFP SalI rev	pRRL-RASGRP-IRES-GFP	745
1+2	BamHI AgeI ZYX fw and ZYX-GFP rev	PCR product 1 and 2	1760
3+4	BamHI AgeI ZYX fw and ZYX-GFP rev	PCR product 3 and 4	1760
1/2+6	BamHI AgeI ZYX fw and GFP SalI rev	PCR product 1/2 and 6	2496
3/4+6	BamHI AgeI ZYX fw and GFP SalI rev	PCR product 3/4 and 6	2496
5+6	BamHI AgeI ZYX fw and GFP SalI rev	PCR product 5 and 6	2496

For pGEM-T system subcloning, a 3' poly-adenosine overhang was added by using 11 µL PCR product, 2 µL PCR *Taq* polymerase buffer (10x), 0.5 µL dNTPs (2.5 mM) and 0.1 µL *Taq* polymerase (250 U), incubated for 10 min at 72 °C. PCR products were ligated with T4 DNA ligase (3.3.8) and transformed to 5-alpha competent *E. coli* (3.3.9). Positive clones were confirmed by colony PCR (3.3.10) and Sanger sequencing (3.3.2).

3.3.7. Restriction enzyme treatment

Plasmids and PCR products were incubated with restriction enzymes (1 U/µL) for 1 h, 37 °C in a thermocycler with corresponding buffer according to manufacturer's instructions. For pRRL-vectors, pGEM-T vectors and *pRRL-RASGRP-IRES-GFP* were digested with restriction enzymes (1 U/µL) for 1 h, 37 °C *BamHI* and *SalI*, separated by DNA gel electrophoresis (see 3.3.11) and recovered by QIAquick gel extraction kit. Finally, they were ligated to pRRL-ZYX WT-GFP, pRRL-ZYX c.188-GFP, pRRL-ZYX c.1258-GFP constructs (3.3.8). IRES-RFP constructs were obtained by digesting pRRL-IL3RAwt-IRES-RFP with *AgeI* and *SpeI.* ZYX variants were amplified by *AgeI* ZYX fw and *SpeI* rev primers from pGEM-T subclones and digested with *AgeI* and *SpeI* as well. Vector backbone and ZYX constructs were cleaned by DNA gel electrophoresis (3.3.11) and recovered by QIAquick gel extraction kit. Finally, the constructs were ligated to pRRL-ZYX WT-IRES-RFP, pRRL-ZYX c.188-IRES-RFP, pRRL-ZYX c.1258-IRES-RFP (3.3.8).

3.3.8. Ligation

The ligation mix was prepared with a vector to insert ratio 1:6, adding 1 µL T4 DNA ligase (5 U/µL), 1 µL T4 DNA ligase buffer (10x), filled up with dH_2O to a total volume of 10 µL. Ligation mixture was stored at 4 °C for 12-15 h and used for transformation.

3.3.9. Transformation

For the amplification of cloned plasmids, 5-alpha competent *E. coli* were used for transformation. Competent cells were thawed on ice, 25 µL cells were used per 5-10 µL ligation solution or plasmid. The cell-ligation mix was incubated 30 min on ice, heat shocked at 42 °C for 40 sec in a thermomixer and kept 1 min on ice. 250 µL pre-warmed LB medium without antibiotics was added to the sample and incubated, shaking at 350 rpm at 37 °C. The tubes were centrifuged for 1 min at 5000 rpm, resuspended in 80 µL LB medium and plated with spatula on LB-Agar plates with ampicillin (50 µg/mL) and incubated at 37 °C overnight.
jshdhd

3.3.10. Colony PCR

To confirm successful cloning of plasmids, either in *pGEM-T* or *pRRL* vectors, 10-30 colonies per genotype were picked from LB-Agar plates and diluted in 10 µL nuclease free dH_2O. 5 µL were used for colony PCR, 5 µL were used for setting up a plasmid mini prep in LB medium with ampicillin for positive selection (3.3.11). The total volume per PCR was 15 µL, adapted to the mastermix (Table 4) with corresponding primers and program (Table 5). The elongation time was adapted to the expected size. For pRRL-ZYX WT-GFP, pRRL-ZYX c.188-GFP, pRRL-ZYX c.1258-GFP primers BamHI AgeI ZYX fw and GFP SalI rev were used. For pRRL- ZYX WT-IRES-RFP, pRRL-ZYX c.188-IRES-RFP, pRRL-ZYX c.1258-IRES-RFP constructs, primers AgeI ZYX fw and SpeI ZYX rev were used.

3.3.11. Plasmid DNA extraction from *E.coli* (mini prep, maxi prep)

Plasmid DNA was extracted, dependent on cultivated volume of LB medium with ampicillin containing transformed *E.coli*. Mini prep was conducted as stated in the plasmid mini prep kit protocol, using up to 5 mL cultivated medium. Maxi prep was conducted in accordance with the manufacturer's protocol, using 100 mL cultivated medium. Plasmid DNA was eluted twice from the column with either 30-50 µL nuclease free dH_2O for mini preps or 100-300 µL nuclease free dH_2O for maxi preps. Nucleic acid concentrations were determined by UV light absorbance with NanoDrop and purity checked by 260/280 nm and 260/230 nm ratios.

3.3.12. Lentivirus production

The generation of stable cell lines, overexpressing transgenic ZYX was established with a lentiviral system. Helper plasmids were needed, one encoded the lentiviral envelope, the Vesicular stomatitis virus-G Protein (*ENV*), one plasmid encoded the Gag-Pol polyprotein, containing virion proteins and enzymes (*GAG/POL*), one helper plasmid carried an RNA-splicing regulator (*REV*) and the *pRRL*-derived transfer vector of interest.

HEK293T cells were seeded to 60-70 % confluency in 10 cm cell culture dishes, one day before. Medium was aspirated and replaced with fresh medium, 1-2 h before

before transfection. The 1 mL mix, sufficient for two cell culture dishes, was prepared at RT in medium without supplements (DMEM plain) using 30 µg plasmid DNA (pRRL-), 6 µg REV, 10 µg GAG/POL, 6 µg ENV and mixed gently. 100 µl PEI (1 µg/µL) were added to the plasmid-medium mix, inverted, and set for assembly for 30 min at RT. 500 µL of the mix were added dropwise to the cell culture dish, swirled gently and incubated at 37 °C. Medium was changed with 12 mL fresh medium, 12 h after transfection. Medium was left 2-3 days and supernatants were collected, filtered through 0.45 µm filter and ultra-centrifuged at 22,000 rpm, for 2.5 h at 4 °C. Virus particle pellet was resuspended in 200-400 µL RPMI-1640 medium without supplements, aliquoted to 50 µL each vial and kept in -80 °C or used directly for transduction.

3.4. Genetic engineering of cells

3.4.1. Transduction to HCT116 or BLaER1 cells

Freshly split cells in low passage were used for transduction. Around 30,000-50,000 cells were resuspended in 100 µL medium (HCT116 in DMEM completely supplemented, BLaER1 cells in RPMI-1640 completely supplemented) and added to the thawed virus vial, kept for 30-60 min at 37 °C in the waterbath. Dependent on cell count and cell type, 24- or 48-well plates were prefilled with supplemented medium, and cells were gently transferred to plates. Medium was changed after 12- 16 h, and transduction efficiency determined by fluorescence microscopy and flow cytometry analysis (3.5.3). Transfection controls expressing selection markers (pRRL-GFP, pRRL-IRES-RFP) were always included.

3.4.2. Transfection of cells

For transient protein expression, cells were transfected with a 1:2 ratio of DNA/PEI mix in water or plain medium, using between 5-50 µg DNA and double the amount of PEI (1 µg/mL). DNA/PEI were mixed gently and assembled for 20 min at RT, added dropwise to the cells and incubated for 16 h. The medium was changed, and protein of interest expression was verified 24-48 h later.

3.4.3. CRISPR-Cas9 mediated knockout in HCT116, BLaER1 cells and iPSCs

Zyxin

Genetic engineering of *ZYX* KO in HCT116 cells, BLaER1 cells and iPSCs was generated by the Alt-R CRISPR-Cas9 system from IDT. Single guide RNAs were designed at the former website of Feng Zhang (http://crispr.mit.edu) or Benchling (https://www.benchling.com/crispr/), suggesting sgRNAs with the lowest off-target effects on the genome. sgRNAs were designed to disrupt the *ZYX* gene at Exon 4 (Table 11).

sgRNAs and universal 67mer trans-activating crispr RNA (tracrRNA, labelled with PE) were reconstituted in TE Buffer and a RNA duplex was formed (sgRNA:tracrRNA) by 5 min 95 °C, cooled down and assembled with the Cas9-protein in the next step, building

the ribonucleoprotein complex. The ribonucleoprotein complex was electroporated to the 300,000 target cells with the Cell line nucleofactor kit V and Lonza nucleofector technology system, using program “HCT116 SE ENII3” for HCT116 cells and program “SG CA 137” for BLaER1 cells, including a PBS electroporation control without the addition of ribonucleoprotein complex. Electroporated cells were plated in 96-well plates and single sorted by flow cytometry for PE after 24 h (3.5.3). Genetic engineering of cells was confirmed by Sanger sequencing (Table 9).

MD2

For MD2 genetic engineering of iPSCs, ssDNA oligomers guide1, guide 2 and MD2 3 bp deletion oligomer were cloned into pSpCas9(BB)-2A-GFP (PX458) backbone. The backbone vector was digested by *BpiI* for 30 min 37 °C, separated by agarose gel electrophoresis and linearized plasmid DNA was recovered (3.3.3). ssDNA oligos forward and reverse pairs were annealed and phosphorylated by T4 polynucleotide kinase. 1µL ssDNA (oligo1 fw, 100 µM), 1µL ssDNA (oligo1 rev, 100 µM), 1 µL T4 ligation buffer (10x), 0.5 µL T4 polynucleotide kinase, added up to 10µL with nuclease free dH_2O, were incubated for 30 min 37 °C, 5 min 95 °C, cooled down to RT and diluted 1:250 in nuclease free dH_2O (Table 11).

For ligation, 50 ng linearized backbone with 1 µL (1:250) oligos, 1 µL T4 ligation buffer, 0.5 µL T4 ligase, added up to 10 µL with nuclease free dH_2O was incubated 1 h at 37 °C. Ligation mix was transformed in competent *E.coli*, positive clones selected from LB agar plates with ampicillin and Sanger sequenced with validated standard pLKO.1 primer fw/rev from Eurofins Genomics (Table 11).

Table 11 List of components for genetic engineering by CRISPR-Cas9 system for *ZYX* and *MD2* genes.

Components	Primer sequence 5'-3' or info
Guides/oligomers	
ZYX guide 1 sgRNA	TGGATATGTGCCCCCACCAG
ZYX guide 2 sgRNA	TGAGCCGGAGCCGGAACCTG
guide1 ssDNA KO MD2 fw	CACCGTCTACTATTTGAGGGCCTAA
guide1 ssDNA KO MD2 rev	AAACTTAGGCCCTCAAATAGTAGAC
guide2 ssDNA KO MD2 fw	CACCGTTTTGCAGAGCTCTGAAGGG
guide2 ssDNA KO MD2 rev	AAACCCCTTCAGAGCTCTGCAAAAC
MD2 3 bp del oligomer for patient variant	AATATCACCTAACCGTGACCAATAACG TTTTGTATTTTATATTTTGTTTGCAGAGA CTGTGAATACAATATCATTCTCCTTCAAA GGAATAAAATTTTCTAAGGTATTGTTCAA GATTTATTTTGTACTGTCTAACC
guide1 ssDNA 3 bp del KO fw MD2	CACCGAACAATATCATTCTCCTTCA
guide1 ssDNA 3 bp del KO rev MD2	AAACTGAAGGAGAATGATATTGTTC
Plasmids	
pSpCas9(BB)-2A-GFP (PX458)	Plasmid backbone for cloning, GFP
pSpCas9(BB)-2A-GFP (PX458-MD2g1)	Plasmid harbouring guide 1 MD2 for KO
pSpCas9(BB)-2A-GFP (PX458-MD2g2)	Plasmid harbouring guide 2 MD2 for KO
pSpCas9(BB)-2A-GFP (PX458-MD2 3 bp del)	Plasmid harbouring guide for MD2 3 bp del
Primers for Sanger sequencing	
ZYX guide1/2 CRISPR KO fw	GTAAGGGACCGGAGAGTAGGAA
ZYX guide1/2 CRISPR KO fw	AGCCTGTGCCAGCAGAAAGAGC
MD2 guide1/2 CRISPR KO fw	CACAGGGCCCCTTTTAACTATACA
MD2 guide1/2 CRISPR KO rev	GGAGGAACATAAAGGCAGAAGTCA
MD2 variant CRISPR fw	CCCCACCACATTCACTACTTTG
MD2 variant CRISPR rev	TTGTGAATTGCTTGTTTCAAATGCT
pLKO.1 fw	Eurofins Genomics standard primer
pLKO.1 rev	Eurofins Genomics standard primer

CRISPR-Cas9 mediated genetic engineering of *MD2* KO and its patient variant (3 bp del) in iPSCs, was performed by using the Lonza nucleofector technology system. iPSCs cells were used in a low passage and grown in 6-well plates. 1-2 wells were used per electroporation setup and cells were supplemented with 10 µM rho kinase inhibitor Y-27632 24 h before treatment.

On the day of electroporation, 6-well plates were coated with 1 mL of 1:100 matrigel dilution in DMEM/F12 and incubated 1 h at 37 °C. Plates were washed one time with PBS and 2 mL pre-warmed mTeSR plus medium, supplemented with 10 µM rho kinase inhibitor Y-27632 was added to each well. Plates were kept at 37 °C.

Human stem cell Nucleofector^{TM} kit 2 was used and supplement 1 (18 µL/reaction) was added to nucleofector solution (82 µL/ reaction) in a 1.5 mL tubes and incubated at 37 °C. iPSCs were washed once with PBS and detached with 0.5 mL accutase (1 mg/mL) per well, incubated for 5-10 min at 37 °C. 0.5 mL mTeSR plus was added per well to dissociate into single cells by pipetting 4-6 times. Cells were transferred to a 15 mL falcon tube, an aliquot was stained with trypan blue and counted by neubauers counting chamber. 1-1.5 x10^6 cells were used per setup, pelleted at 115 rpm 3 min at RT in a 1.5 mL tube. The pellet was resuspended in 100 µL pre-warmed supplemented nucleofector solution.

Both MD2 KO PX458 vectors were used for maximum efficiency, by adding 2.5 µg PX458-MD2g1 and 2.5 µg PX458-MD2g2 to the 100 µL cell suspension. For the patient variant, 5 µg PX458-*MD2* 3 bp del and 8 µL ssODN were added to the 100 µL cell suspension, plus one electroporation control. The vector-ssODN mix was electroporated to the target cells with the Lonza nucleofector technology system, using program “B-016”. Cells were transferred to pre-incubated 6-well plates. To inhibit the non-homologous end joining pathway, engineered patient specific variant (3 bp del) of iPSCs were supplemented with SCR7 (10 µM) 8 to 24 h after nucleofection, inhibiting DNA ligase IV.

For cultivation of single clone iPSCs and sorting, cells were treated with 10 µM rho kinase inhibitor Y-27632 for 24 h, detached by accutase treatment and sorted by flow cytometry for GFP positive single cells in bulk. Collection occurred in 700 µL mTeSR plus medium, supplemented with 10 µM Y-27632 and 1 % penicillin-streptomycin. 3000 to 5000 cells were plated on 10 cm cell culture dishes, coated with matrigel 1:100, containing 6 mL mTeSR plus, 4 mL mTeSR plus conditioned medium and 1 % penicillin-streptomycin. Conditioned medium was collected each day from passaged iPSCs, filtered through 0.45 µm pore size, to allow growth of single iPSCs to colonies

after sorting. Cells were grown to small colony size (5-10 days), picked for single clone growth in 24-well plates and sequencing.

For clone sequencing, small amounts of cells were collected in 1.5 mL tubes, mixed with 50 µL 50 mM NaOH and incubated 15 min at 95 °C. Subsequently, 5 µL 1M Tris pH 7.5 were added. A small amount (1-2 µL) of the solution were used for Sanger sequencing (3.3.2) with corresponding primers (Table 9).

3.5. Cell biology techniques

3.5.1. Protein expression analysis by SDS-PAGE

To analyze protein expression, residual medium was removed by a PBS wash and cells were collected in 1.5 mL tubes. Cells were lysed for 1 h on ice with 20-50 µL cell lysis buffer. The buffer was prepared with 100 µL cell lysis buffer (10x) mixed with 60 µL protease inhibitor cocktail (PIC), 10 µL phenylmethanesulfonyl fluoride protease inhibitor (PMSF, 0.1 M), and 830 µL dH_2O. After lysis on ice, cells were spun down for 10 min, 15,000 rpm at 4 °C, supernatants were collected in 1.5 mL tubes and the protein yield was quantitatively analyzed by measuring absorbance at 595 nm in bradford solution on a BioTek synergy H1 hybrid reader and Gen5.11 software.

Protein samples were mixed with 5x Laemmli buffer (1 mL 1.5 M Tris-HCl, pH 6.8, 3 mL Glycerol, 0.6 mL 20 % SDS, 1.8 mg bromophenolblue, added up to 10 mL with dH_2O) and fresh 3 % ß-mercaptoethanol. Samples were denatured for 10 min at 95 °C, short spun and separated by sodium dodecyl sulfate–polyacrylamide gel electrophoresis (SDS-PAGE) with 7 µL pre-stained protein ladder (10 to 180 kDa) for molecular weight determination.

Large gels were purchased as precast (26-well 12 % Criterion™ TGX Stain-Free™ protein gel with criterion system), 15-well gels were usually self-made with Mini-PROTEAN tetra vertical system from Bio-Rad). The amount of acryl-bisacrylamide determined gel percentage of separating gels (Table 12). First separating gels were casted and polymerized for 15-20 min at RT. Stacking gels were casted on top, respective combs inserted and polymerized for 15 min RT. After loading of protein samples, gels were run at 80 V for 20 min, then 80 min at 120 V. Running buffer contained 14.1 g glycine, 3.03 g Tris, 1 g SDS up to 1 L with H_2O.

Table 12 Preparation of separating and stacking gel for SDS-PAGE.

Component	Separating gel (13 %)	Separating gel (10 %)
1.5 M Tris-HCl (pH 8.8)	2.9 mL	2.9 mL
Acryl-bisacrylamide	3.4 mL	2.6 mL
SDS (10 %)	77.5 µL	77.5 µL
dH_2O	2.3 mL	3.1 mL
TEMED	5.75 µL	5.75 µL
APS (20 %)	37.6 µL	37.6 µL
	Stacking gel (6 %)	
0.5 M Tris-HCl (pH 6.8)	360 µL	
Acryl-bisacrylamide	487,5 µL	
SDS (10 %)	28.75 µL	
dH_2O	1.95 mL	
TEMED	2.87 µL	
APS (20 %)	18.8 µL	

Protein transfer was accomplished by either semi-dry Trans-Blot® Turbo™ transfer system 2.5 V for 20 min or wet blotting for 60-90 min at 400 mA using mini Trans-Blot® electrophoretic transfer cell from Bio-Rad (Table 13). Gels were soaked in corresponding buffer (Bjerrum Schafer-Nielsen Buffer containing 48 mM Tris, 39 mM glycine, 20 % methanol, 0.037 % SDS (pH 9.2) in 1L dH_2O or Transfer buffer containing 25 mM Tris, 192 mM glycine, 10 % methanol/ethanol, 0.1 % SDS in 1L dH_2O (pH 8.3). Assembly occurred with three layers of Whatman paper, followed by the gel and activated 0.45 µm PVDF membrane, stacked with another three layers of Whatman paper, removal of all bubbles for clean transfer and blotting was conducted at system specific times, voltage or current (Table 13).

Table 13 Transfer systems for immunoblotting.

	Trans-Blot® Turbo™ Transfer System	Mini Trans-Blot® electrophoretic transfer cell
Membrane	0.45 µm PVDF	0.45 µm PVDF
Kind of transfer	Semi-dry	Wet
Membrane activation	Methanol	Methanol or Ethanol
Buffer	Bjerrum Schafer-Nielsen buffer	Transfer buffer
Time	20 min	60-90 min
Voltage/ current	2.5 V	400 mA

Transferred membranes were blocked with either 5 % BSA in PBS with 0.1 % Tween-20 (PBST) or 10 % milk in PBST buffer for 1 h at RT. This was followed by primary antibody incubation for 12-16 h on orbital shakers at 4 °C. After three PBST washing steps for 10 min at RT, membranes were incubated for 1 h at RT, with a HRP-conjugated secondary antibody, binding the specific isotype of the primary antibody. For visualization of specific protein expression patterns, membranes were washed three times with PBST for 10 min at RT, semidried and incubated for 3-5 min darkened with SuperSignal west dura extended duration substrate for chemiluminescence detection and imaged with the ChemiDoc XRS+ system and image lab software. Several proteins could be detected on one membrane by incubating membranes with western blot stripping buffer for 15 min RT, washing three times 10 min with PBST and repeating sequentially primary and secondary antibody application (Table 14). Equal loading of membranes was probed with either anti-Actin or anti-GAPDH at the final detection.

Table 14 Antibodies for immunoblotting.
Diluted either in 10 % milk (milk) or 5 % BSA (BSA) in PBST.

Antibodies	Clone	Supplier	Order no.	Diluent	Dilution
Primary antibody					
NF-κB p65	D14E12	Cell Signaling Technology	8242S	milk	1:1000
Phospho-NF-κB p65 (Ser536)	93H1	Cell Signaling Technology	3033S	BSA	1:1000
p38 MAPK	polyclonal	Cell Signaling Technology	9212S	milk	1:1000
Phospho-p38 MAPK (Thr180/Tyr182)	D3F9	Cell Signaling Technology	4511S	BSA	1:1000
p44/p42 MAPK (Erk1/2)	polyclonal	Cell Signaling Technology	9102S	milk	1:1000
Phospho-p44/42 MAPK (Erk1/2) (Thr202/Tyr204)	D13.14.4E	Cell Signaling Technology	9101S	BSA	1:1000
NLRP3	D2P5E	Cell Signaling Technology	13158S	milk	1:1000
IL-1beta	polyclonal	R&D/ biotechne	AF-201-NA	milk	1:1000
Caspase-1	polyclonal	Enzo Life Sciences	BML-SA101-0100	milk	1:1000
Zyxin	EPR4302	Abcam	ab109316	milk	1:10,000
MD-2	polyclonal	Biozol	LS-C158083-400	milk	1:1000
GAPDH	6C5	Santa Cruz Biotechnology	sc-32233	milk	1:1000
β-Actin HRP	C4	Santa Cruz Biotechnology	sc-47778 HRP	milk	1:5000
Secondary antibody					
Anti-rabbit IgG, HRP-linked	-	Cell Signaling Technology	7074S	milk	1: 3000
Mouse anti-goat IgG, HRP-linked	-	Santa Cruz Biotechnology	sc-2354	milk	1: 3000
HRP Goat Anti-Mouse IgG	-	BD Biosciences	554002	milk	1: 3000

3.5.2. ELISA

To verify secreted cytokines of interest, the sandwich enzyme-linked immunosorbent assay (ELISA) was performed. According to manufacturer's protocol for human TNF ELISA (BD OptEIA) and human IL-1β/IL-1F2 Duo Set (R&D biotechne) supernatants collected from former experiments were analyzed, protein-binding 96-well plates were coated with capture antibody in corresponding buffer overnight at 4 °C. After three washing steps with PBS and 0.05 % Tween-20 (PBST), plates were blocked with 1 % BSA in PBST for 2 h at RT. Samples were thawed on ice and diluted in 1 % BSA in PBST, if needed. After blocking and three PBST washing steps, samples were transferred in duplicates to the plates on ice, always including a standardized dilution series of recombinant protein for subsequent concentration calculations. Plates were sealed and kept at 4 °C for 12-16 h. After washing five times, detection antibody was incubated for 2 h at RT. Plates were washed five times, followed by 1 h streptavidin-conjugated HRP incubation (kept dark) at RT and another washing step seven times. 100 µL TMB solution (1x) was added, the substrate for HRP and incubated for 5-15 min at RT (kept dark). Reaction was stopped by addition of 50 µL 2 M H_2SO_4 and plates were spectrophotometrically analyzed, measuring the absorbance at 490 nm with the BioTek Synergy H1 Hybrid Reader and Gen5.11 Software.

3.5.3. Flow cytometry and cell sorting

Flow cytometry was conducted on the BD Biosciences LSRFortessa. Data were analyzed with FlowJo v10 software. Samples were prepared in FACS Buffer (PBS with 2 % FBS), filtered through cell strainer snap cap of 5 mL round-bottom tubes before acquisition.

For staining, cells of interest were collected on ice in 15 mL Falcon tubes, pelleted by centrifugation, washed once with PBS, and resuspended in FACS Buffer. Staining for several human antigens occurred in 200 µL total volume (Table 15). If Brilliant Violet (BV) colors were part of the panel, 50 µL Brilliant stain buffer was used in the staining solution. Incubation of antibodies was conducted for 1 h on ice, light protected. Cells were washed once with FACS buffer and resuspended in 200 µL FACS buffer for analysis.

Table 15 Conjugated antibodies (anti-human) for flow cytometry.

Antibodies	Clone	Supplier	Order no.	Dilution
Anti-CD14 APC	MIH1	BD Biosciences	587926	1:200
Anti-CD45 FITC	HI30	Biolegend	304038	1:200
Anti-CD34 BV421	561	BioLegend	343610	1:200
Anti-CD274 APC	MIH1	BD Biosciences	563741	1:200
Anti-CD86 BV421	FUN-1	BD Biosciences	562432	1:200
Anti-CD163 PE	GHI/61	Biolegend	333606	1:200
Anti-HLA-DR PE-Cy7	L243	BD Biosciences	335830	1:200
Anti-CD14 FITC	M5E2	BD Biosciences	555397	1:100
Anti-TLR4 PE-Cy7	SA15-21	BioLegend	145408	1:40
Anti-CD284 (TLR4) PE	TF901	BD Biosciences	564215	1:200

Before sorting, CRISPR-Cas9 engineered iPSCs needed to be kept in mTeSR plus medium, supplemented with 10 µM Rho kinase inhibitor Y-27632 for 24 h. Cells were detached by accutase treatment and sorted by flow cytometry for PE or GFP positive single cells. Collection occurred in 700 µL mTeSR plus medium, supplemented with 10 µM Y-27632 and 1 % penicillin-streptomycin.

Cell sorting was performed by BD FACSAria II cell sorter. Cells were collected, washed, and diluted in 700 µL FACS buffer. Cells were filtered through cell strainer snap cap of 5 mL round-bottom tubes immediately before acquisition. A 15 mL falcon tube with 5 mL corresponding complete medium was prepared for bulk sorting (HCT116 and BLaER1 cells). Single cell clones (e.g. CRISPR-Cas9 engineered HCT116 or BLaER1 cells) were collected in 96- to 24-well plate formats.

3.6. Microscopy

3.6.1. Immunofluorescence microscopy

For detection of immunofluorescently labeled proteins in HCT116 cells, around 50,000 cells were seeded on glass coverslips, 12 mm in 24 well plates. Cells were cultured for 16-24 h. For fixation, cells were washed with PBS and incubated with 3.7 % PFA in PBS for 10 min at RT. After three PBS washing steps for 10 min, slides were quenched with 50 mM NH_4CL in PBS for 15 min at RT. Permeabilization of cells occurred with 1 % BSA in 0.05 % saponin-PBS for 1 h at RT, followed by 5 min washing with PBS. For primary antibody application, coverslips were transferred to a humidified chamber, adding 80 µL to the sample and incubated at 4 °C for 12-16 h (Table 16). Samples were washed three times with PBS and the secondary antibody was applied to a 24-well plate, incubated for 2 h at RT, followed by three washes for 5 min. F-Actin was stained, if needed, with phalloidin for 1 h at RT. DNA was stained with DAPI 0.5 µg/mL for 5 min at RT. Samples were washed two times 5 min with PBS and mounted on glass slides with 10 µL fluorescence mounting medium (Table 16). Slides were dried for 12-18 h at RT and analyzed by confocal microscopy using Zeiss LSM 800, 40x/1.4 NA or 63x/1.4 NA oil objectives and ZEN blue software Version 2.6.

Table 16 Primary antibodies, secondary antibodies and fluorescent stains for confocal microscopy.

Antibodies	Clone	Supplier	Order no.	Host	Dilution
Primary antibody					
Anti-Zyxin	polyclonal	Sigma Aldrich	HPA004835	rabbit	1:400
Anti-Vinculin	hVIN-1	Sigma Aldrich	V9131	mouse	1:400
Anti-VASP	A-11	Santa Cruz Biotechnology	sc-46668	mouse	1:400
Secondary antibody or other stains					
Goat anti-Rabbit IgG (H+L) Cross-Adsorbed Secondary Antibody, Alexa Fluor 633	polyclonal	Thermo Fisher Scientific	A-21070	goat	1:800
Goat anti-Mouse IgG (H+L) Cross-Adsorbed Secondary Antibody, Alexa Fluor 488	polyclonal	Thermo Fisher Scientific	A-11001	goat	1:800
Alexa Fluor® 633 phalloidin	-	Thermo Fisher Scientific	A22284	-	1:250
DAPI (5 mg/m)	-	Sigma Aldrich	D9542	-	1:10,000

3.6.2. Migration analysis

To analyze migratory capacities of cells, one Ibidi culture insert was adhered per well, in a 6-well format. These culture inserts left an untouched 500 µm gap, while cells were seeded on both sides. HCT116 cells were freshly split and 150,000 cells in 200 µL resuspended and plated per site of the insert. Cells were grown confluent for 3-4 days and supplied with 100 µL fresh medium per day due to evaporation. The culture inserts were removed, cells were washed with PBS and wells filled with 2 mL fresh medium. Migration of cells was monitored for 24 h and images acquired by AxioVert microscope using Axio Vision software from Zeiss.

3.6.3. Cytospin and histological stain

For morphological analysis of iPSC-derived monocytoid cells, 10,000 cells in PBS were spun on coated cytoslides with the required equipment of Tharmac Cellspin I for 5 min. Slides were dried at RT for 16 h and stained 2 min with May-Grünwald's eosine-methylene blue solution modified, washed twice with dH_2O for 1 min. Giemsa's azur eosin-methylene blue solution was diluted 1:20 in Sorenson's phosphate buffer (for 0.133 M pH 7.2, mix 71.5 mL 133 mM Na_2HPO with 28.5 mL KH_2PO_4) and slides were incubated 17 min, followed by washing twice with dH_2O. Slides were dried at RT for 16 h and analyzed by AxioVert Microscope and Axio Vision software from Zeiss.

3.6.4. Transepithelial electrical resistance measurement (TEER)

Epithelial barrier integrity was measured over time by transepithelial electrical resistance of a cellular monolayer. HCT116 cells were seeded in transwell cell culture inserts, diameter of 6.5 mm, pore size 8.0 µm in corresponding plates and grown confluently, measuring daily TEER with EVOM2 epithelial Volt/Ohmmeter.

3.6.5. Colony formation assay

To investigate the clonogenicity of cells, 750 cells per six well were seeded in 3 mL. Each condition was seeded in triplets and analyzed 2 weeks after seeding. Each well was washed once with 1 mL PBS and fixed with 1 mL 4% PFA for 10 min, stained with 0.05 % (w/v) crystal violet in 1 % methanol/ PBS solution for 1 h, washed two times with PBS and dried overnight.

3.7. Generation of iPSC-derived macrophages

3.7.1. iPSC differentiation to monocytic progenitors and macrophage-like cells

Differentiation of iPSCs occurred in 6 well plates, using 3 wells per genotype. iPSCs were split as described before and 10-20 equal-sized colonies seeded per well. Medium was changed daily and grown for 3 days until colonies reached size of 1 mm, which was day 0 of the differentiation process. Detailed protocols have been published [218, 219].

For CD14+ cell differentiation from iPSCs, cells were cultivated (2 mL per well) in specific media and supplements over 28 days with additional 7 days of macrophage-lineage direction, and medium was changed daily (Figure 10).
After 6 days, 5-6 colonies were selected for ongoing cultivation while residual colonies were aspirated. Floating cells during media change were collected and used for FACS analysis to confirm differentiation process over time.

CD14+ cells were isolated by positive selection using either human CD14 microbeads or EasySep™ human CD14 positive selection kit II according to manufacturer's protocol. Isolation efficiency was proven by FACS analysis and cells used for experiments. After positive selection, macrophage-like cells were differentiated by the addition of M-CSF for 7 days, and medium was changed every two days.

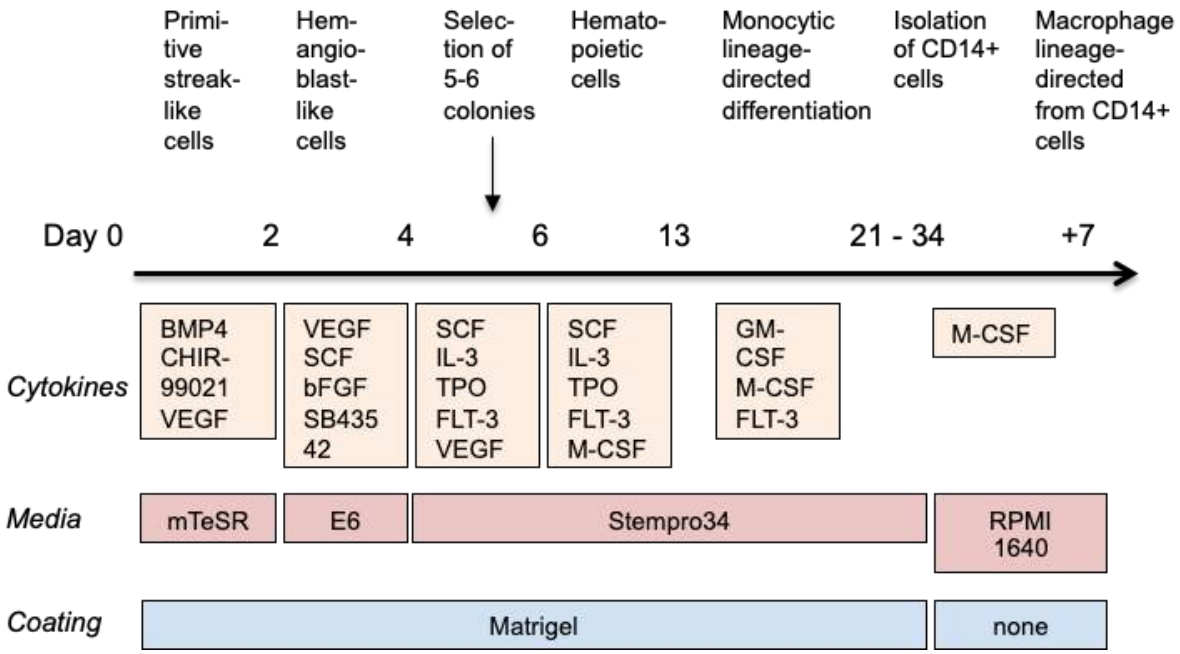

Figure 10 iPSC differentiation scheme for CD14+ cells in monolayer culture.
Cultivation conditions and cytokine concentrations for day 0-2: BMP4 (80 ng/mL), CHIR-99021 (2 µM), VEGF (80 ng/mL) in mTeSR medium. Day 2-4: VEGF (80 ng/mL), SCF (50 ng/mL), bFGF (25 ng/mL), SB43542 (2 µM) in Essential 6 medium (E6). Day 4-6: SCF (50 ng/mL), IL-3 (50 ng/mL), TPO (5 ng/mL), FLT-3 (50 ng/mL), VEGF (50 ng/mL) in StemPro-34 medium. Day 6-13: SCF (50 ng/mL), IL-3 (50 ng/mL), TPO (5 ng/mL), FLT-3 (50 ng/mL), M-CSF (50 ng/mL) in StemPro-34 medium. Day 13-21/31: GM-CSF (25 ng/mL), M-CSF (50 ng/mL), FLT-3 (50 ng/mL) in StemPro-34 medium. After CD14+ cell isolation, additional 7 days: M-CSF (100 ng/mL) in RPMI-1640 complete medium. Modified from Yanagimachi et al. and Fan et al. [218, 219].

3.7.2. M1/M2 polarization of human macrophages

Pro- and anti-inflammatory macrophage properties were analyzed from former differentiated iPSCs. Around 200,000 isolated CD14+ cells were seeded per well and condition in a 12-well format. Cells were differentiated with 100 ng/mL M-CSF for seven days and medium was changed daily. After 7 days, macrophage-like cells were washed twice with medium and rested for 4-6 h in RPMI-1640 complete medium without M-CSF. For M0 macrophages no cytokines were added. Pro-inflammatory M1 macrophages were differentiated by stimulation with LPS (50 ng/mL) and IFN-γ (20 ng/mL). Anti-inflammatory M2 macrophages were differentiated by the stimulation with IL-4 (20 ng/mL), IL-10 (20 ng/mL), TGF-β (20 ng/mL). Cells were incubated for each condition 24 h at 37 °C.

3.7.3. Gentamycin protection assay of iPSC-derived macrophages

To determine bacterial uptake of *Salmonella typhimurium*, 20 000 macrophages were plated in triplets in 24 well plates in RPMI medium with 10 % FCS, without antibiotics for up to 12 h. *Salmonella typhimurium* were a kind gift from Dr. Felipe Romero. Macrophages were incubated with a multiplicity of infection of 10, for 3 h or 6 h. Followed by a treatment with gentamycin (50 mg/mL) for 1 h. Cells were washed with PBS and complemented with RPMI complete medium with 100 ug/mL gentamycin for 2 h. After incubation, cells were washed twice with PBS. Cells were lysed with 200 µL 1 % Triton-X in dH_2O and pipetted on LB plates in serial dilutions. Plates were kept overnight at 37 °C and colony formation units were analyzed.

3.8. Statistics

For statistical analysis the commercial GraphPad PRISM v.6 and v.10 software was used. Data was analyzed via ANOVA or two-tailed paired Student's *t* test. Mean values were presented with standard deviation. Statistical significance was presumed for *p*-values <0.05 and indicated in text and figures. Values, which did not reach statistical significance (>0.05), were not mentioned specifically.

4. Results

4.1. Identification of two patients with rare biallelic homozygous *ZYX* sequence variants and inflammatory bowel disease

Two rare biallelic homozygous genetic variants of *ZYX* were identified on the human genome assembly GRCh37.p13 upon WES analysis. Both variants were found on the human transcript ENST00000322764.5, on chromosome position chr7:143078852-143078852 for patient 1 (P1) and on chr7:143085695-143085695 for patient 2 (P2). Both variants were on protein coding exons (P1 Exon 2, P2 on Exon 7), found at the consensus coding sequence CCDS5883. Both rare homozygous missense variants in the *ZYX* gene were confirmed by Sanger sequencing of patients and their first-degree relatives, showing an autosomal recessive mendelian inheritance pattern, segregating with the disease phenotype of both patients (Figure 11).

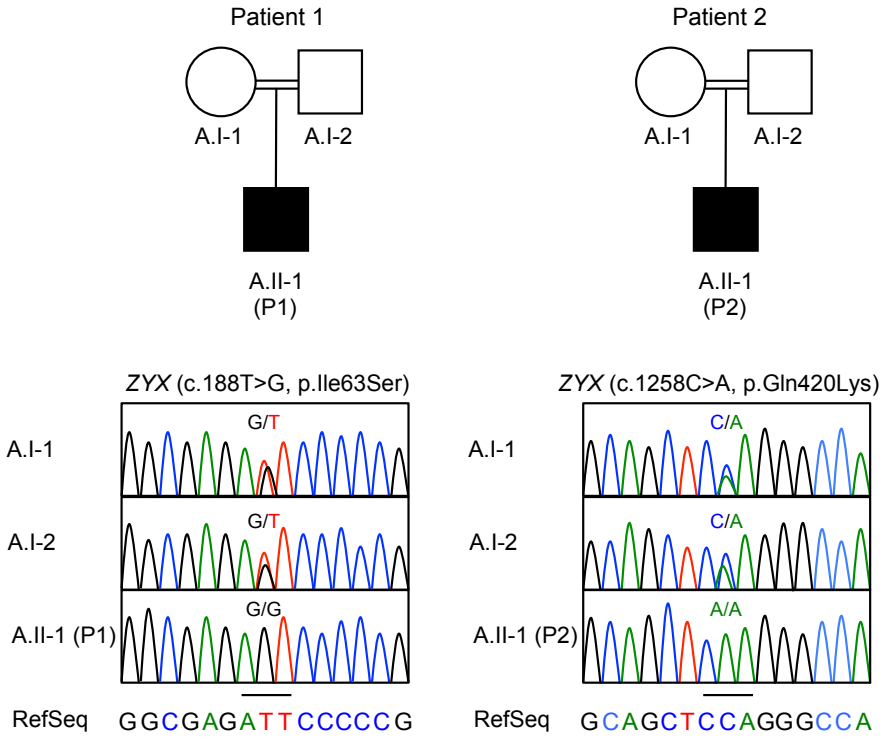

Figure 11 Segregation analysis of two homozygous variants of *ZYX* from two independent families.
Pedigrees of both families presented one affected child with IBD. Sanger sequencing of first-degree relatives and patient 1 from a consanguineous Algerian family, confirmed a rare homozygous missense variant in the *ZYX* gene (c.188T>G, p.Ile63Ser). Patient 2 from a consanguineous Syrian family carried another rare homozygous missense variant of *ZYX* (c.1258, Gln420Lys), which was confirmed by Sanger Sequencing, indicating the segregation of both variants with the IBD disease phenotype.

Patient 1 from Arab origin and a consanguineous family (2nd degree), had an age of onset of 8 years and was diagnosed with IBD at the age of 11. The patient suffered from fatigue, abdominal pain, vomiting, non-bloody diarrhea, and fissures. The disease was classified by the Paris classification as stricturing and penetrating disease behavior. Endoscopic and histopathological examinations confirmed inflammatory and atrophic chronic gastritis, diffuse inflammatory infiltrates in terminal ileum and crypt abscesses in the ascending colon. Initially, the patient had slightly increased white blood cell count > 12,000 cells/µl and increased platelet count > 700,000 cells/µL, interpreted as a sign of chronic systemic inflammation. The patient showed no response to mesalazine (5-ASA) 50 mg/kg/d and only partial response to corticosteroids 1,5 mg/kg/d for 2 months and azathioprine treatment 3mg/kg/d for 4 years. Due to the refractory course, the patient had to undergo colostomy and bowel resection at the age of 12.

Patient 2 born to a consanguineous family (2nd degree) with Arab origin had an age of diagnosis of VEO-IBD at 2 years. The patient presented with growth failure, poor weight gain/weight loss, fatigue, nausea, vomiting, abdominal pain, non-bloody and bloody diarrhea, constipation, and rectal bleeding. The disease was classified by the Paris classification as non-stricturing and non-penetrating. The patient suffered from severe viral infections requiring hospitalization. Endoscopy showed inflammation of the transverse colon, descending colon, sigmoid and rectum as well as perianal disease. Histopathology confirmed inflammation with neutrophil leukocytes in lamina propria, but no granuloma. Under immunosuppressive therapy, the patient still had increased white blood cell count > 19,000 cells/µl and increased platelet count > 600,000 cells/µl. Neutrophils were > 45 %, monocytes > 8 %, lymphocytes > 45 %, eosinophils 0.2 % basophils 0.8 %. Serum immunoglobulin analysis showed IgA above normal range, IgG below, as well as IgD and IgM at normal range. In addition to VEO-IBD, the patient was diagnosed with cow milk allergy. The patient showed no response to antibiotics but good response to corticosteroids and short-term diet with Modulen® IBD formula.

4.2. Zyxin protein structure and variant prediction

The prediction of both missense variants on the proteins functional effect was evaluated by bioinformatics using PolyPhen (polymorphism phenotyping) and SIFT (sorting intolerant from tolerant) values [220, 221].

PolyPhen ranges from 0.0 (tolerated) to 1.0 (deleterious). The variant I63S (P1) and P2 variant p.Q420K (P2) were both predicted to be deleterious variants of *ZYX* by PolyPhen (P1: 0.838, P2: 0.997). SIFT ranges from 0.0-0.05 are declared as deleterious, 0.05-1.0 as tolerated. Both patients' variants were predicted to be deleterious (P1: 0, P2: 0.02) by SIFT. At that time of performing the PhD thesis, variants at genome aggregation database (gnomAD) were also not found in healthy individuals [222].

For protein structure visualization, the tool AlphaFold was used to predict the structure of Zyxin upon artificial intelligence implementation [223, 224] (Figure 12). In P1, the p.Ile63Ser amino acid change leads to a change of an aliphatic, non-polar and neutral charged isoleucine to a hydroxylic, polar and neutral charged serine. While in P2, the p.Gln420Lys variant leads to a change of polar and neutral charged glutamine to a cationic, positive charged lysine. Both variants are located beside or in a functional domain of the ZYX protein, suggesting a probable functional impact (Figure 12). Whereas p.I63S is located at the N terminus near the proline-rich ENAH/VASP binding site, the p.Q420K variant was predicted to affect the Actin-binding LIM domain.

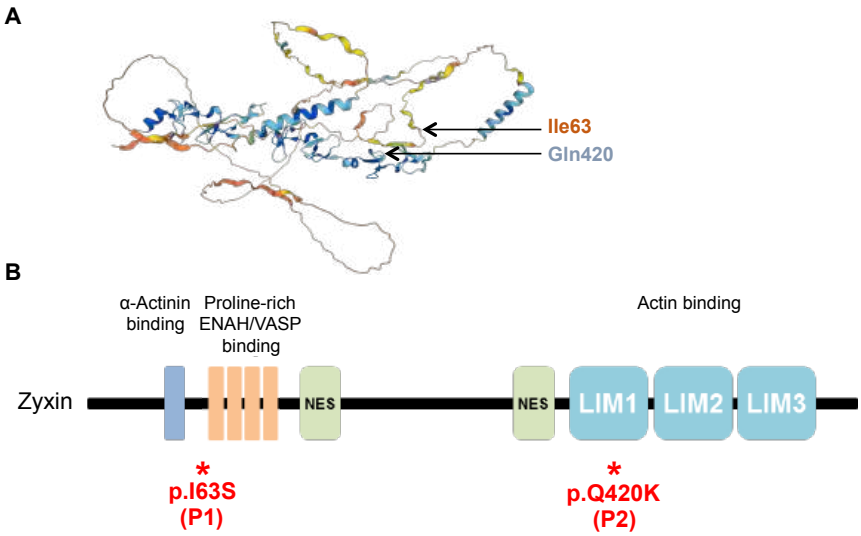

Figure 12 Prediction of the protein structure of Zyxin by Alphafold (A) and (B) functional domains.

A) Homozygous missense variants of ZYX occur at position p.63 and p.420. The color code reflects the confidence score of the model structure (orange: very low, blue: very high). B) The variant identified in patient 1 (P1, p.I63S) variant occurs between the functional α-Actinin and ENAH/VASP binding site. The second variant (P2, p.Q420K) occurs in the LIM1 domain, which is part of the Actin binding. NES, nuclear export signal. Modified from Hoffman et al. and Oldenburg et al. [188, 189].

4.3. Cell models

4.3.1. Functional validation of *ZYX* variants in heterologous HCT116 coloncarcinoma cells

To investigate the functional impact of both patient variants (I63S, Q420K), we established a heterologous cellular model. First, we generated a stable CRISPR/Cas9-mediated knockout of *ZYX* (*ZYX*$^{-/-}$) in HCT116 coloncarcinoma cells. Next, we fused ZYX wild-type (WT) and mutant (I63S, Q420K) variants on the C-terminus with green-fluorescent protein (GFP, *pRRL-ZYX-GFP* constructs) and generated stable overexpression of ZYX-GFP fusion proteins in HCT116 *ZYX*$^{-/-}$ cells. Immunoblotting confirmed the lack of the Zyxin protein in the generated knockout cell line as well as similar expression patterns and molecular weights for wild-type and mutant ZYX-GFP fusion proteins (Figure 13).

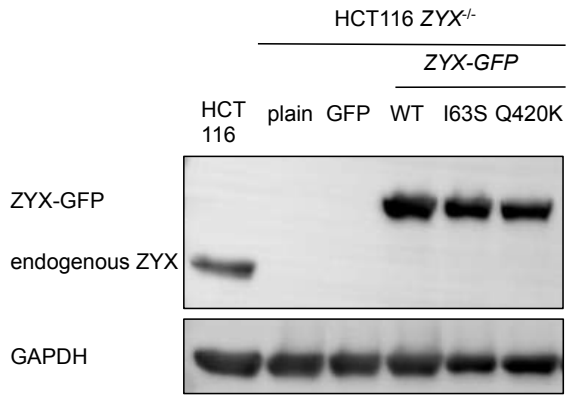

Figure 13 Overexpression analysis of heterologous HCT 116 *ZYX*$^{-/-}$ cells.
Cells were lentivirally transduced and overexpressing variants of ZYX (wild-type (WT), I63S, Q420K) fused with a C-terminal green-fluorescent protein (GFP). Immunoblotting of endogenous ZYX and overexpression of ZYX (WT, I63S, Q420K)-GFP variants in *ZYX*$^{-/-}$ HCT116 cells, and glyceraldehyde-3-phosphate dehydrogenase (GAPDH). (n=3)

Zyxin is a key regulator for actin assembly and critical for adherent junction formation, maintaining physical integrity of the epithelial barrier [225]. Therefore, we analyzed the monolayer integrity and permeability of HCT116 and HCT116 *ZYX*$^{-/-}$ cells by a measurement of transepithelial electrical resistance (TEER) over 10 days. Physiological TEER increased over time similarly in the HCT116 and HCT116 *ZYX*$^{-/-}$monolayer, suggesting no differences over the course of time (Figure 14).

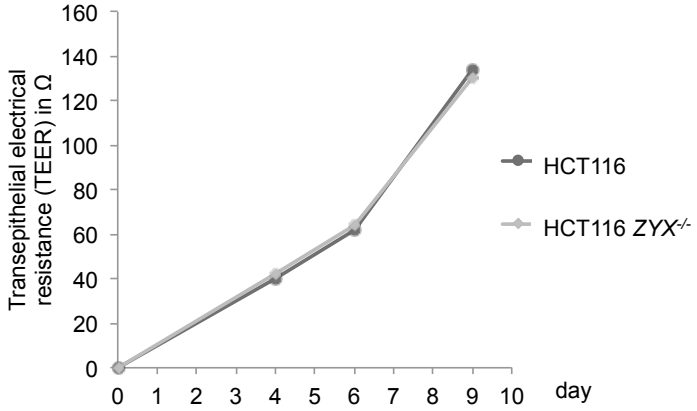

Figure 14 The establishment of a stable monolayer is independent of Zyxin in HCT 116 cells.
Measurement of transepithelial electrical resistance (TEER) over 10 days of a HCT116 and *ZYX*$^{-/-}$ deficient cells in monolayers. (n=1)

Previous studies have shown that mouse fibroblasts deficient in Zyxin have a higher migratory capacity than wild-type cells, a knockdown via single-hairpin RNA in canine kidney cells led to a similar migratory capacity like wild-type, and knockdown in human oral squamous cell carcinoma cells led in contrast to a significant slower migration [188, 226, 227]. To determine the impact of the identified *ZYX* variants on migratory capacities, we first assessed ZYX deficient and reconstituted HCT116 cells (WT, I63S, Q420K) by a migration assay. As cells reached confluency, we removed a culture insert, which left a gap of 500 µm and observed cell migration over 24 h. Time lapse microcopy showed physiological migration and closing of the redefined gap without any significant differences among all genotypes (Figure 15A).

It was previously shown that Zyxin impairs the proliferation in colorectal cancer cell lines [185]. To investigate the formation from of cell colonies from single cells, we performed a colony formation assay over two weeks. ZYX deficiency seemed to impair the colony formation in HCT 116 cells and only with GFP reconstituted cells. All heterologous lines (ZYX WT, I63S, Q420K) showed similar proliferation capacity (Figure 15B).

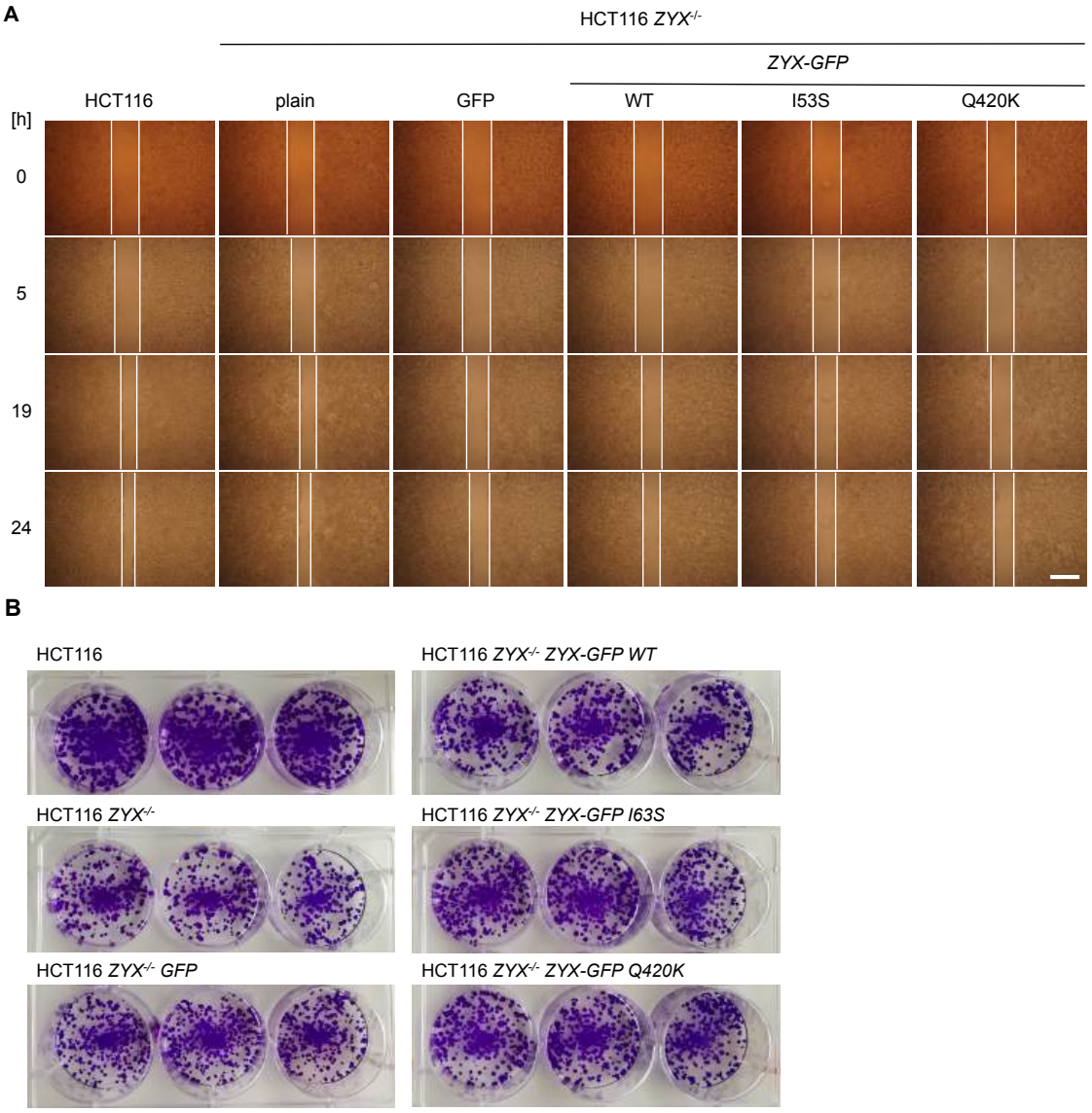

Figure 15 Analysis of migratory and proliferative capacities in heterologous HCT116 cells.

A) Migration capacity measured over 24 h on a monolayer, leaving a defined gap of 500 µm, monitoring migration capacity by time-lapse light microscopy, scale bar 500 µm. (n=3). B) Colony formation assay on heterologous HCT 116 cells after 2 weeks. (n=2)

To study colocalization of known interaction partners in focal adhesions, we assessed the spatial distribution of Zyxin with its interacting focal adhesion proteins such as Vinculin, which is part of the force transduction layer, and VASP, a directly interacting protein in the proximal actin regulatory layer [174]. Prior data suggested that VASP is absent in ZYX-deficient mouse fibroblasts, while Vinculin localization persists independently of ZYX [188]. We performed immunofluorescent staining of Vinculin or VASP in combination with a DAPI staining for nucleus visualization. We analyzed *ZYX*$^{-/-}$ HCT116 cells and their overexpressed GFP-tagged ZYX variants (WT, I63S, Q420K) in *ZYX*$^{-/-}$ HCT116 cells by confocal immunofluorescence microscopy (Figure 16). Vinculin is present in *ZYX*$^{-/-}$ HCT116 cells and no aberrations among the ZYX variants (WT, I63S, Q420K)-GFP in *ZYX*$^{-/-}$ HCT116 cells could be observed (Figure 16). In contrast, VASP could not be detected at focal adhesions in *ZYX*$^{-/-}$ HCT116 cells, but colocalized with all three overexpression variants at the cell edges (Figure 16).

Notably, the analysis of actin by a phalloidin staining in all reconstituted cells did not reveal any changes of the actin skeleton in steady-state conditions. A normal localization of Zyxin at the leading edges of the cells was seen, independent of which Zyxin variant was overexpressed (Figure 16).

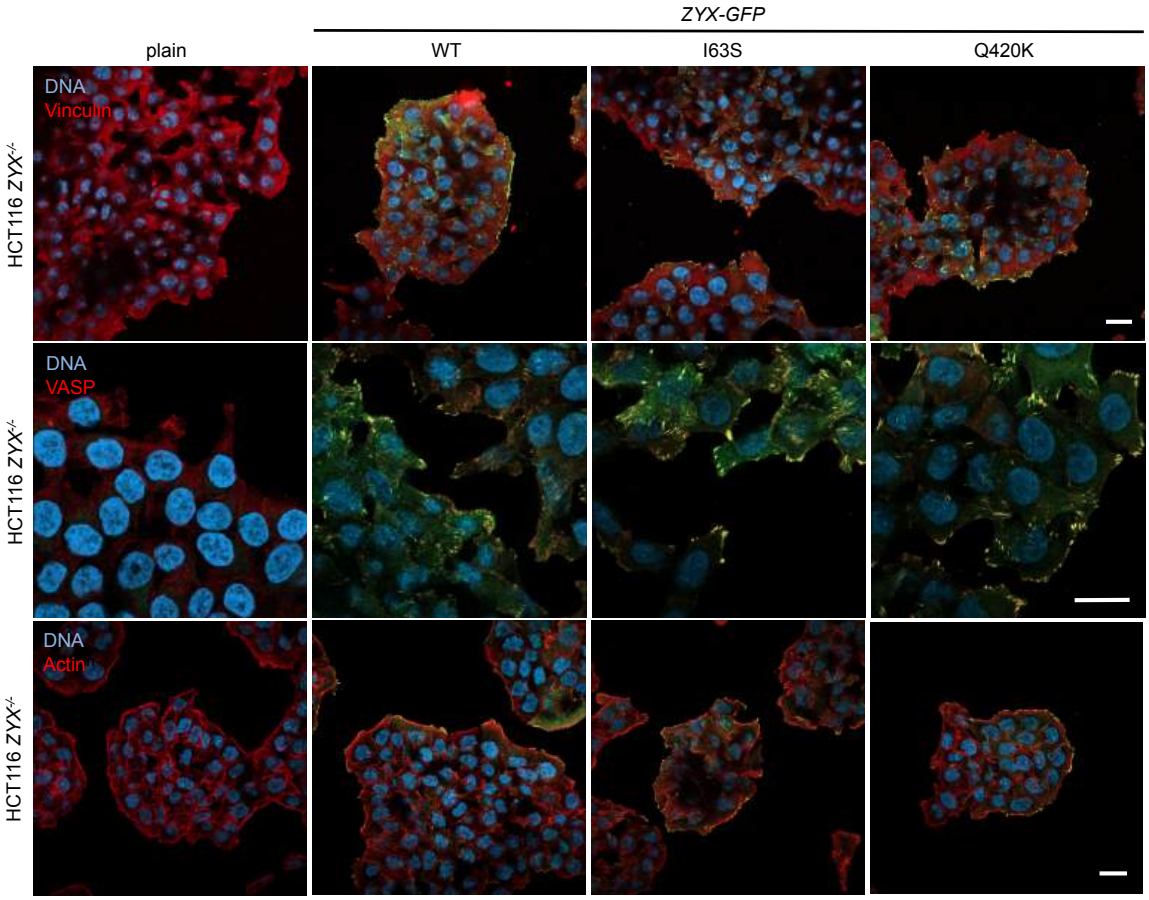

Figure 16 Protein colocalization is not altered in heterologous *ZYX*$^{-/-}$ HCT116 cells. Protein localization in HCT116 *ZYX*$^{-/-}$ cells, and HCT116 *ZYX*$^{-/-}$ cells overexpressing ZYX WT-GFP, ZYX I63S-GFP, ZYX Q420K-GFP was determined by confocal immunofluorescence microscopy using antibodies for either Vinculin or Vasodilator stimulated phosphoprotein (VASP) or phalloidin for Actin staining. DAPI was used to visualize DNA of the nucleus. Yellow indicates protein colocalization. Scale bar 50 µm. (n=2)

To analyze the influence of Zyxin on *CXCL10* induction, ZYX-deficient HCT116 cells were stimulated with Polyinosinic:polycytidylic acid (Poly I:C). Poly I:C simulates double-stranded RNA (dsRNA) during viral replication and activates the expression of *CXCL10* through TLR3 [183]. Previously, it was shown that Zyxin stabilizes dsRNA responses in HeLa cells and THP-1 macrophages [183]. *CXCL10* and baseline *ZYX* expression were determined by qPCR, showing a decreased *CXCL10* expression upon Poly I:C stimulation in ZYX-deficient HCT116 cells, independent of transfection agent Lipofectamine 3000 (Figure 17A). Overexpression of *ZYX* (*WT, I63S, Q420K*) was confirmed by qPCR, but no clear reduction of *CXCL10* expression was observed in the overexpressed ZYX variants, since GFP overexpression in ZYX-deficient HCT116 cells by itself led to a substantial *CXCL10* induction (Figure 17B).

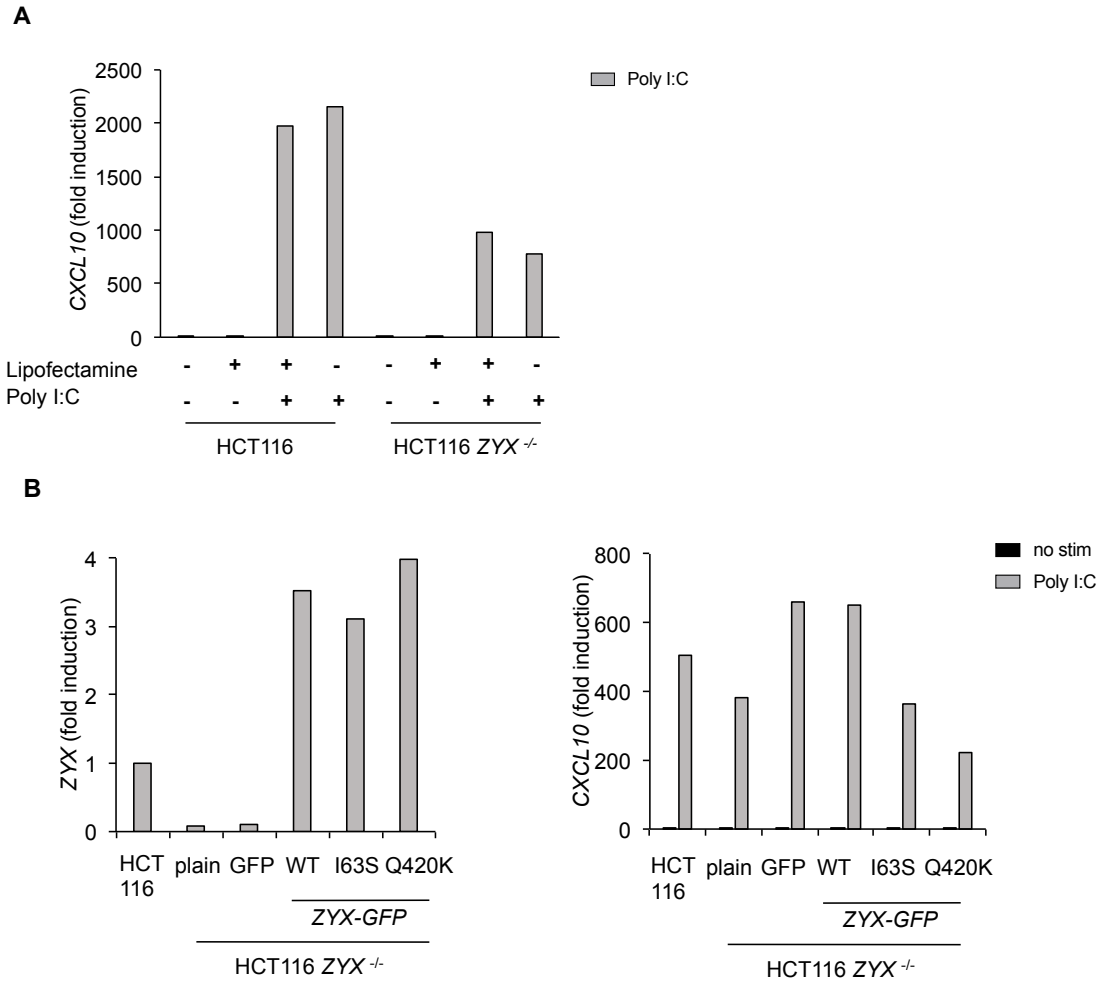

Figure 17 ZYX deficiency impairs *CXCL10* mRNA expression upon Poly I:C stimulation.

HCT116, HCT116 *ZYX*$^{-/-}$ (plain), and HCT116 *ZYX*$^{-/-}$ stable overexpressing variants of *ZYX (WT, I63S, Q420K)-GFP* were used for the determination of *CXCL10* mRNA expression upon Poly I:C stimulation (5 µg/mL) ± Lipofectamine 3000 for 6 h. A) *CXCL10* expression was determined by qPCR, normalized to *GAPDH* in HCT116 and HCT116 *ZYX*$^{-/-}$ cells. Cells were stimulated ± Lipofectamine 3000. (n=1) B) Representative *CXCL10* and *ZYX* mRNA expression was determined by qPCR, normalized to *GAPDH*. Cells were stimulated without Lipofectamine 3000. (n=2)

4.3.2. Investigating *ZYX* deficiency variants in BLaER1 cells.

As there were no clear results on the influence of ZYX and its variants on the colorectal carcinoma cell line HCT116, we decided to study its influence on BLaER1 monocyte transdifferentiation model [203]. We generated CRISPR/Cas9-mediated *ZYX* knockout cells (BLaER1 *ZYX*$^{-/-}$) and analyzed their TLR3 response upon Poly I:C stimulation. FACS analysis showed that the general protocol for transdifferentiation worked for ZYX deficient BLaER1 cells, as indicated by CD14+ monocytoid cells (Figure 18A). Immunoblotting of BLaER1 cells and BLaER1 *ZYX*$^{-/-}$ revealed an impairment of NF-κB, P38 and P44/42 Mitogen-activated protein kinase (MAPK) signaling and its phosphorylation when stimulated by Poly I:C (Figure 18B). Further, a decreased type I interferon response in ZYX deficient monocytoid BLaER1 cells was detected, as suggested by a reduced expression of *IFNB1, CXCL10* and *IL8* upon Poly I:C stimulation (Figure 18C), confirming previous data from HeLa cells and THP-1 macrophages [183]. In addition, pro-inflammatory induction of *TNF* expression was induced and lower in ZYX deficient monocytoid BLaER1 cells (Figure 18C).

Additionally, we investigated the inflammasome activation in Zyxin-deficient BLaER1 cell model. The inflammasome is a multi-protein complex, activated by two activation steps. First, DAMPs or PAMPs induce pro-inflammatory cytokine production (IL-1β and IL-18) through NF-κB signaling, a process named priming. A second signal (e.g. extracellular ATP, RNA viruses, or pore-forming toxins) leads to an activation and the usually inactive NLRP3 undergoes a conformational change [79, 228]. NLRP3 assembles to oligomers and provides a platform to recruit apoptosis-associated speck-like protein containing a CARD (ASC) through their pyrin domain [79, 228]. The other part of ASC activates Caspase-1 (CASP1) through their Caspase activation and recruitment domain (CARD) effecting the cleavage of CASP1 to active CASP1 which consecutively cleaves pro-IL-1β to the active, mature IL-1β form [79]. In our studies, we could show that ZYX deficiency resulted in significant alteration of NLRP3 activity and IL-1β secretion upon LPS and Nigericin stimulation after 3 h (short-term) but not within 18 h of LPS ± Nigericin (long-term) stimulation (Figure 18D).

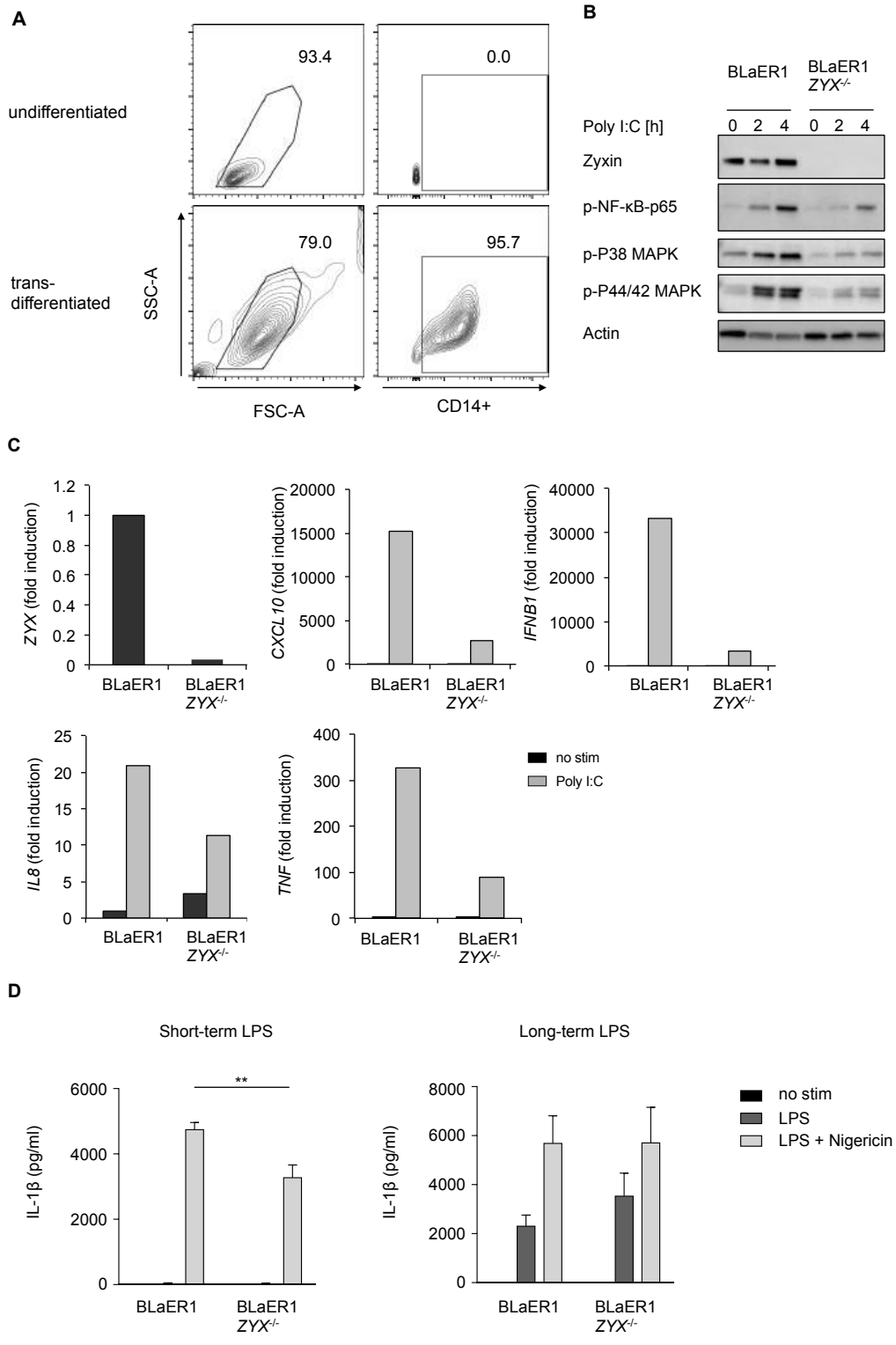

Figure 18 Impaired signaling and pro-inflammatory cytokine production in monocytoid *ZYX*$^{-/-}$ BLaER1 cells.

A) Representative FACS analysis of CD14+ cells after 7 days transdifferentiation. (n=2) B) Immunoblotting of transdifferentiated BLaER1 cells and BLaER1 *ZYX*$^{-/-}$ upon Poly I:C (2 µg/mL) stimulation for up to 4 h for NF-κB and MAPK key molecules. (n=3) C) Representative *ZYX, CXCL10, IFNB1*, *IL8* and *TNF* mRNA expression was determined by qPCR, normalized to *GAPDH*. Cells were treated 6 h with Poly I:C (2 µg/mL) or not stimulated (no stim). (n=3) D) Knockout of *ZYX* alters NLRP3 inflammasome activity. IL-1β secretion measured by ELISA

upon LPS stimulation 20 ng/mL for 3 h (short term LPS) or 200 ng/mL for 18 h (long term LPS) ± Nigericin. ** p<0.01. (n=3)

Further, we wanted to test the ZYX variants in a heterologous monocytoid model and reconstituted BLaER1 *ZYX*$^{-/-}$ cells by stable and lentiviral transduction of *pRRL-ZYX-IRES-RFP* (WT, I63S, Q420K) constructs. FACS analysis confirmed that cells sorted for RFP with similar mean fluorescence intensity (MFI), followed by transdifferentiation, were able to generate similar CD14+ cells for all reconstituted cell lines (Figure 19A).

Since our experiments showed that ZYX deficiency impairs NLRP3 inflammasome activity by short-term LPS (20 ng/mL) + Nigericin stimulation for 3 h, we repeated the experiment with all reconstituted BLaER1 cell lines and examined IL-1β secretion by ELISA (Figure 19B). While ZYX deficiency showed a lower IL-1β secretion for BLaER1 *ZYX*$^{-/-}$ and BLaER1 *ZYX*$^{-/-}$ *IRES-RFP* upon LPS + Nigericin, reconstitution with *ZYX* constructs was not able to achieve IL-1β secretion levels like normal BLaER1 cells (Figure 19B, left). Furthermore, 18 h stimulation with LPS or LPS (200 ng/mL) + Nigericin did not show any differences in IL-1β secretion in all heterologous cells (Figure 19B, right).

However, immunoblotting revealed a very low expression of ZYX in reconstituted BLaER1 *ZYX*$^{-/-}$ cells in comparison to the endogenous level of BLaER1 cells (Figure 19C). Despite this, ZYX deficiency sustained a delay in phosphorylation of NF-κB-p65, P38 MAPK and P44/42 upon Poly I:C (2 µg/mL) for up to 4 h (Figure 19C). In consideration of low ZYX (WT, I63S, Q420K) protein expression, the phosphorylation of NF-κB and MAPK signature proteins could be still detected after 4 h Poly I:C stimulation, suggesting a low impact of the ZYX patient variants (I63S, Q420K) on NF-κB and MAPK signaling.

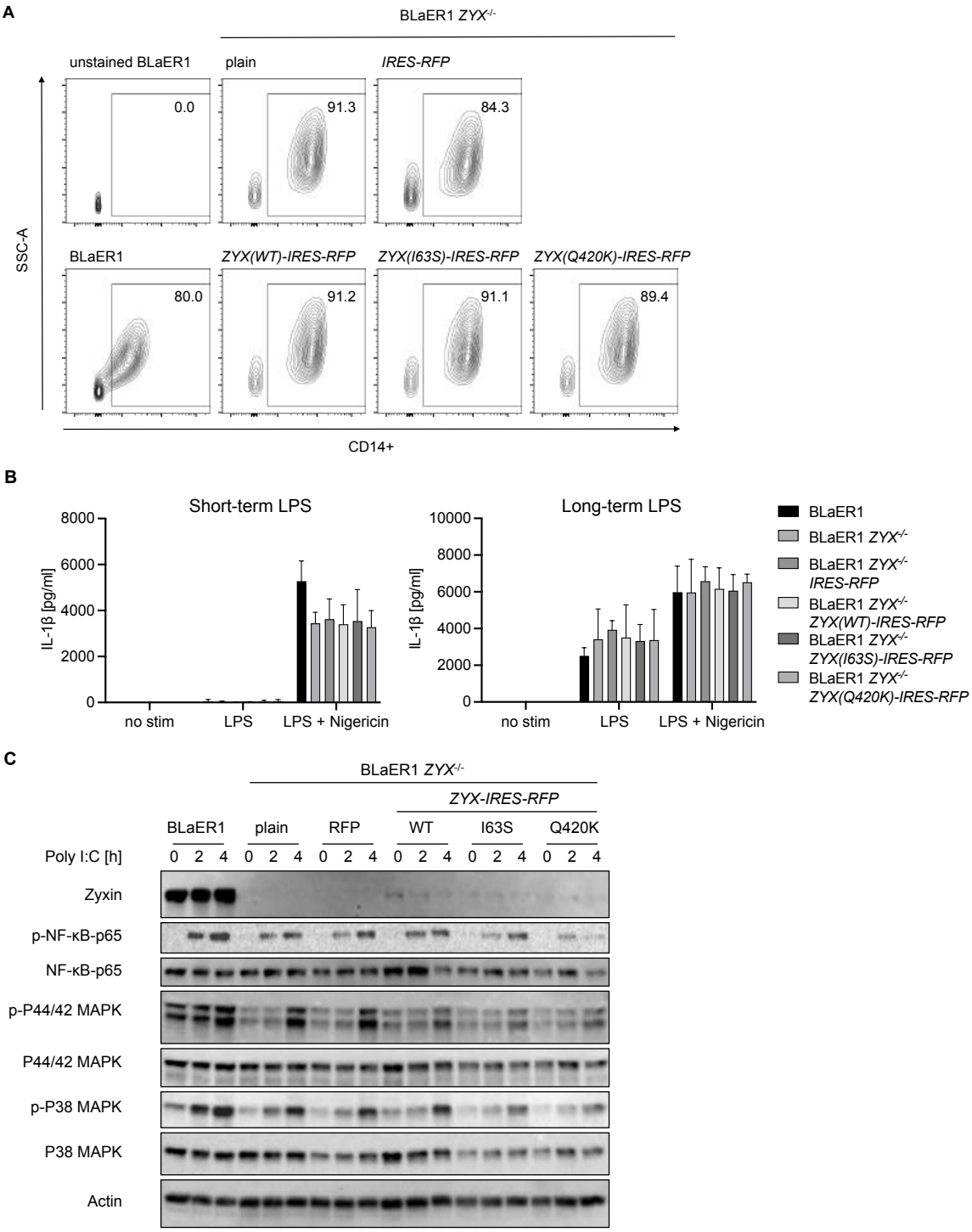

Figure 19 Reconstitution of *ZYX* variants in BLaER1 *ZYX*$^{-/-}$ cells.
A) Transdifferentiation of BLaER1 and BLaER1 *ZYX*$^{-/-}$ cells, reconstituted RFP and ZYX variants (wild-type (WT), I63S, Q420K). (n=3) B) IL-1β secretion was measured by ELISA upon LPS stimulation (20 ng/mL) for 3 h (short-term, left) or LPS stimulation (200 ng/ mL) 18 h (long-term, right) LPS ± Nigericin. (n=2). C) Immunoblotting revealed low ZYX protein upon reconstitution of BLaER1 *ZYX*$^{-/-}$ cells with *ZYX-IRES-RF*P constructs. Knockout of *ZYX* (plain and RFP only) led to less NF-κB and MAPK signaling upon Poly I:C (2 µg/mL) stimulation for up to 4 h. (n=3)

4.3.3. Assessment of ZYX deficiency in iPSC-derived macrophages

To assess our previous findings from our ZYX deficient cell lines (HCT 116, BLaER1), we examined genetically engineered induced pluripotent stem cells (iPSCs). We generated ZYX-deficient iPSCs (iPSCs *ZYX*$^{-/-}$) and WT clones, differentiated these into macrophage-like cells and studied their pro-inflammatory cytokine secretion and signaling.

FACS analysis confirmed that ZYX-deficient iPSCs (iPSCs *ZYX*$^{-/-}$) were able to derive macrophage-like cells from iPSCs, with similar surface protein expression upon the differentiation process as compared to WT clones. More than 80 % of all clones were positive for hematopoietic cell marker CD45, and over 45 % of the floating cells were positive for CD14 on day 13 (Figure 20A). Immunoblotting confirmed ZYX knockout in iPSCs (Figure 20B). Cell morphology was analyzed by cytospin of WT and *ZYX*$^{-/-}$ iPSCs with May-Grünwald and Giemsa staining, which revealed macrophage-like cells in light microscopy (Figure 20C).

Two clones of iPSCs WT and iPSCs *ZYX*$^{-/-}$ were used to analyze TLR3- and TLR4-mediated signaling in iPSC-derived macrophages. LPS stimulation (20 ng/mL) ± Nigericin for 3 h showed similar IL-1β secretion for the WT macrophages, compared to ZYX-deficient cells (D). LPS stimulation (200 ng/mL) ± Nigericin for 18 h, revealed unequal IL-1β secretion for the WT clones, while *ZYX*$^{-/-}$ cells were similar to WT (Figure 20D). However, Poly I:C (2 µg/mL) stimulation for up to 4 h revealed no major differences in NF-κB and MAPK signaling, since a stable phosphorylation pattern for iPSCs-derived macrophages *ZYX*$^{-/-}$ was established within 2 h of stimulation (Figure 20E).

Collectively, our experimental studies using different cellular models (HCT116, BLaER1, iPSCs) could not unveil a functional defect of the identified Zyxin patient-derived variants. Despite this, the analysis of ZYX deficiency suggested a potential role in inflammasome activity by the help of Zyxin in BLaER1 cells and an impact on pro-inflammatory cytokine induction (*IL8, TNF*) and type I IFN responses (*CXCL10, IFNB*).

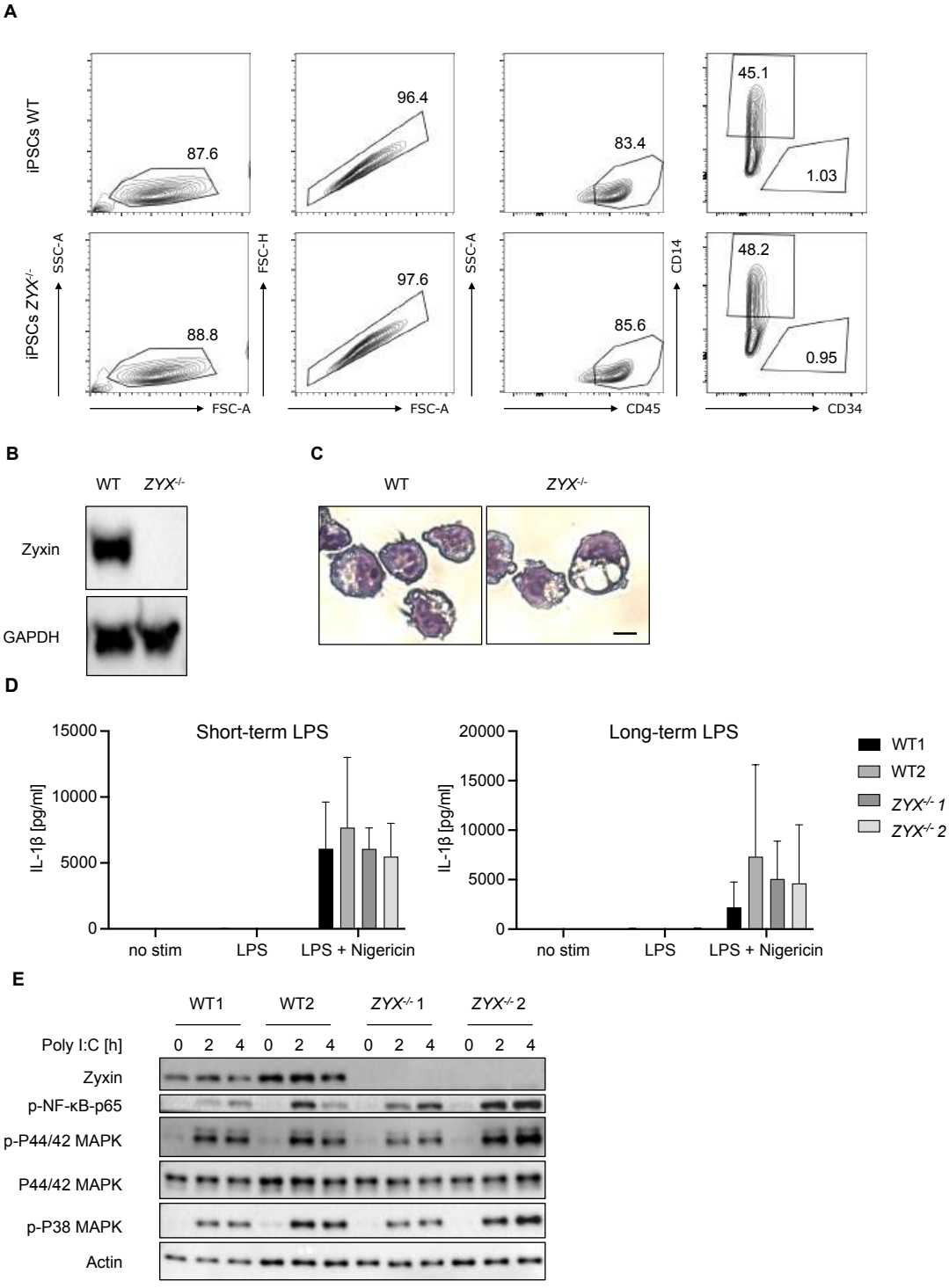

Figure 20 Analysis of iPSC-derived macrophages wild-type (WT) and ZYX deficient (*ZYX*$^{-/-}$).

A) FACS analysis of iPSC-derived macrophages on day 13, determining surface expression of CD45, CD34 and CD14. (n=3) B) Immunoblotting for Zyxin expression of iPSCs. (n=3) C) Cell morphology analysis by May-Grünwald and Giemsa staining on day 13 (n=1). Scale bar 10 µm. D) IL-1β secretion measured by ELISA upon LPS stimulation (20 ng/mL) for 3 h (short-term LPS) ± Nigericin and LPS stimulation (200 ng/mL) for 18 h (long-term LPS) ± Nigericin. (n=2) E) Immunoblotting for NF-κB and MAPK signaling upon Poly I:C (2 µg/mL) stimulation for up to 4 h on different iPSC-derived macrophage clones. (n=3)

4.4. Identification of a VEO-IBD patient with a rare biallelic homozygous 3 bp in-frame deletion in *LY96*

A rare biallelic homozygous 3 bp in-frame deletion of *LY96* was identified on the human genome assembly GRCh37.p13 upon WES analysis. The variant was found on the human transcript ENST00000284818.2, on chromosome position chr8:74939034, in the protein coding exon 4, as part of consensus coding sequence CCDS6216, encoding the protein MD2. The homozygous 3 bp in-frame deletion in the *LY96* gene (c.347_349delCAA, p.Thr116del) in patient A.II-1 (P1) and sibling A.II-5 (P2) was confirmed by Sanger sequencing of the patient and first-degree relatives (Figure 21A). The inheritance pattern showed an autosomal recessive mendelian pattern with incomplete penetrance regarding the intestinal phenotype. The younger sibling (A.II-5, P2) had a previous diagnosis of recurrent infections such as pneumonia and otitis media, without an IBD phenotype. In contrast, both parents were heterozygous (A.I-1, A.I-2), while non-affected siblings represented either homozygous wild-type (A.II-7) or heterozygous alleles (A.II-2, -3, -6, -8). No material was available for individual A.II-4.

The index patient A.II-1 was diagnosed with IBD within his first year of life. He suffered from frequent bloody diarrhea since the age of three months and was hospitalized subsequently due to two deep anal ulcers. He was treated with corticosteroids and additional immunomodulators such as azathioprine, methotrexate, cyclosporine as well as anti-TNF (infliximab, adalimumab) and anti-$\alpha_4\beta_7$ integrin antibody therapy (vedolizumab) resulting only in partial disease improvement. At the age of 6 years, he developed persistent pneumonia that required lobectomy of the left lower lobe and lingula. Physical examination revealed a short stature and clubbed fingers. Besides mild hypoalbuminemia, hyperimmunoglobulinemia, and positive IgA anti-*Saccharomyces cerevisiae* antibodies, further immunologic and genetic examination of known immunodeficiencies were not conclusive. At the age of 12 years, the index patient underwent laparoscopic subtotal colectomy and ileostomy, which improved the patient's general status and weight gain. The younger brother of the index patient (A.II-5), harboring the same genetic variant of *LY96*, had a history of pneumonia and otitis media, but had yet not developed an IBD phenotype.

4.5. The patient variant possibly alters MD2-LPS interaction

The prediction analysis of the 3 bp in-frame deletion on the function of MD2 could not be evaluated by PolyPhen and SIFT values. At the time of evaluation, no homozygous variant at gnomAD was found in healthy individuals or our internal variant database. For protein structure visualization, the crystal structure of human MD2 was used from protein data bank number 2E56 (Figure 21B) [229].

The membrane bound TLR4 receptor requires its accessory protein MD2 and dimerizes upon LPS binding with another TLR4-MD2-LPS complex, leading to subsequent signaling through the TIR domains, and initiating an intracellular cascade of MYD88 dependent and independent signaling [230]. MD2 binding to LPS is thereby crucial for TLR4-mediated downstream signaling function. The identified 3 bp in-frame deletion (Thr116) lies in close proximity of the LPS binding site of MD2 (Val119-Ser123) and suggested a potential interference with LPS-dependent signaling (Figure 21B). TLR4 signaling was formerly described to be a sensitive signaling pathway regulating bacterial handling and homeostasis in patients with IBD [231].

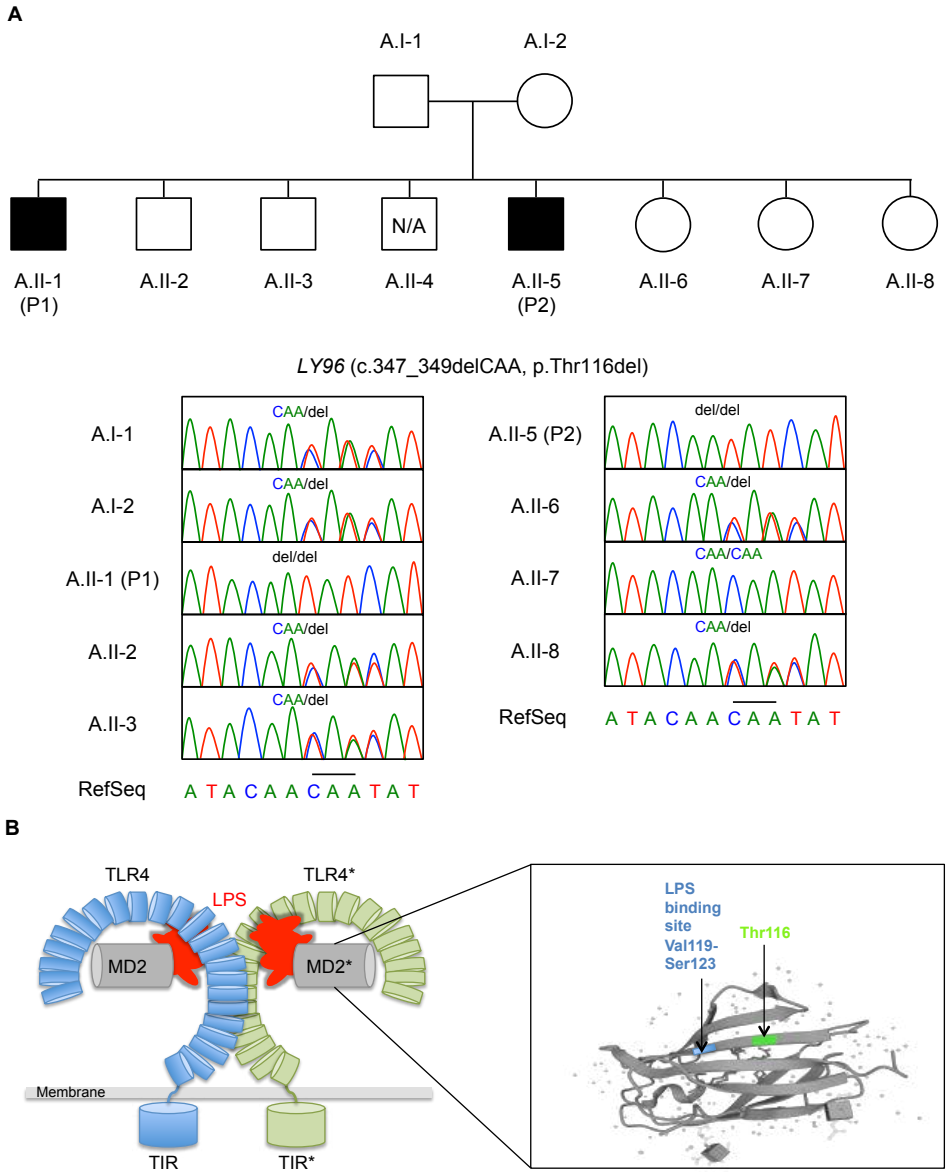

Figure 21 Segregation analysis of a rare homozygous 3 bp in-frame deletion in the *LY96* gene (c.347_349delCAA, p.Thr116del).

A) Pedigree of the non-consanguineous family. A rare homozygous 3 bp in-frame deletion in *LY96* was confirmed by Sanger Sequencing in the VEO-IBD patient (A.II-1, P1) and a younger sibling (A.II-5, P2). N/A, no material available. B) The membrane bound TLR4 receptor requires the accessory protein MD2 and dimerizes upon LPS binding with another TLR4*-MD2*-LPS complex, leading to MYD88-dependent and -independent signaling. The magnified crystal structure of PDB2E56 displays the identified deletion of threonine 116 (green) in close proximity to the LPS binding site of MD2 (Val119-Ser123 in blue). Modified from Park and Lee, modified from Ohto et al. [229, 232].

4.6. Analysis of patient-derived monocytes with a homozygous 3 bp in-frame deletion in *LY96*

4.6.1. Impaired LPS signaling in patient-derived monocytes

Previous studies of human and mouse models underlined the critical function of MD2 in mediating LPS responsiveness through TLR4 [233, 234].

First, we assessed the impact of the variant on protein expression. Immunoblotting of PBMC lysates revealed a reduced expression of MD2 in the index patient (A.II-1) and sibling (A.II-5) in comparison to healthy donors (HD) and the father (A.I-1) (Figure 22A).

To evaluate possible alterations in TLR4 signaling, we investigated LPS responses in PBMC-derived monocytes from healthy donors and family members (Figure 22B). We next analyzed IL-1β secretion of PBMC-derived macrophages by ELISA upon long-term (18 h, 200 ng/mL) LPS ± Nigericin treatment to test for inflammasome activation (Figure 22B). Interestingly, the monocytes of the index patient (A.II-1, P1) and sibling (A.II-5, P2) revealed a significant lower IL-1β secretion in comparison to healthy controls.

To assess the decreased IL-1β secretion in greater detail, we evaluated IL-1β protein expression, induction and secretion in supernatants (SNT) and lysates by immunoblot analysis (Figure 22C). The healthy travel control (TC), healthy sibling (A.II-3) and father (A.I-1) revealed induction of pro-IL-1β and IL-1β in lysates and supernatants, while only slight induction could be detected in the index patient (A.II-1) and sibling (A.II-5) harboring the 3 bp deletion in *LY96*.

Taken together, these results suggested an impaired LPS-mediated pro-inflammatory cytokine production driven by MD2 dysfunction in PBMC-derived monocytes.

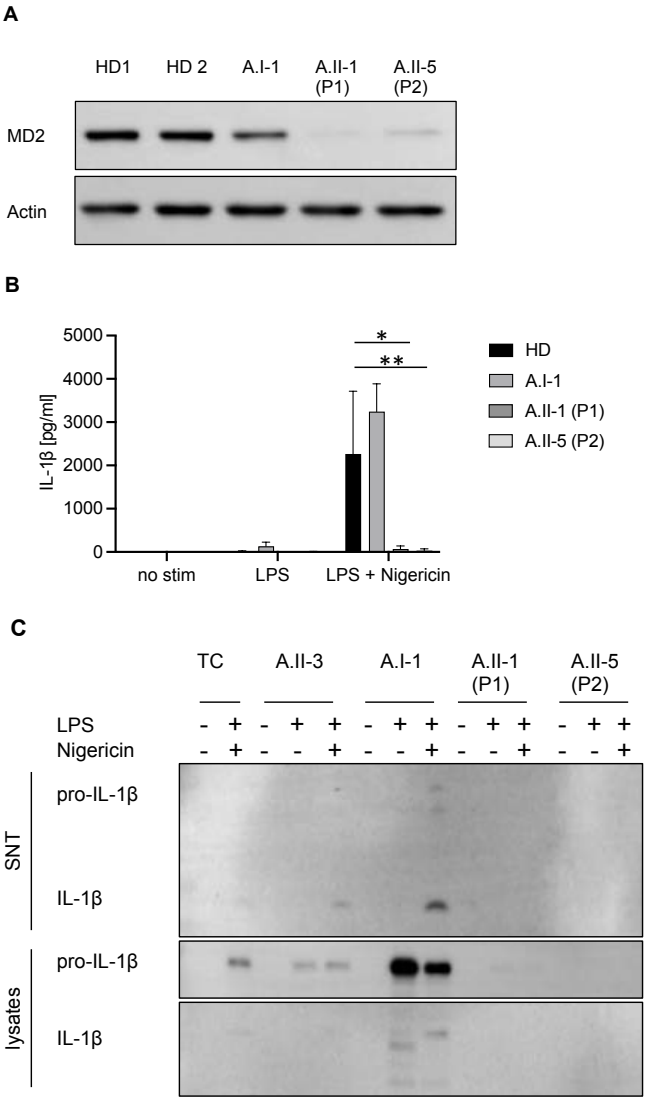

Figure 22 Dysfunctional MD2 leads to LPS hyporesponsiveness in PBMC-derived monocytes.

A) Reduced MD2 expression in PBMCs from the index patient (A.II-1) and sibling (A.II-5) were detected in comparison to the heterozygous father (A.I-1) and 2 healthy donors (HD) (n=1). B) MD2 deficiency alters NLRP3 inflammasome activity in PBMC-derived monocytes of the index patient (A.II-1) and sibling (A.II-5) in comparison to healthy donors (HD), and the father (A.I-1). IL-1β secretion measured ELISA upon LPS stimulation (200 ng/mL for 18 h) ± Nigericin. (n=2) C) Immunoblotting of supernatants (SNT) and lysates from monocytes reveals a reduced induction and secretion of pro-IL-1β and IL-1β in the patient and sibling harboring the deletion of Thr116 in MD2 (A.II-1, A.II-5) in comparison to travel control (TC) or unaffected family members upon 200 ng/mL LPS ± Nigericin stimulation for 18 h. (n=2). * $p<0.05$, ** $p<0.01$

4.7. Assessment of functional relevance of MD2 deficiency in iPSC-derived macrophages

4.7.1. Generation of iPSC lines with KO or patient-specific mutation by CRISPR/Cas9-mediated engineering

To evaluate the potential dysfunction of MD2 and to gain further pathomechanistic insights, we engineered an iPSC model by CRISPR-Cas9 editing. Knockout of MD2 in iPSC single clones occurred by disrupting the *LY96* with a 146bp deletion (KO). The index patient variant was implemented by a knockout of the 3 bp in-frame deletion in iPSC single clones (further mentioned as T116del) and wild-type iPSC single clones (WT) were obtained following engineering without specific guide RNAs.

In line with the established protocol to generate iPSC-derived macrophages, over 90 % of cells were CD45 positive and no differences in CD14 and CD34 surface expression patterns and morphologies could be detected for MD2-deficient cells during the differentiation process on day 13, 16, or 20 (Figure 23A-C). For functional studies, iPSC-derived macrophages were harvested between day 21 and 34. FACS analysis of CD45-positive cells for TLR4 and CD14 expression occurred in steady state conditions. No differences in the mean fluorescence intensity of TLR4 and CD14 were detected for MD2-deficient cells in comparison to wild-type (Figure 23D).

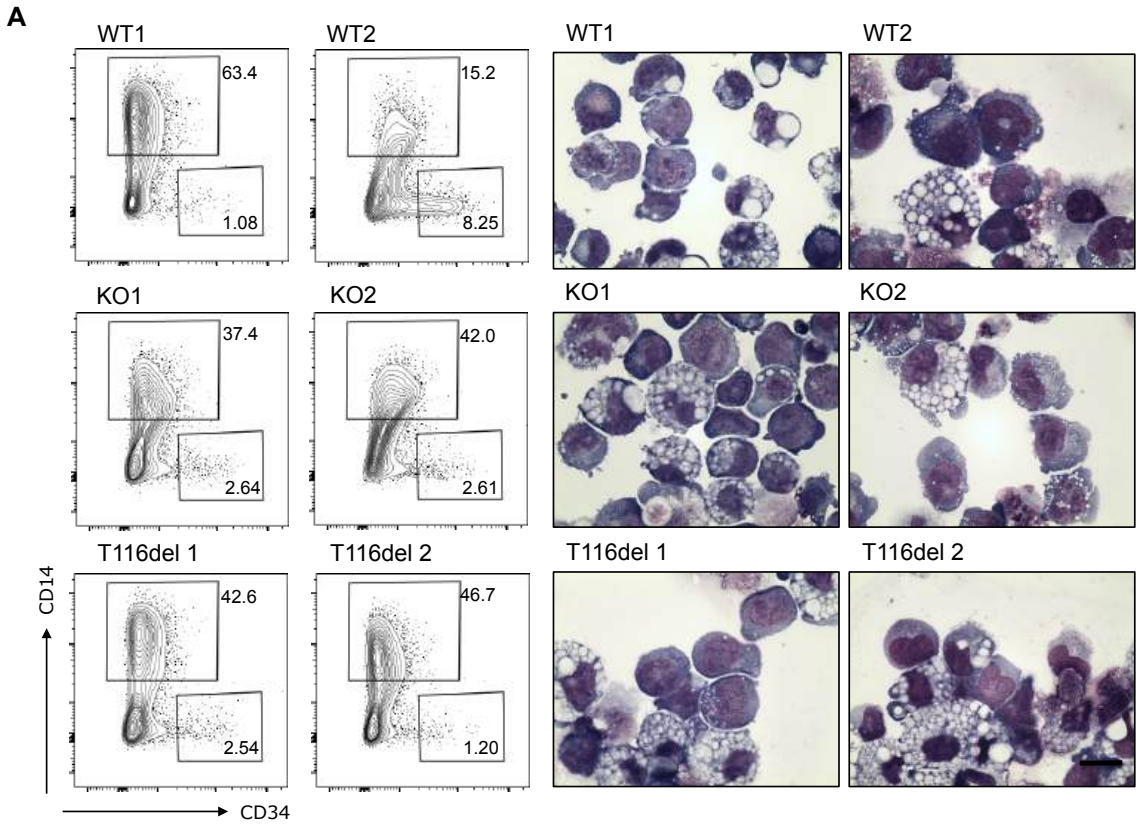
A
WT1
WT2
63.4
1.08
15.2
8.25
KO1
KO2
37.4
2.64
42.0
2.61
T116del 1
T116del 2
42.6
2.54
46.7
1.20
CD14
CD34

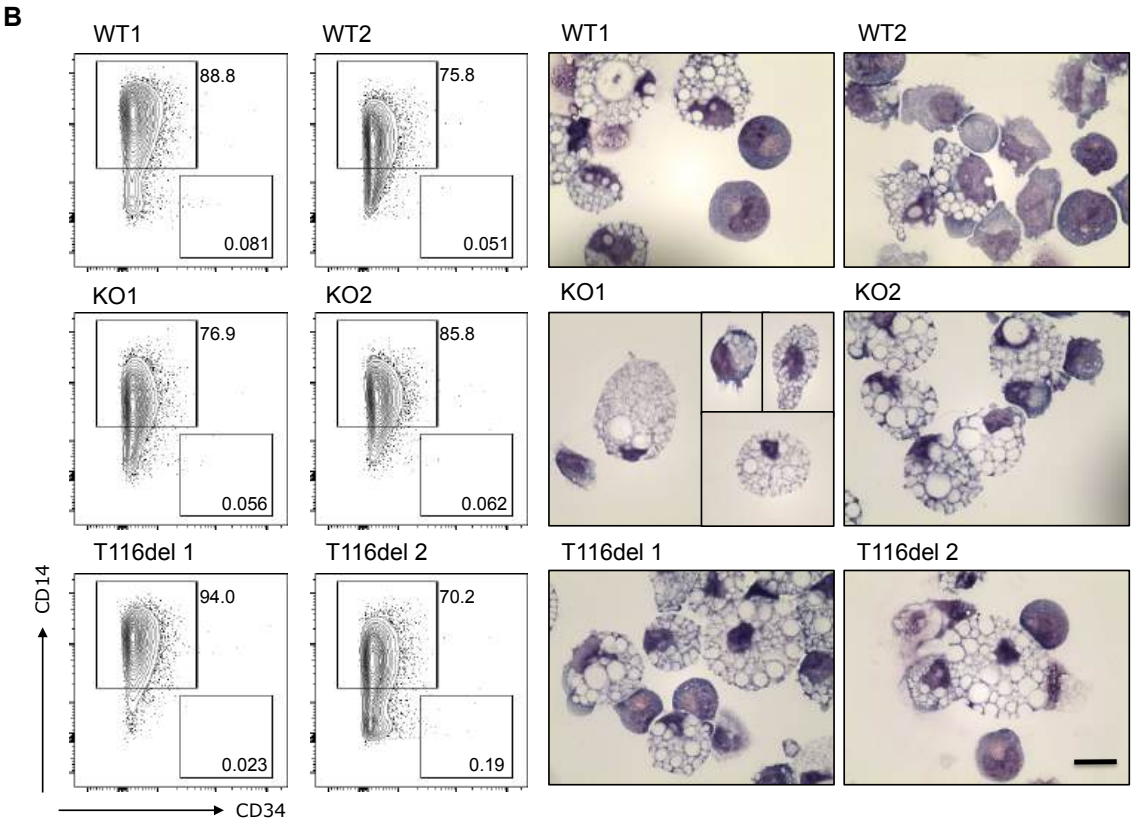
B
WT1
WT2
88.8
0.081
75.8
0.051
KO1
KO2
76.9
0.056
85.8
0.062
T116del 1
T116del 2
94.0
0.023
70.2
0.19
CD14
CD34

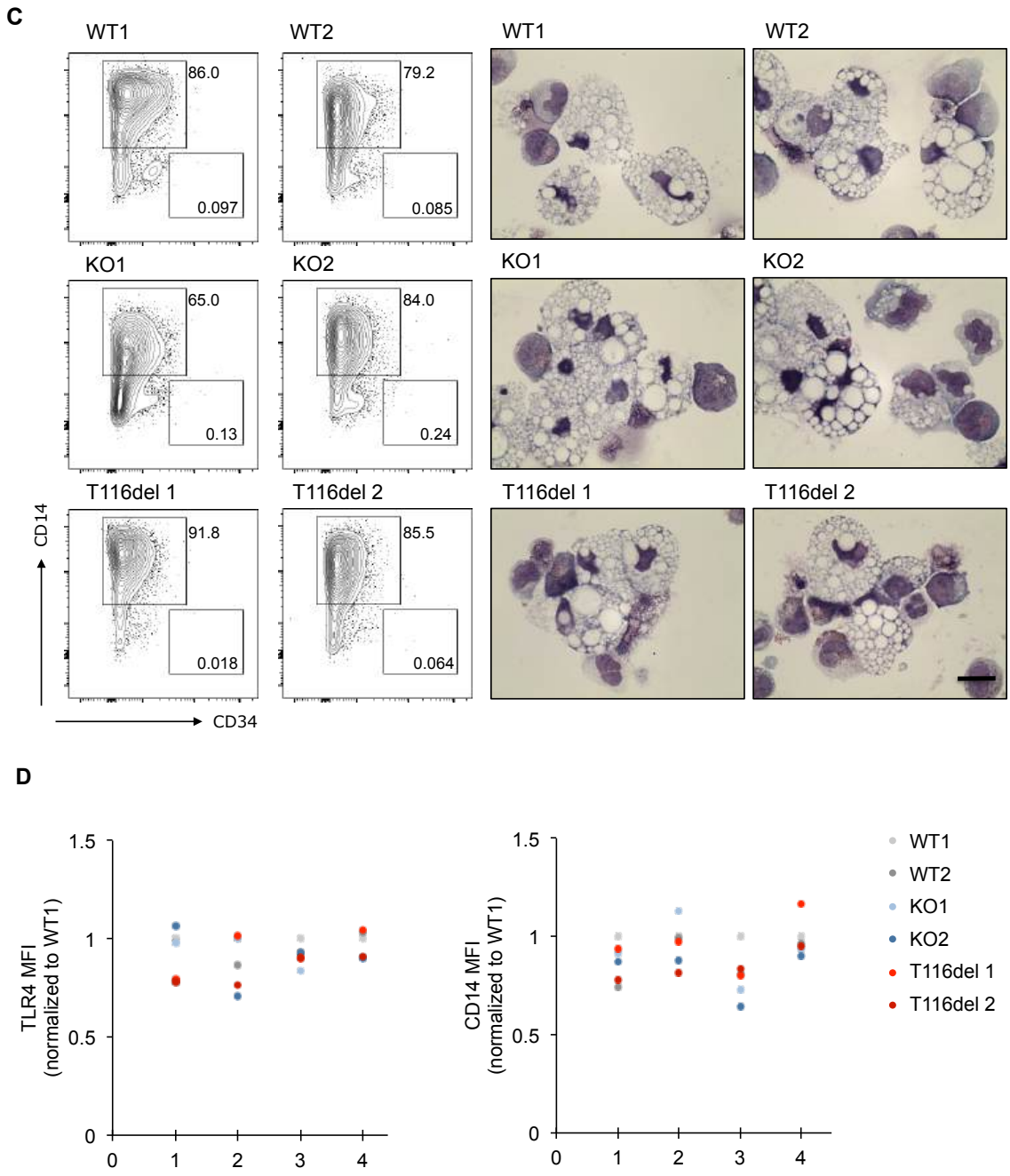

Figure 23 MD2 (KO, T116del) has no impact on the differentiation of iPSCs to macrophages.

iPSC-derived macrophages (single clones WT1, WT2, KO1, KO2, T116del 1, T116del 2) were analyzed for hematopoietic- and macrophage-specific cell surface protein expressions by FACS. Cells were gated for hematopoietic marker CD45 and analyzed for the hematopoietic precursor marker CD34 and macrophage surface marker CD14, during the macrophage differentiation process on day 13 (A), day 16 (B) and day 20 (C). In parallel, cell morphologies were evaluated of iPSC-derived macrophages by May-Grünwald and Giemsa stainings using light microscopy. Scale bar 10 µm. (n=3). D) iPSC-derived macrophages were harvested between day 21 and 34. CD45-positive cells were analyzed by FACS for the mean fluorescence intensity (MFI) of TLR4 and CD14 expression normalized to WT1 in steady state conditions, without major differences in MFI upon MD2 deficiency or T116del variant (n=1).

4.7.2. LPS responsiveness of MD2-deficient iPSC-derived macrophages

While undifferentiated iPSC clones remained unresponsive to LPS (Figure 24A), iPSC-derived macrophages responded to LPS. Temporal differences in LPS responsiveness upon MD2 deficiency were detected by immunoblotting (Figure 24B-C). Whereas iPSC-derived WT macrophages showed a physiological phosphorylation of target downstream signaling compounds like NF-κB-P65, P38 and P44/42 MAPK to LPS, a delayed and reduced LPS-mediated signal transduction could be detected in MD2 deficient macrophages (Figure 24B). Furthermore, MD2 deficient macrophages seemed less reactive to LPS in a dose-dependent manner (Figure 24C).

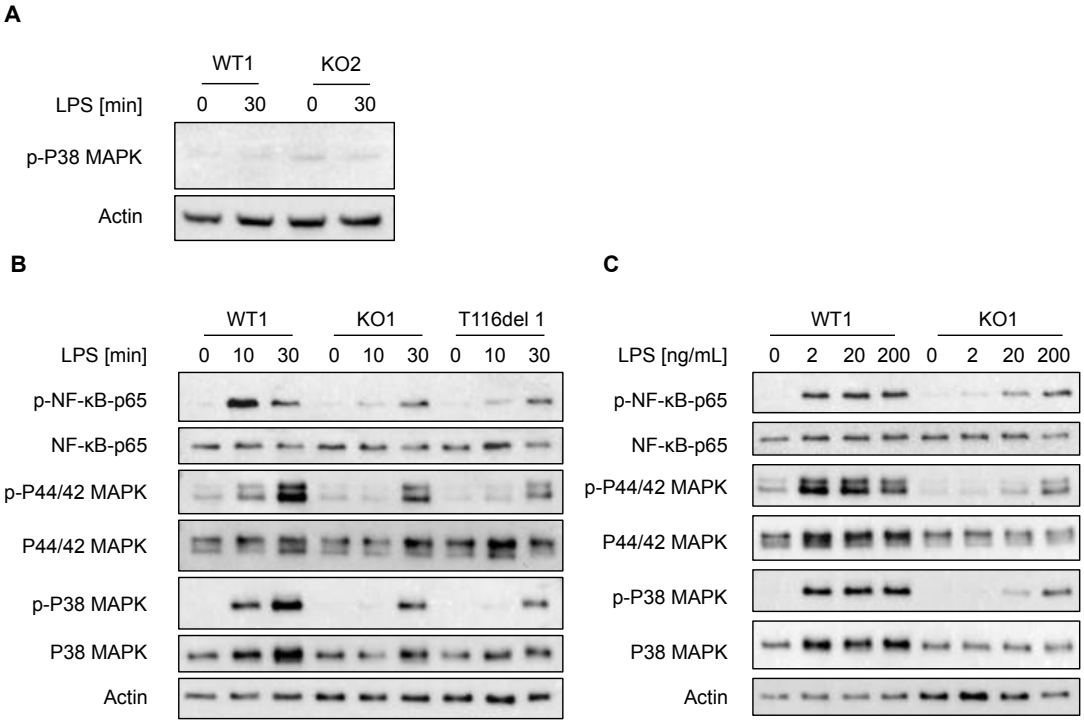

Figure 24 MD2 deficiency alters dynamic and responsiveness to LPS in iPSC-derived macrophages.
A) Immunoblotting of undifferentiated iPSC clones wild-type 1 (WT1) and knockout (KO2) were stimulated for 30 min with 200 ng/mL LPS and remained unresponsive to induce P38 mitogen-activated protein kinase (MAPK) phosphorylation by LPS stimulation. (n=1) B) iPSC-derived macrophages were stimulated for up to 30 min with LPS (200 ng/mL). Immunoblotting revealed a delay in phosphorylation of the NF-κB subunit p65, P38 and P44/42 MAPK signaling (n=3). C) Analysis of dose-dependent LPS responsiveness (2-200 ng/mL, 30 min) of iPSC-derived WT and MD2 knockout (KO1) macrophages showed an impaired phosphorylation of downstream signaling compounds (n=2).

4.7.3. MD2 deficiency amends pro-inflammatory cytokine responses in iPSC-derived macrophages

For the functional validation of the impaired LPS responses and NLRP3 inflammasome activity, we performed a short-term (3 h) LPS ± Nigericin stimulation of iPSC-derived macrophages to evaluate the release of IL-1β (Figure 25A). Short-term stimulation with LPS and Nigericin led to significantly lower IL-1β secretion in MD2 knockout iPSC-derived macrophages (KO1, KO2) or macrophages harboring the index patient variant (T116del 1, T116del 2) in comparison to WT macrophages. In WT iPSC-derived macrophages, LPS alone was able to induce low amounts of IL-1β, which was undetectable in MD2-deficient (KO, T116del) cells. Interestingly, ELISA revealed also a significantly reduced cytokine production for TNF in MD2-deficient cells upon LPS stimulation (Figure 25B).

Immunoblotting of the lysates underlined that the inflammasome activity is impaired upon MD2 deficiency (Figure 25D). LPS alone induced NLRP3 and pro-IL-1β expression in WT macrophages, but to a lesser extent in MD2-deficient cells (KO and T116del). Treatment with LPS plus Nigericin, the second signal, lead to the detection of cleaved CASP1 and less pro-IL-1β, since it is cleaved to mature IL-1β and extracellular secreted in WT macrophages. The cleavage of pro-IL-1β seemed to be compromised in MD2-deficient cells, supporting the findings of the altered IL-1β secretion by ELISA.

To investigate the effects of LPS responsiveness on other pro-inflammatory cytokines, we investigated the induction of *IL6* after 18 h stimulation LPS by real-time PCR in iPSC-derived macrophages from all genotypes (Figure 25C). Remarkably, these results showed significant lower *IL6* induction after 18 h of LPS stimulation, when MD2 is impaired (KO, T116del).

Notably, the deletion of one amino acid (p.T116del) of the patient-specific mutation displayed a functional disturbance of affected pro-inflammatory cytokine secretion (IL-1β, TNF) or induction (*IL6*) similar to the complete knockout of MD2.

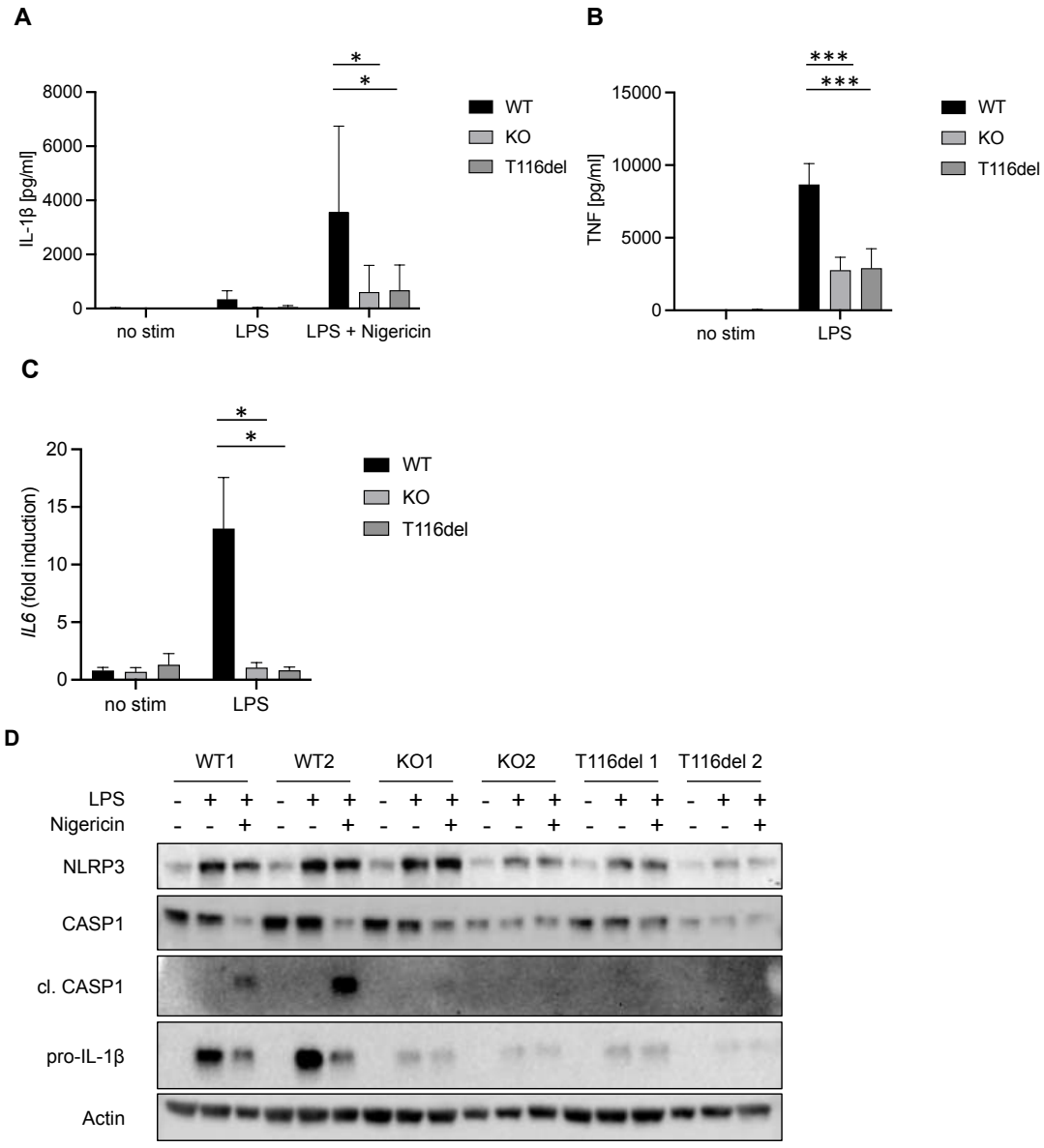

Figure 25 MD2 deficiency affects pro-inflammatory cytokine responses.
Analysis of iPSC-derived macrophages with a wild-type (WT) genotype, knockout (KO) or expression of the MD2 patient variant (T116del). A) MD2 deficiency alters NLRP3 inflammasome activity in iPSC-derived macrophages with MD2 knockout (KO1, KO2) and MD2 patient variant (T116del 1, T116del 2) compared to wild-type (WT1, WT2). IL-1β secretion measured by ELISA upon LPS stimulation 20 ng/mL for 3 h. (n=3) B) TNF ELISA showed an impairment of TNF secretion upon LPS stimulation 20 ng/mL for 3 h. measured by a representative TNF ELISA in iPSC-derived macrophages of MD2 knockout (KO1, KO2) and MD2 patient variant (T116del 1, T116del 2) compared to wild-type (WT1, WT2). (n=3) C) Analysis of real-time PCR of *IL6*, normalized to GAPDH upon LPS stimulation 20 ng/mL for 18 h. (n=2). D) Immunoblotting of lysates from short term LPS (20 ng/mL for 3 h) ± Nigericin stimulation for key inflammasome molecules NLRP3, CASP1, cleaved (cl.) CASP1 and IL-1β. (n=2). * $p<0.05$, *** $p<0.001$

4.7.4. Altered surface expression patterns upon M1/M2 polarization in MD2 deficient (KO, T116del) iPSC-derived macrophages

Macrophages can have completely opposing functions dependent on the exposure to stimulating cytokines. M1 macrophages are stimulated by LPS and IFN-γ, which promote pro-inflammatory processes and pathogen elimination [235]. M2 macrophage polarization is induced by IL-4, IL-10 and TGF-β, which plays a role in supporting processes like tissue repair and apoptotic cell clearance [235].

To discriminate the effects of MD2 deficiency (KO, T116del) on the capacity of M1 and M2 generation from our iPSCs, we stimulated our macrophages with the M1/M2 specific cytokines and analyzed their morphology as well as surface expression markers. Our iPSC-derived macrophages polarized to M1 and M2 phenotypes appeared normal in their cell morphology and independent of MD2 deficiency, when analyzed by May-Grünwald and Giemsa staining using light microscopy (Figure 26A). FACS analysis revealed that all cells were positive for CD14. Macrophages were analyzed for positive CD86, CD 163, CD274 and HLA-DR surface expression.
While an overall normal expression pattern of CD14 could be detected in all *in vitro* polarized macrophages, MD2-deficient (KO, T116del) M1 macrophages displayed higher surface expression of CD86 and HLA-DR in contrast to WT M1 macrophages (Figure 26B). Moreover, M2 macrophage differentiation based on CD163 surface expression showed a similar pattern amongst all genotypes (Figure 26B).

According to our previous findings, we were keen on the effect of pro-inflammatory cytokine production in our polarized macrophages. We investigated the supernatants of the M1 and M2 macrophages for IL-1β and TNF secretion after 24h of polarization (Figure 26C-D). We found significantly reduced cytokine levels in MD2-deficient (KO, T116del) M1 macrophages, supporting former findings of an impaired LPS responsiveness (Figure 26C-D).

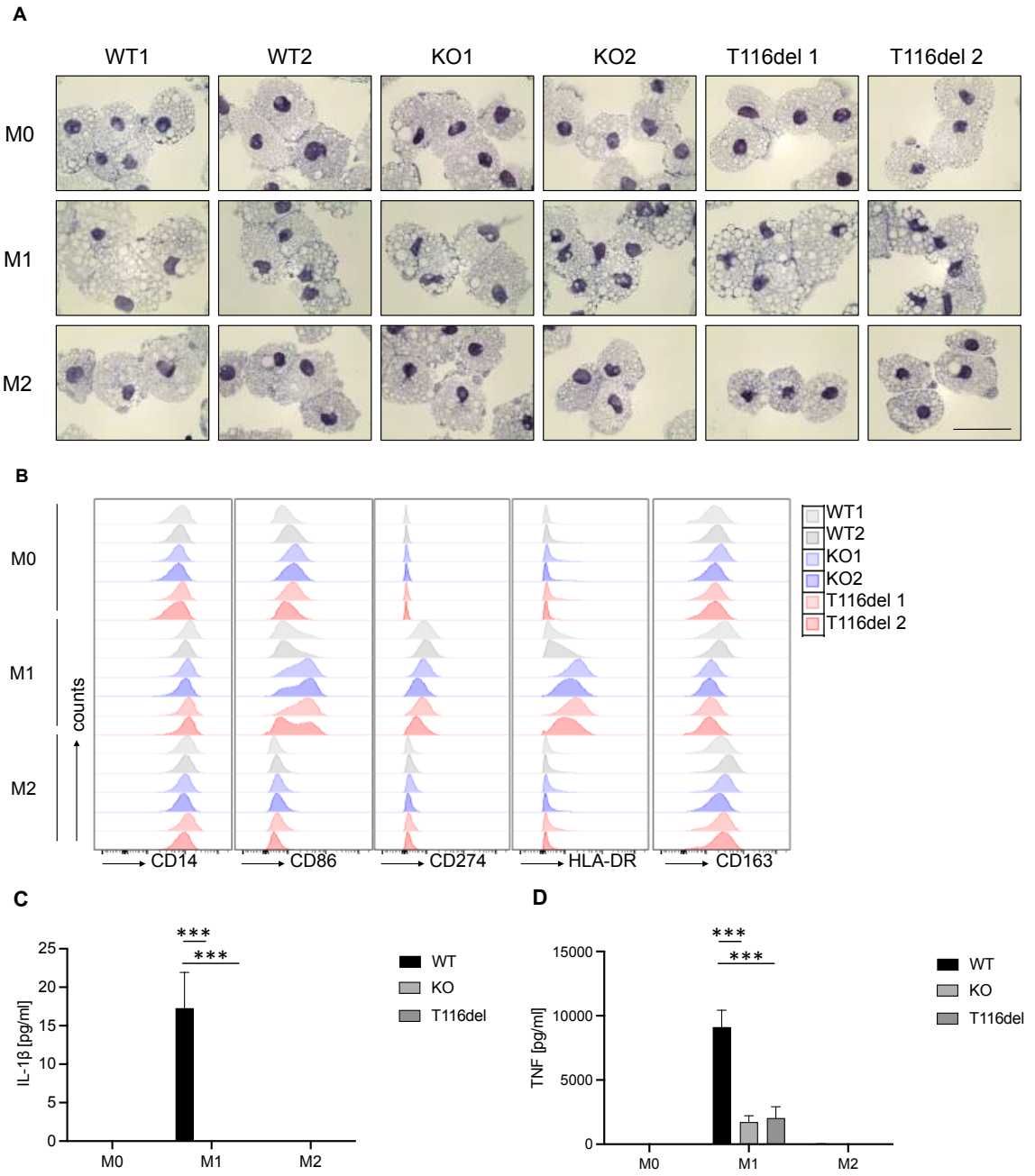

Figure 26 M1/M2 macrophage polarization of wild-type (WT) and MD2-deficient (KO, T116del) iPSC-derived macrophages.

Generation of M0 (no cytokines), polarization of M1 macrophages (LPS 50 ng/mL, IFN-γ 20 ng/mL) and M2 macrophages (IL-4 20 ng/mL, IL-10 20 ng/mL, TGF-β 20 ng/mL) for 24 h. A) Corresponding May-Grünwald and Giemsa staining of iPSC-derived macrophages were evaluated by light microscopy indicating no obvious alterations in cell morphologies. Scale bar 10 µm. (n=1) B) FACS analysis of surface expression markers CD86, CD163, CD274, HLA-DR. (n=3). C) IL-1β secretion of M0, M1 and M2 macrophages analyzed by ELISA upon polarization for 24 h. (n=2). D) Analysis of TNF secretion of M0, M1 and M2 macrophages by ELISA upon polarization for 24 h (n=2). *** p<0.001

4.7.5. Impaired handling of *Salmonella typhimurium* in MD2 deficient (KO, T116del) iPSC-derived macrophages

To assess bacterial handling of MD2-deficient iPSC-derived macrophages, we conducted a gentamycin protection assay by challenging macrophages with *Salmonella typhimurium* for 3 h and 6 h, in collaboration with Yue Li. After 3 h and 6 h only half of the colony-formation units were formed in MD2-deficient macrophages in comparison to WT macrophages (Figure 27). This suggested either increased killing or a lower phagocytosis capacity due to MD2 deficiency.

Interestingly, the investigation of the MD2 variant towards its function and bacterial handling displayed nearly identical features to a complete knockout of MD2.

Collectively, our data demonstrate that the index patient variant of a 3 bp in-frame deletion interferes with crucial LPS responsiveness in iPSC-derived macrophages, as indicated by cytokine secretion (IL-1β, TNF), induction of cytokine expression (*IL6*) and immunoblotting.

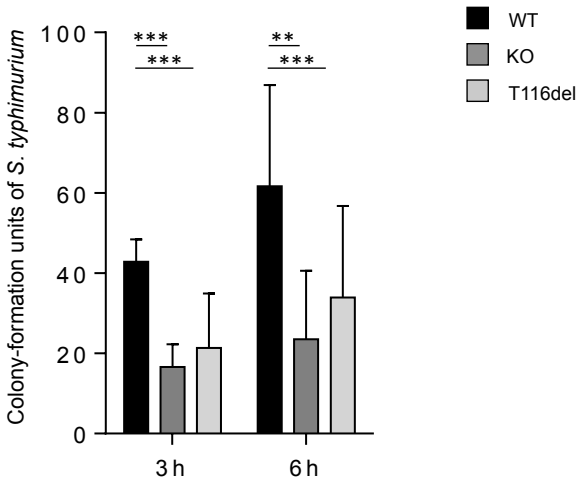

Figure 27 Handling of *Salmonella typhimurium* is impaired in MD2-deficient (KO, T116del) iPSC-derived macrophages.
Gentamycin protection assay of macrophages showed less colony-formation units of *S. typhimurium* after inoculation for 3 h or 6 h (n=3). ** p<0.01, *** p<0.001

5. Discussion

5.1. Patients with rare germline sequence variants and IBD

In the landscape of IBD, there have been increasing numbers of unclassified phenotypes over recent decades [31, 32]. In patients with an onset below six years of age, determined as VEO-IBD, incidences have increased dramatically [236]. These patients often present with a more severe and progressive disease course than common forms of an UC or CD phenotype. Furthermore, these patients are often accompanied with a higher potential of extra-intestinal manifestations. Consequently, conventional therapies often remain unsuccessful in VEO-IBD patients, necessitating surgeries, such as ileostomies or colectomies [237]. Therefore, there is an enormous demand to improve the clinical management of those patients by developing strategies to understand the pathomechanisms of IBD and to ultimately find possible treatment targets for therapeutic approaches.

The pathogenesis of IBD is multifactorial and highly heterogeneous, whereby environmental factors, complex immunological dysfunctions, epithelial barrier defects, imbalances of the microbial flora and genetic susceptibility can overlap with each other [48]. WES analyses were pioneering improvements for the comprehension of VEO-IBD and the role of monogenic variants in IBD pathogenesis [46, 144]. Our WES analysis of VEO-IBD patients revealed homozygous biallelic monogenic variants in *ZYX* or *LY96* genes, following an autosomal recessive Mendelian inheritance pattern. With this work, we shed light on the relevance and underlying pathomechanisms of the newly identified *ZYX* and *LY96* variants.

5.2. Analysis of the relevance of Zyxin variants in two unrelated VEO-IBD patients

5.2.1. Zyxin variants do not impair colocalization of proteins of focal adhesions

Prior to this work, there were no described cases of patients with IBD and monogenic variants in *ZYX*. Our first index patient was diagnosed with early-onset IBD at the age of 8, with a stricturing and penetrating disease behavior, atrophic gastritis, inflammatory infiltrates, and crypt abscesses. Our second patient had an age of onset of 2 years and was presented with growth failure, poor weight gain, non-bloody and bloody diarrhea, as well as a non-stricturing and non-penetrating disease behavior. Furthermore, he had severe viral infections that required hospitalization.

The epithelial barrier plays a key role of separating the luminal environment to the inside of the body and usually allows only selective absorption of nutrients or water, while preventing the entry of dangerous toxins, viruses or pathogens [238]. It is composed of the apical lumen, the mucus layer, and the basal monolayer of epithelial cells, forming a physical barrier. In IBD, abrogated protein functions of E-cadherin, FERMT1, TTC7A or EpCAM have been demonstrated to disturb the epithelial integrity and polarity of cells [167, 239-241]. As a consequence, increased permeability enables the infiltration of pathogens from the lumen to the lamina propria and can promote a continuous inflammation of the intestine and systemic immunological responses in susceptible individuals [242]. Pro-inflammatory cytokines such as IFN-γ or TNF can weaken the epithelial barrier and induce endocytosis of tight junction proteins (e.g. Junction adhesion molecule-1, Occludin or Claudin-1) independent of apoptosis [243]. Additionally, these proteins were found downregulated in samples of IBD patients [244]. The cell-cell contacts of the epithelial monolayer are well orchestrated by multiprotein complexes in apical tight junctions, adherens junctions and basal desmosomes, all contributing to an intact intestinal barrier function [245].

Zyxin is part of the adherens junctions, a multiprotein complex, linking the cytoskeleton to the extracellular matrix, which promotes actin dynamics and mechanosensitivity [182]. It acts as a scaffolding protein of cytoskeletal components facilitating migration, proliferation, and differentiation [177, 246].
Zyxin is ubiquitously expressed among all cell types but particularly in granulocytes and monocytes [247, 248]. Highest tissue RNA expression of *ZYX* is found in the endometrium and intestine based on the human protein atlas [247, 248]. The structure of Zyxin exhibits several functional domains. The N-terminus harbors the α-Actinin binding site, a proline-rich domain of ActA repeats that enables the interaction with ENAH/VASP and other actin binding proteins. Nuclear export signals promote shuttling of Zyxin between the cytosol and nucleus, and three C-terminal actin binding LIM domains associate Zyxin to focal adhesions [179, 249, 250]. Zyxins interactions with focal adhesion proteins such as Vinculin, Paxillin and VASP have been studied in detail [251].

Based on current research data, we hypothesized that ZYX variants might affect the function of focal adhesions and the linkage of the actin cytoskeleton to the extracellular matrix resulting in impaired epithelial barrier function. We investigated the function of Zyxin in intestinal epithelial HCT116 cells, genetically engineered by CRISPR/Cas9. We reconstituted the ZYX-deficient coloncarcinoma HCT116 cells with the stable overexpression of GFP-fused ZYX wild-type, ZYX p.I63S (near the proline-rich ENAH/VASP binding site) and ZYX p.Q420K (near the Actin-binding LIM domain).

Our colocalization studies by confocal microscopy revealed normal localization of Vinculin with all overexpressed ZYX variants on the leading edges of the cells and ablation of Zyxin had no impact on the Vinculin localization at focal adhesions [188]. In contrast, Zyxin deficiency in HCT116 cells led to a lack of VASP on the leading edges, as previously published in ZYX deficient mouse fibroblasts [188]. However, overexpression of all ZYX variants was able to restore and colocalize VASP to the leading edges of the cells at the focal adhesion. Accordingly, our hypothesized possible defect of the p.I63S variant near the VASP-binding site could not be proven. Furthermore, it has been proposed that ZYX deficiency leads to more ventral stress fibers and actin remodeling, although our phalloidin staining of HCT116 cells could not

confirm these findings in our study [252]. Moreover, the localization of Zyxin at the leading edges to the attached actin filaments seemed completely normal.

To better understand the functional relevance of the identified variants on cytoskeletal architecture and mechanosensing, force-induced recruitment of Zyxin to focal adhesion could provide more insights, along with its capability to shuttle to the nucleus. This could be investigated by mechanosensitive gene induction and Zyxin-regulated proteins upon mechanical stretch stress (e.g. Akt, CCAR1 or SIRT1) [182, 246, 253-255].

5.2.2. Normal monolayer generation and migratory behavior of Zyxin-deficient HCT116 cells

IBD patients tend to display increased permeability of the epithelial barrier in the intestine [256, 257]. Deficiency of tight junction proteins such as EpCAM or Occludin have been shown to result in decreased transepithelial resistance in colon carcinoma cell line T84 and MDCK cells or enhanced in CaCO2 cells [258]. To investigate permeability of cell monolayers, we analyzed transepithelial resistance upon ZYX deficiency in HCT116 cells. We could not to detect any differences. Wild-type and ZYX-deficient HCT116 cells increased resistance over time uniformly.

Zyxin can act as a tumor suppressor but can also promote progression, dependent on the entity [186]. *ZYX* overexpression was found in hepatocellular carcinoma, malignant renal tumors, and breast cancer, where its expression was shown to directly correlate with the malignancy severity status [259-261]. A study from 2018 provided additional evidence to the oncogenic role of Zyxin in colon cancer, as depletion of *ZYX* in a xenograft mouse model compromised cancer proliferation, migration, and development [262]. Zyxin can be phosphorylated and shuttled to the nucleus, by a transient interaction to focal adhesions [251, 263]. This transient association of ZYX to focal adhesion was postulated to promote oncogenesis and progression by weakening the focal adhesions. Since migratory capacities are a crucial factor for the functionality of focal adhesive proteins, small interfering RNA-mediated knockdown of ZYX in oral squamous cell carcinoma cells resulted in decreased migration, while Zyxin-depleted mouse fibroblasts showed a higher migration rate [188, 227]. Additionally, Zyxin

mediated vascular repair in endothelial cells was noted after wounding carotid artery's in mice and was indispensable for wound healing in MDCK cells [226, 264]. Our investigation of the migratory capacity and wound closure of our reconstituted heterologous HCT116 cells revealed no major difference between all analyzed samples. These data suggest no impairment of migratory capacities in HCT116 cells overexpressing each of our patient-derived variants. Furthermore, the colony formation assay showed no differences amongst the ZYX variants, concluding no major proliferative impairment. Migration assays through transwells towards extracellular matrix attractants (e.g. collagen type I or IV, laminin, or fibronectin) could help to better understand the migratory capacity of the ZYX variants, since it was shown that Zyxin-deficient vascular smooth muscle cells abrogate their migratory behavior [265].

5.2.3. Zyxin deficiency alters IFN I responses in cell models

Our investigations did not reveal obvious phenotypes in epithelial HCT116 cells in cytoskeletal and colocalization studies, TEER measurements and migration studies. Zyxin has been proposed to be involved in the endothelial exocytosis of von Willebrand factor, in which it helps to remodel the actin skeleton around secreted granules [266]. A recent study has shown that Zyxin binds to RIG-I and the mitochondrial protein MAVS and regulates interferon responses upon viral particle stimulation in HeLa and THP-1 macrophages [183].

Clearance of infected cells is crucial for stable homeostasis and prevents spreading of viral infections in the body. Specific sensors for PAMPs, viral DNA and RNA are part of the first line defense of the innate immune system. Poly I:C mimics dsRNA, which is found upon replication of a virus in a cell and is recognized by endosomal TLR3 [267]. TLR3 induces TRIF-dependent NF-κB and MAPK signaling, leading to pro-inflammatory responses such as TNF, IL-6 or IL-8 secretion, but can also initiate anti-viral responses such as IFN-β induction through the IRF3 pathway [268]. Besides TLR3, Poly I:C can alternatively be recognized by cytosolic sensor RIG-I and MDA-5 inducing type I IFN responses [269].

We showed that HCT116 can respond to Poly I:C stimulation, as indicated by induction of the interferon-inducible gene *CXCL10*. CXCL10 is a chemoattractant for regulatory T cells, natural killer cells, monocytes and is upregulated in the colonic mucosa of IBD patients [270]. Zyxin deficiency in HCT116 led to a lower induction of *CXCL10*, while overexpression of our *ZYX-GFP* constructs did not reveal substantial differences affecting *CXCL10* expression through our patient variants. However, lentiviral transduction and an up to fourfold higher *ZYX* expression may overshadow detectable effects and suggests the use of alternative plasmids or CRISPR/Cas9-mediated genetic engineering of the patient variants in HCT116 cells.

Zyxin is highly expressed in monocytes, therefore BLaER1 cells were used as a human monocytoid model. Investigations of genetically CRISPR/Cas9-engineered BLaER1 cells highlighted that ZYX deficiency was not only shown to reduce induction of antiviral *IFNB* and subsequent *CXCL10*, but also impaired pro-inflammatory *IL8* and *TNF* production. Furthermore, we could demonstrate that ZYX deficiency abrogated NF-κB, P38 and P44/42 MAPK phosphorylation in monocytoid BLaER1 cells but less conclusively in iPSC-derived macrophages. Unfortunately, reconstitution of BLaER1 ZYX-deficient cells with *ZYX-IRES-RFP* constructs revealed no stable overexpression of the Zyxin variants, even though RFP signals were similar based on the MFI among all groups. Optimization of the expression constructs may provide more reliable investigations of the ZYX variants. Stable CRISPR/Cas9-mediated knock-in of the variants could be another possible solution to circumvent (over-) expression systems.

Zyxin seems not to be the only focal adhesion and actin remodeler, which has been shown to influence type I interferon responses. Zyxin and focal adhesion kinase (FAK) are both part of focal adhesions and Zyxin-mediated repair responses are controlled by FAK [271]. FAK has been implicated in viral IFNB responses, since FAK deficiency leads to a higher RNA virus susceptibility and impairs NF-κB and IFN-β signaling [272]. FAK as well as RIG-I and Zyxin, are associated with MAVS [272]. The role of a functional actin skeleton for RIG-I was proposed to ensure proper antiviral signaling, while enabling quick shuttling to mitochondria, which may also similarly apply to Zyxin [273]. Furthermore, FAK deficiency in a DSS-induced colitis model drastically impaired epithelial cell proliferation healing [169]. Additional investigations of the antiviral response are needed to understand the underlying mechanisms of action, considering

that one patient suffered from recurrent and hospitalized infections. The diminished pro-inflammatory cytokine induction in Zyxin-deficient cells could explain an impact on viral clearance, leading to an imbalance in the intestinal homeostasis, which may necessitate further investigation.

5.2.4. Zyxin influences inflammasome activation

Prior to this work, Zyxins role in TLR4 signaling had not been studied, especially not in the NLRP3 inflammasome activation. The inflammasome is built upon LPS priming, while a second signal coming from DAMPs, ATP or membrane perforation, subsequently triggers IL-1β secretion of the cells [228].

We showed a significantly lower production of pro-inflammatory IL-1β upon 3 h LPS with Nigericin stimulation in Zyxin-deficient cells, but similar secretion after 18 h, shedding new light on the role of Zyxin in TLR4-dependent inflammatory processes. A more concise monitoring of the spatiotemporal response to LPS would be necessary to elucidate the role of Zyxin in this early response by monitoring inflammasome key molecules (e.g. NLRP3, CASP1, IL-1β) and its possible impact on other pro-inflammatory cytokines (TNF, IL-6, IL-8). Furthermore, TLR4 internalization studies by FACS and microscopy could provide more insights of Zyxin and its variants.

Interestingly, there are various proteins that have overlapping functions with Zyxin, while a compensatory effect of other proteins cannot be ruled out in our patients. ZYX null mice did not reveal impacts on general organ development, behavior, fertility, or viability of mice, assuming a counterbalancing function of proteins of the same protein family [274].

5.2.5. Zyxin variants in the current SNP databases

At the time of our study, Zyxin was not described in the context of VEO-IBD and *ZYX* seemed like a plausible candidate gene to study, since it was found in two independent patients. Furthermore, both identified variants were unique and not found in healthy individuals at that time. But SNP databases grew constantly and incorporated more data over time. Therefore, its significant importance in medicine increased tremendously with

the technological progress and availability of WES within the last two decades [146, 275]. p.I63S (rs201850974) is currently noted in the SNP variant database (gnomAD v2.1.1.) as benign and has an allele frequency of 0.003 in the human population. 5 homozygote variants from genome and exome sequencing of 668 allele counts have been found from African/African American and Latino/Mixed American ethnicity. p.Q420K (rs146818692) was found with an allele frequency of 0.000043 without any homozygotes among 122 allele counts. Nevertheless, both SNPs had not yet been analyzed functionally.

5.2.6. Summary of our findings and outlook

Our work showed that *ZYX* variants from two independent IBD patients seemed to have a normal function on the Zyxin protein distribution, colocalization, association to the actin skeleton as well as ability to proliferate, when analyzed in HCT116 cells. Interestingly, we were able to show that ZYX deficiency impacts IFN I responses in epithelial HCT116 and monocytoid BLaER1 cells and determine its influence on pro-inflammatory cytokine induction and secretion. However, we could not identify any functional defects of our *ZYX* variants (I63S, Q420K). Based on the current dataset, it seems unlikely that the *ZYX* variants are disease causing. Yet, at the beginning of our studies and based on the state of knowledge at the time, it was strongly indicated to verify the two variants mechanistically. Furthermore, we took the opportunity to evaluate a possible target in VEO-IBD, which may have resulted in a better disease management and treatment option for these patients. In particular, our patients who do not respond well to conventional therapies could have gained a new opportunity.

However, we must still consider that IBD remains a very complex disease that is driven by multiple factors and facets that we may not have addressed yet. iPSC-derived organoid development, the bacterial and viral handling of macrophages, their endocytosis capacities (e.g. of TLR4 upon LPS stimulation, TLR3 upon Poly I:C), stress induced responses or crystallographic resolutions of Zyxin could all add another relevant scientific layers to the complex understanding of the identified *ZYX* variants.

5.3. The role of a biallelic 3 bp in-frame deletion in *LY96* of a VEO-IBD patient

Our index patient (A.II-1) was represented with a biallelic 3 bp in-frame deletion (p.T116del) in *LY96*, coding for the MD2 protein. The patient suffered from VEO-IBD, bloody diarrhea, anal ulcers, and had a poor response to conventional treatments. After a lobectomy due to persistent pneumonia at the age of 6 and a laparoscopic subtotal colectomy at the age of 12, the patients' the health status improved. The parents were heterozygous for the identified *LY96* variant. Among the 7 siblings, one (A.II-5) harbored the same variant. The sibling (A.II-5) had no gastrointestinal manifestations to date but was diagnosed with recurrent infections such as pneumonia and otitis media.

5.3.1. Human MD2 deficiency in patient-derived monocytes

The intestine harbors one of the largest and most significant microbial populated surfaces in the body [276]. Constant and tight regulation maintains the homeostatic balance in the gut, continuously distinguishing between the tolerance towards commensal bacteria or combating pathogens, toxins or viruses. The underlying gut-associated lymphoid tissues resemble the largest immune system in the human body to address the dynamic processes of immune tolerance [96]. Disturbances of the microbiome and dysfunctional immunological responses have been shown in various studies to directly impact IBD in susceptible individuals [277-281].

The innate immune system plays an indispensable role in the recognition of microbial and viral compounds through PRRs such as NLRs or TLRs [282]. MD2 and CD14 are accessory proteins of TLR4 and crucial for LPS induced signaling, activating the NF-κB and MAPK pathway in a MYD88-dependent manner, and inducing pro-inflammatory cytokines (e.g. TNF, IL-1β, IL-6 or IL-8) [192]. LPS can also activate TLR4-MD2, independently of MYD88. TLR4-MD2 is internalized by the help of CD14, which leads to IFN-β secretion and activation of IFN-inducible genes (e.g. *CXCL10, CCL2* and *CCL5*) [215, 216].

In physiological conditions, TLR4 and MD2 expression is low in intestinal epithelial cells but has been demonstrated to be high in patients with adult and childhood IBD,

specifically in the terminal ileum of adults and the colon of children [283-285]. Sensing of LPS by TLR4-MD2 has been postulated to occur on the basolateral site of intestinal epithelial cells, which suggested that bacterial invasion-sensing through the epithelial barrier is another step to warrant intestinal homeostasis [285]. Additional infiltration of TLR4-sensitive macrophages to the inflamed mucosa deteriorates the LPS response [286]. Several TLR4 sequence variants, which impair downstream signaling, have been described in patients with VEO-IBD and IBD [287-289]. Murine TLR4- and MYD88-deficient DSS-induced colitis models demonstrated increased rectal bleeding, bloody stools, and severe intestinal inflammation, which showed a dysfunctional bacterial tolerance and clearance [231, 290]. These innate immune defects concomitant with IBD in human and murine models can cause a failure to produce an adequate response to commensal or pathogenic bacteria. Innate immune cells (e.g. granulocytes, macrophages or antigen-presenting cells) have been shown to be key mediators in host defense mechanisms against tissue damage and infection, for example by releasing IL-1β through inflammasome formation [291]. Various inflammatory diseases such as VEO-IBD (e.g. by Caspase-8, RIPK1 or IL-10(R) deficiencies), autoinflammatory diseases (e.g. rheumatoid arthritis, systemic lupus erythematosus, Sjoegren's syndrome), gout or type II diabetes have been associated with a dysregulated inflammasome formation and response [144, 156, 157, 292].

Inflammasomes are multimeric protein complexes, which assemble and recognize inflammatory stimuli such as DAMPs and PAMPs in a two-step process [293, 294]. The inflammasome is formed when PAMPs or DAMPs activate sensors, e.g. LPS activates the NLRP3 inflammasome, and downstream NF-κB-mediated signaling induces pro-IL-1β, pro-IL-18 and NLRP3 expression upon priming [295]. A second signal such as DAMPs and PAMPs promote the usually inactive NLRP3 to undergo a conformational change and assemble to NLRP3 oligomers. These oligomers provide a platform and recruit ASC through their pyrin domain [79, 228]. The other part of ASC activates CASP1, which results in the cleavage to active CASP1. CASP1 consecutively cleaves pro-IL-1β and pro-IL-18 to their active, mature forms [79]. We demonstrated that in patient-derived monocytes, LPS induced TLR4 signaling is abrogated upon the 3 bp in-frame deletion of *LY96*. Activation of the NLRP3 inflammasome led to a diminished expression of pro-IL-1β in the index patient (A.II-1) and sibling (A.II-5) upon LPS and Nigericin stimulation, confirmed by lysate immunoblotting. As a direct consequence of

reduced pro-IL-1β expression, we detected less IL-1β secretion in the patient (A.II-1) and sibling (A.II-5) compared to healthy controls or the father (A.I-1) by ELISA and immunoblotting of the supernatants. In parallel, Capitani et. al described a biallelic loss of function variant of *TLR4* in two individuals, in which one was asymptomatic and the other suffered from severe perianal CD [289]. Similar to our findings, patient-derived monocytes displayed an impaired TLR4-mediated signaling with a diminished response to LPS and production of cytokines (IL-1α, TNF, IL-6) [289].

5.3.2. MD2 deficiency abrogates inflammasome activation in iPSC-derived macrophages

Macrophages play a pivotal role in intestinal inflammation and were shown to induce hypersecretion of pro-inflammatory cytokines in IBD patients (e.g. IL-1β, IL-6, IL8, TNF) [296, 297]. Tight balancing of cytokines is therefore necessary for a regular homeostasis in the gut. Nagai et al. demonstrated that murine MD2 deficiency results in hyporesponsiveness to LPS in bone marrow-derived macrophages, dendritic and B cells, and a higher susceptibility to *Salmonella typhimurium* infection [192]. A studied point mutation at p.C95Y, conserved among human and mice MD2, resulted in impaired NF-κB activity, but normal physical interaction with TLR4 [298].

In our study, we assessed the LPS responsiveness of the patient-specific MD2 variant p.T116del in CRISPR/Cas9-engineered iPSCs with MD2 knockout clones (KO), the patient-specific variant (T116del) and unmodified clones (WT). Similar to our findings from patient-derived monocytes, MD2 knockout and MD2 T116del macrophages displayed a significantly diminished IL-1β secretion upon LPS and Nigericin stimulation. Additionally, our immunoblot analysis of the lysates revealed that cleaved Caspase-1 and pro-IL-1β expressions were abrogated in MD2 KO and MD2 T116del clones.
NLRP3 deficiency has been controversially discussed, but implicated in several studies to attenuate DSS-induced colitis, which was reversed when co-housed with another wild-type mouse strain, exchanging the microbial flora [299, 300]. However, a study from Zaki et al. showed that NLRP3- and CASP1-deficient mice are highly susceptible to DSS-induced colitis [301]. Contrary to previous findings, Zaki et al. revealed that these mice displayed a spreading of commensal bacteria, increased numbers of

macrophages and neutrophils in the lamina propria and submucosa as well as a disrupted epithelial barrier [301]. These studies indicated that not only genetic susceptibility but also the microbial flora contributes to inflammatory intestinal phenotypes. Investigation of our patient specific variant in a murine model could provide excellent insights to microbiome establishment and intestinal homeostasis. Furthermore, the microbial flora could play an additional role in the incomplete penetrance of the IBD phenotype displayed in our index patient, but not the sibling, who harbors the same variant. Besides that, other risk factors such as environmental exposures, infections and diet have to be taken into account for the manifestation of IBD.

5.3.3. MD2 deficiency does not impact the generation of iPSC-derived macrophage and surface marker expression in steady-state

TLR4 deficiency has been shown not to affect the immune cell composition in the periphery, but in activating quiescent hematopoietic stem cell proliferation in acute systemic LPS stress situations [302]. However, we observed that MD2 deficiency (KO, T116del) did not influence the differentiation process to hematopoietic progenitors and macrophages in our iPSC-derived model. Moreover, all analyzed iPSC-derived macrophages harbored a similar CD14 and TLR4 surface expression under steady state conditions, while LPS challenge of these MD2-deficient macrophages revealed a defective TLR4 endocytosis, as we have recently demonstrated by Li et al. [303]. Previous studies have shown that CD14 is necessary for TLR4 endocytosis [304]. TLR4 mutant murine macrophages, which lack their intracellular TIR domain, still display a normal functional internalization of the receptor [304]. Yet, murine MD2 deficient macrophages have been shown to fully abolish endocytosis of TLR4 [305]. The detailed analysis of two MD2 mutations, which impaired either the formation (p.C95A) or oligomerization (p.F126A) of TLR4-MD2 complex, were shown to prevent TLR4 internalization [305].

Emphasizing previous results, MD2 is crucial for proper TLR4 endocytosis and tolerance for *Salmonella typhimurium* relies on functional sensing of LPS. As we have recently demonstrated, bacterial handling capacity of *Salmonella typhimurium* is

impaired in MD2-deficent macrophages [303]. Yet in contrary, the biallelic TLR4 stop codon variant in an asymptomatic and a patient with IBD showed normal *Salmonella typhimurium* handling [289]. This proposes that MD2 has a distinct function in *Salmonella typhimurium* handling in macrophages and may affect bacterial clearance, other than TLR4. This needs to be studied in greater detail, ideally with larger cohort and possible variants from both affected proteins.

5.3.4. MD2 deficiency affects MYD88-dependent signaling

Our identified MD2 patient-specific variant (p.T116del) is located in close proximity to an N-glycosylation site (p.N114), which is essential for normal functionality [303]. Therefore, the defective glycosylation of MD2 seems to impact the dysfunctional downstream signaling (e.g. NF-κB, MAPK) besides previous described hyporesponsiveness upon MD2 deficiency [192, 303, 306].

Our data revealed a reduced phosphorylation of target molecules of the MYD88-dependent pathway (e.g. NF-κB p65, P38 and P44/42 MAPK) upon stimulation of LPS with lower concentrations. Higher concentrations of LPS induced phosphorylation of NF-κB p65, P38 and P44/42 MAPK in MD2-deficient cells, but to a lesser extent than in WT cells. This suggested that downstream signaling is not completely abolished but similar affected between a full knockout of MD2 and the patient-specific variant of MD2.

Furthermore, we showed a significant impairment in TNF secretion and *IL-6* expression induction upon LPS stimulation, pinpointing that the patient-specific MD2 variant mimicked the same dysfunctional phenotype as a complete knockout of MD2. Since anti-TNF is one of the gold standards in IBD therapies, this may also explain the lack of response seen in our patient, yet the complexity of the patients general IBD disease course is not negligible and further detailed analysis would be informative, e.g. analysis of pro-inflammatory cytokine concetrations in blood serum [307].

Our index patient (A.II-1) underwent colectomy at the age of 12, so patient-derived intestinal organoids would be an excellent model to derive from iPSCs for further investigations of complex host-pathogen interactions. Crystal structure analysis by cryo-electron microscopy or X-ray crystallography of the patient-specific MD2 variant and in

complex with LPS may shed more light on its conformational native structure and probable misfolding.

5.3.5. MD2 deficiency alters surface expression of CD86 and HLA-DR in M1 macrophages

Macrophage polarization is necessary for a functional adaption in the intestine in response to different cytokines. *In vitro* polarization has been shown to distinguish between pro-inflammatory M1 macrophages and anti-inflammatory M2 macrophages, while *in vivo* distinction is more difficult since multiple stimuli are present and phenotypes of polarization are reversible [308, 309].

According to their name, M1 macrophages are supposed to trigger Th1-mediated inflammation, whereas M2 macrophages are supposed to initiate Th2 responses, resolving chronic inflammation and tissue repair [310]. The imbalance of M1 and M2 macrophages has been revealed in several inflammatory and chronic diseases such as asthma, rheumatoid arthritis, type 2 diabetes, atherosclerosis, cardiovascular diseases and particularly in IBD [311]. In IBD patients, a prominent accumulation of M1 macrophages occurs in the intestine, while less M2 macrophages are present, disturbing the macrophage equilibrium [312]. Since pro-inflammatory M1 polarization includes not only IFN-γ but also LPS stimulation, we expected differences in surface expression upon MD2 deficiency.

In our studies, we detected higher surface expression of CD86 in MD2-deficient M1 macrophages (KO, T116del). CD86 is a ligand for CD28 on naïve T cells but also for inhibitory CTLA-4 on cytotoxic T cells [313, 314]. Furthermore, a higher expression of the MHC II molecule HLA-DR in MD2-deficient M1 macrophages (KO, T116del) was detected, while CD274 (PD-L1) expression seemed normal among all M1-polarized macrophages. This pattern of higher CD86 and HLA-DR surface expression may implicate a higher activation status than in WT macrophages. On the contrary, inflamed tissues of a small analysis of 10 CD patients revealed that macrophages in the inflamed mucosa have an increased number of CD14(hi)HLA-DR(dim) cells, while healthy tissue was prominently populated with CD14(hi)HLA-DR(hi) cells [296].

It has been shown that murine MD2- or TLR4-deficient B cells are not able to upregulate CD86 upon Lipid A stimulation, which is the hydrophobic and functional endotoxin part of LPS [315]. MD2- or TLR4-deficient bone marrow-derived macrophages and dendritic cells seemed irresponsive to Lipid A, but neither were analyzed in macrophage polarization conditions [192]. Functional IL-1β and TNF secretion of M1 macrophages were significantly reduced in our study, when analyzed by ELISA. Another study from 2022 in human monocyte THP-1 cells demonstrated that M1 polarization with IFN-γ and LPS led to increased CD86 and HLA-DR expression [316]. For M1 polarization, stimulatory IFN-γ can be released by natural killer or T cells which induces MHC class II expression like HLA-DR on antigen-presenting cells (macrophages, B cells, dendritic cells) enhancing CD4+ T cell responses [317]. Furthermore, IFN-γ alone has been shown to generate potent pro-inflammatory macrophages and high CD86 expression upon LPS priming, leading to a strong Th1 response by IL-17 and IFN-γ secretion [318]. IFN-γ is also capable of inducing MHC I molecules to subsequently activate CD8+ T cells [319, 320]. The higher surface expression markers (CD86, HLA-DR) on M1 macrophages may suggest a higher sensitivity to IFN-γ in the absence of MD2 but its impact on T cell responses *in vivo* can only be speculated, since the pro-inflammatory secretion of IL-1β and TNF still seemed impaired. The capacity of M1 macrophages with MD2 deficiency in T cell activation need further investigation in co-culture conditions with T cells, to define their impact on CD4+ or CD8+ T cell priming.

5.3.1. MD2 deficiency in extraintestinal manifestations

Extraintestinal manifestations are common in IBD and particularly in VEO-IBD patients, with nearly 50 % developing at least one comorbidity [145].

Our MD2-deficient index patient was diagnosed with VEO-IBD, yet the other sibling harboring the same MD2 variant has not shown any IBD symptoms to date. Despite this, both suffered from pneumonia, leading to lobectomy in the index patient, pointing towards the importance of MD2 in response to Gram-positive bacteria.

MD2 does not only oligomerize with TLR4 but also with TLR2. TLR2-MD2 facilitates apart from LPS responses, also response to compounds of Gram-positive bacteria [193]. TLR2 plays a specific role in recognizing fragments of *Streptococcus pneumoniae* such as lipoteichoic acid, peptidoglycan or lipoproteins, inducing IL-8 secretion via NF-κB signaling [321]. Recently, TLR4- and MYD88-deficient mice have been shown to display impaired macrophage response in *Streptococcus pneumonia*-infected mice by affecting pro-inflammatory cytokine secretion [322].

Community acquired pneumonia through Gram-positive *Streptococcus pneumoniae* infection is one of the leading causes of childhood mortality under the age of 5 years [323]. Similar to the otitis media phenotype of the sibling without IBD, TLR2 deficiency in a murine model had been shown to impair macrophage recruitment, leading to prolonged duration of the middle ear infection and dysfunctional *Streptococcus pneumoniae* clearance [324]. These clinical manifestations suggest, that besides historical and environmental factors of both MD2 variant-harboring individuals, TLR2-MD2 could play an essential role in their pneumonia and otitis phenotype, which should be studied in greater detail. Unfortunately, no bacteria have been isolated from the patients to provide further insights to support our hypothesis. A recent study of biallelic TLR4 deficiency in IBD patients showed normal TLR2 responses, drawing attention to MD2 as a common accessory protein of TLR2 and TLR4. Interestingly, the TLR4-deficient cohort segregation analysis also revealed incomplete penetrance of variant-harboring individuals similar to our family with MD2 deficiency [289].

5.3.2. Summary of our findings and outlook

In conclusion, we were able to shed light on the role of MD2 and the functional analysis of a 3 bp deletion leading to a similar phenotype as a complete knockout of MD2 in iPSC-derived macrophages. Interestingly, a dysfunctional LPS response in patient monocytes and iPSC-derived macrophages uncovered a possible impact on bacterial handling and its influence on the tolerance of commensal bacteria in the context of IBD. For the development of future targeted IBD therapies, it can be derived from our study that impairing TLR4 signaling and MD2 elimination may not be an ideal approach. When designing targeted therapies, further mechanistic approaches are needed to understand the role of MD2.

These investigations could include omics-approaches to investigate transcription and expression patterns of iPSC-derived macrophages or other derived immune cells, when challenged with microbial stimuli. Inflammatory responses and possible compensatory or excessive effects on other cell types could provide more functional insights from murine models, harboring the index patient variant as well. Microbial challenges of these mice could generate further insights in bacterial handling and may propose possible treatment options for our patient, such as prebiotics or specific antibiotics [325]. Furthermore, the investigation of iPSC-derived bone marrow organoids, in a xenograft model could help to elucidate MD2s role in detail, as recently described from Frenz-Wiessner et. al [326].

Taken together, future mechanistic studies on MD2 in intestinal homeostasis, innate and adaptive immunity are necessary to potentially reveal new personalized treatment options and shed light on the complex, multilayered disease of VEO-IBD.

6. References

1. Engel, M.A., M. Khalil, and M.F. Neurath, Highlights in inflammatory bowel disease--from bench to bedside. Clin Chem Lab Med, 2012. 50(7): p. 1229-35.
2. Kaser, A., S. Zeissig, and R.S. Blumberg, Inflammatory bowel disease. Annu Rev Immunol, 2010. 28: p. 573-621.
3. Sobczak, M., et al., Current overview of extrinsic and intrinsic factors in etiology and progression of inflammatory bowel diseases. Pharmacol Rep, 2014. 66(5): p. 766-75.
4. Ng, S.C., et al., Worldwide incidence and prevalence of inflammatory bowel disease in the 21st century: a systematic review of population-based studies. Lancet, 2018. 390(10114): p. 2769-2778.
5. Collaborators, G.I.B.D., The global, regional, and national burden of inflammatory bowel disease in 195 countries and territories, 1990-2017: a systematic analysis for the Global Burden of Disease Study 2017. Lancet Gastroenterol Hepatol, 2020. 5(1): p. 17-30.
6. Auvin, S., et al., Incidence, clinical presentation and location at diagnosis of pediatric inflammatory bowel disease: a prospective population-based study in northern France (1988-1999). J Pediatr Gastroenterol Nutr, 2005. 41(1): p. 49-55.
7. Cosnes, J., et al., Epidemiology and natural history of inflammatory bowel diseases. Gastroenterology, 2011. 140(6): p. 1785-94.
8. Santiago, M., et al., What forecasting the prevalence of inflammatory bowel disease may tell us about its evolution on a national scale. Therap Adv Gastroenterol, 2019. 12: p. 1756284819860044.
9. Baumgart, D.C. and W.J. Sandborn, Inflammatory bowel disease: clinical aspects and established and evolving therapies. Lancet, 2007. 369(9573): p. 1641-57.
10. Kelsen, J. and R.N. Baldassano, Inflammatory bowel disease: the difference between children and adults. Inflamm Bowel Dis, 2008. 14 Suppl 2: p. S9-11.
11. Prelipcean, C.C., et al., What is the impact of age on adult patients with inflammatory bowel disease? Clujul Med, 2013. 86(1): p. 3-9.
12. Nimmons, D. and J.K. Limdi, Elderly patients and inflammatory bowel disease. World J Gastrointest Pharmacol Ther, 2016. 7(1): p. 51-65.
13. Crohn, B.B., L. Ginzburg, and G.D. Oppenheimer, Regional ileitis; a pathologic and clinical entity. Am J Med, 1952. 13(5): p. 583-90.

14. Wehkamp, J., et al., Inflammatory Bowel Disease. Dtsch Arztebl Int, 2016. 113(5): p. 72-82.
15. Ordás, I., et al., Ulcerative colitis. Lancet, 2012. 380(9853): p. 1606-19.
16. Ungaro, R., et al., Ulcerative colitis. Lancet, 2017. 389(10080): p. 1756-1770.
17. Solem, C.A., et al., Fistulas to the urinary system in Crohn's disease: clinical features and outcomes. Am J Gastroenterol, 2002. 97(9): p. 2300-5.
18. Ye, B.D., et al., Clinical features and long-term prognosis of Crohn's disease in Korea. Scand J Gastroenterol, 2010. 45(10): p. 1178-85.
19. Mekhjian, H.S., et al., Clinical features and natural history of Crohn's disease. Gastroenterology, 1979. 77(4 Pt 2): p. 898-906.
20. Molodecky, N.A., et al., Increasing incidence and prevalence of the inflammatory bowel diseases with time, based on systematic review. Gastroenterology, 2012. 142(1): p. 46-54.e42; quiz e30.
21. Van Limbergen, J., et al., Definition of phenotypic characteristics of childhood-onset inflammatory bowel disease. Gastroenterology, 2008. 135(4): p. 1114-22.
22. Bryant, R.V., et al., Systematic review: histological remission in inflammatory bowel disease. Is 'complete' remission the new treatment paradigm? An IOIBD initiative. J Crohns Colitis, 2014. 8(12): p. 1582-97.
23. Satsangi, J., et al., The Montreal classification of inflammatory bowel disease: controversies, consensus, and implications. Gut, 2006. 55(6): p. 749-53.
24. Fumery, M., et al., Natural History of Adult Ulcerative Colitis in Population-based Cohorts: A Systematic Review. Clin Gastroenterol Hepatol, 2018. 16(3): p. 343-356.e3.
25. Harbord, M., et al., Third European Evidence-based Consensus on Diagnosis and Management of Ulcerative Colitis. Part 2: Current Management. J Crohns Colitis, 2017. 11(7): p. 769-784.
26. Hanzel, J., et al., Emerging therapies for ulcerative colitis. Expert Rev Clin Immunol, 2022. 18(5): p. 513-524.
27. Langholz, E., et al., Course of ulcerative colitis: analysis of changes in disease activity over years. Gastroenterology, 1994. 107(1): p. 3-11.
28. Baumgart, D.C. and W.J. Sandborn, Crohn's disease. Lancet, 2012. 380(9853): p. 1590-605.

29. Rogler, G., et al., Extraintestinal Manifestations of Inflammatory Bowel Disease: Current Concepts, Treatment, and Implications for Disease Management. Gastroenterology, 2021. 161(4): p. 1118-1132.
30. Thia, K.T., et al., Risk factors associated with progression to intestinal complications of Crohn's disease in a population-based cohort. Gastroenterology, 2010. 139(4): p. 1147-55.
31. Guindi, M. and R.H. Riddell, Indeterminate colitis. J Clin Pathol, 2004. 57(12): p. 1233-44.
32. Yantiss, R.K. and R.D. Odze, Diagnostic difficulties in inflammatory bowel disease pathology. Histopathology, 2006. 48(2): p. 116-32.
33. Prenzel, F. and H.H. Uhlig, Frequency of indeterminate colitis in children and adults with IBD - a metaanalysis. J Crohns Colitis, 2009. 3(4): p. 277-81.
34. Tremaine, W.J., Is indeterminate colitis determinable? Curr Gastroenterol Rep, 2012. 14(2): p. 162-5.
35. Rinawi, F., et al., The natural history of pediatric-onset IBD-unclassified and prediction of Crohn's disease reclassification: a 27-year study. Scand J Gastroenterol, 2017. 52(5): p. 558-563.
36. Thurgate, L.E., et al., An Overview of Inflammatory Bowel Disease Unclassified in Children. Inflamm Intest Dis, 2019. 4(3): p. 97-103.
37. Benchimol, E.I., et al., Epidemiology of pediatric inflammatory bowel disease: a systematic review of international trends. Inflamm Bowel Dis, 2011. 17(1): p. 423-39.
38. Rogers, B.H., L.M. Clark, and J.B. Kirsner, The epidemiologic and demographic characteristics of inflammatory bowel disease: an analysis of a computerized file of 1400 patients. J Chronic Dis, 1971. 24(12): p. 743-73.
39. Silverberg, M.S., et al., Toward an integrated clinical, molecular and serological classification of inflammatory bowel disease: report of a Working Party of the 2005 Montreal World Congress of Gastroenterology. Can J Gastroenterol, 2005. 19 Suppl A: p. 5a-36a.
40. Levine, A., et al., Pediatric modification of the Montreal classification for inflammatory bowel disease: the Paris classification. Inflamm Bowel Dis, 2011. 17(6): p. 1314-21.

41. Assa, A., F. Rinawi, and R. Shamir, The Long-Term Predictive Properties of the Paris Classification in Paediatric Inflammatory Bowel Disease Patients. J Crohns Colitis, 2018. 12(1): p. 39-47.
42. Ruemmele, F.M., et al., Characteristics of inflammatory bowel disease with onset during the first year of life. J Pediatr Gastroenterol Nutr, 2006. 43(5): p. 603-9.
43. Hyams, J., et al., The natural history of corticosteroid therapy for ulcerative colitis in children. Clin Gastroenterol Hepatol, 2006. 4(9): p. 1118-23.
44. Markowitz, J., et al., Corticosteroid therapy in the age of infliximab: acute and 1-year outcomes in newly diagnosed children with Crohn's disease. Clin Gastroenterol Hepatol, 2006. 4(9): p. 1124-9.
45. Shim, J.O., Recent Advance in Very Early Onset Inflammatory Bowel Disease. Pediatr Gastroenterol Hepatol Nutr, 2019. 22(1): p. 41-49.
46. Uhlig, H.H., et al., The diagnostic approach to monogenic very early onset inflammatory bowel disease. Gastroenterology, 2014. 147(5): p. 990-1007.e3.
47. Glocker, E.O., et al., Infant colitis--it's in the genes. Lancet, 2010. 376(9748): p. 1272.
48. Sartor, R.B., Mechanisms of disease: pathogenesis of Crohn's disease and ulcerative colitis. Nat Clin Pract Gastroenterol Hepatol, 2006. 3(7): p. 390-407.
49. Kaplan, G.G. and S.C. Ng, Understanding and Preventing the Global Increase of Inflammatory Bowel Disease. Gastroenterology, 2017. 152(2): p. 313-321.e2.
50. Wild, C.P., Complementing the genome with an "exposome": the outstanding challenge of environmental exposure measurement in molecular epidemiology. Cancer Epidemiol Biomarkers Prev, 2005. 14(8): p. 1847-50.
51. Rogler, G. and S. Vavricka, Exposome in IBD: recent insights in environmental factors that influence the onset and course of IBD. Inflamm Bowel Dis, 2015. 21(2): p. 400-8.
52. Agrawal, M., et al., Early life exposures and the risk of inflammatory bowel disease: Systematic review and meta-analyses. EClinicalMedicine, 2021. 36: p. 100884.
53. Piovani, D., et al., Environmental Risk Factors for Inflammatory Bowel Diseases: An Umbrella Review of Meta-analyses. Gastroenterology, 2019. 157(3): p. 647-659.e4.
54. Lopes, E.W., et al., Lifestyle factors for the prevention of inflammatory bowel disease. Gut, 2022.

55. Oligschlaeger, Y., et al., Inflammatory Bowel Disease: A Stressed "Gut/Feeling". Cells, 2019. 8(7).
56. Schaubeck, M., et al., Dysbiotic gut microbiota causes transmissible Crohn's disease-like ileitis independent of failure in antimicrobial defence. Gut, 2016. 65(2): p. 225-37.
57. Mentella, M.C., et al., Nutrition, IBD and Gut Microbiota: A Review. Nutrients, 2020. 12(4).
58. Frank, D.N., et al., Disease phenotype and genotype are associated with shifts in intestinal-associated microbiota in inflammatory bowel diseases. Inflamm Bowel Dis, 2011. 17(1): p. 179-84.
59. Gomez de Agüero, M., et al., The maternal microbiota drives early postnatal innate immune development. Science, 2016. 351(6279): p. 1296-302.
60. Jakobsson, H.E., et al., Decreased gut microbiota diversity, delayed Bacteroidetes colonisation and reduced Th1 responses in infants delivered by caesarean section. Gut, 2014. 63(4): p. 559-66.
61. Ley, R.E., D.A. Peterson, and J.I. Gordon, Ecological and evolutionary forces shaping microbial diversity in the human intestine. Cell, 2006. 124(4): p. 837-48.
62. Whitman, W.B., D.C. Coleman, and W.J. Wiebe, Prokaryotes: the unseen majority. Proc Natl Acad Sci U S A, 1998. 95(12): p. 6578-83.
63. O'Hara, A.M. and F. Shanahan, The gut flora as a forgotten organ. EMBO Rep, 2006. 7(7): p. 688-93.
64. Zheng, J., et al., The role of gut microbiome in inflammatory bowel disease diagnosis and prognosis. United European Gastroenterol J, 2022. 10(10): p. 1091-1102.
65. Matijašić, M., et al., Gut Microbiota beyond Bacteria-Mycobiome, Virome, Archaeome, and Eukaryotic Parasites in IBD. Int J Mol Sci, 2020. 21(8).
66. Qin, J., et al., A human gut microbial gene catalogue established by metagenomic sequencing. Nature, 2010. 464(7285): p. 59-65.
67. Zoetendal, E.G., M. Rajilic-Stojanovic, and W.M. de Vos, High-throughput diversity and functionality analysis of the gastrointestinal tract microbiota. Gut, 2008. 57(11): p. 1605-15.
68. Zhang, Y.Z. and Y.Y. Li, Inflammatory bowel disease: pathogenesis. World J Gastroenterol, 2014. 20(1): p. 91-9.

69. Soderholm, A.T. and V.A. Pedicord, Intestinal epithelial cells: at the interface of the microbiota and mucosal immunity. Immunology, 2019. 158(4): p. 267-280.
70. Paone, P. and P.D. Cani, Mucus barrier, mucins and gut microbiota: the expected slimy partners? Gut, 2020. 69(12): p. 2232-2243.
71. Birchenough, G.M., et al., New developments in goblet cell mucus secretion and function. Mucosal Immunol, 2015. 8(4): p. 712-9.
72. Ayabe, T., et al., Secretion of microbicidal alpha-defensins by intestinal Paneth cells in response to bacteria. Nat Immunol, 2000. 1(2): p. 113-8.
73. Loonen, L.M., et al., REG3γ-deficient mice have altered mucus distribution and increased mucosal inflammatory responses to the microbiota and enteric pathogens in the ileum. Mucosal Immunol, 2014. 7(4): p. 939-47.
74. Edwards, J.A., et al., Role of regenerating islet-derived proteins in inflammatory bowel disease. World J Gastroenterol, 2020. 26(21): p. 2702-2714.
75. Cerutti, A. and M. Rescigno, The biology of intestinal immunoglobulin A responses. Immunity, 2008. 28(6): p. 740-50.
76. Cao, A.T., et al., Interleukin (IL)-21 promotes intestinal IgA response to microbiota. Mucosal Immunol, 2015. 8(5): p. 1072-82.
77. Pietrzak, B., et al., Secretory IgA in Intestinal Mucosal Secretions as an Adaptive Barrier against Microbial Cells. Int J Mol Sci, 2020. 21(23).
78. Lin, R., et al., Clinical significance of soluble immunoglobulins A and G and their coated bacteria in feces of patients with inflammatory bowel disease. J Transl Med, 2018. 16(1): p. 359.
79. Franchi, L., et al., The inflammasome: a caspase-1-activation platform that regulates immune responses and disease pathogenesis. Nat Immunol, 2009. 10(3): p. 241-7.
80. Zambetti, L.P., et al., The rhapsody of NLRPs: master players of inflammation...and a lot more. Immunol Res, 2012. 53(1-3): p. 78-90.
81. West, A.P., A.A. Koblansky, and S. Ghosh, Recognition and signaling by toll-like receptors. Annu Rev Cell Dev Biol, 2006. 22: p. 409-37.
82. Rehwinkel, J. and M.U. Gack, RIG-I-like receptors: their regulation and roles in RNA sensing. Nat Rev Immunol, 2020. 20(9): p. 537-551.
83. Briard, B., D.E. Place, and T.D. Kanneganti, DNA Sensing in the Innate Immune Response. Physiology (Bethesda), 2020. 35(2): p. 112-124.

84. Tang, D., et al., PAMPs and DAMPs: signal 0s that spur autophagy and immunity. Immunol Rev, 2012. 249(1): p. 158-75.
85. Coleman, O.I. and D. Haller, Bacterial Signaling at the Intestinal Epithelial Interface in Inflammation and Cancer. Front Immunol, 2017. 8: p. 1927.
86. Kumar, M., M. Garand, and S. Al Khodor, Integrating omics for a better understanding of Inflammatory Bowel Disease: a step towards personalized medicine. J Transl Med, 2019. 17(1): p. 419.
87. Wéra, O., P. Lancellotti, and C. Oury, The Dual Role of Neutrophils in Inflammatory Bowel Diseases. J Clin Med, 2016. 5(12).
88. Danne, C., et al., CARD9 in neutrophils protects from colitis and controls mitochondrial metabolism and cell survival. Gut, 2022.
89. Yunna, C., et al., Macrophage M1/M2 polarization. Eur J Pharmacol, 2020. 877: p. 173090.
90. Han, X., et al., Roles of Macrophages in the Development and Treatment of Gut Inflammation. Front Cell Dev Biol, 2021. 9: p. 625423.
91. Molnár, T., et al., Clinical significance of granuloma in Crohn's disease. World J Gastroenterol, 2005. 11(20): p. 3118-21.
92. Schulz-Kuhnt, A., et al., Innate Lymphoid Cells as Regulators of Epithelial Integrity: Therapeutic Implications for Inflammatory Bowel Diseases. Front Med (Lausanne), 2021. 8: p. 656745.
93. Foti, M. and P. Ricciardi-Castagnoli, Antigen sampling by mucosal dendritic cells. Trends Mol Med, 2005. 11(9): p. 394-6.
94. Mabbott, N.A., et al., Microfold (M) cells: important immunosurveillance posts in the intestinal epithelium. Mucosal Immunol, 2013. 6(4): p. 666-77.
95. Mörbe, U.M., et al., Human gut-associated lymphoid tissues (GALT); diversity, structure, and function. Mucosal Immunol, 2021. 14(4): p. 793-802.
96. Brandtzaeg, P., et al., Terminology: nomenclature of mucosa-associated lymphoid tissue. Mucosal Immunol, 2008. 1(1): p. 31-7.
97. Jovani, M. and S. Danese, Vedolizumab for the treatment of IBD: a selective therapeutic approach targeting pathogenic a4b7 cells. Curr Drug Targets, 2013. 14(12): p. 1433-43.
98. Fuss, I.J., et al., Disparate CD4+ lamina propria (LP) lymphokine secretion profiles in inflammatory bowel disease. Crohn's disease LP cells manifest

increased secretion of IFN-gamma, whereas ulcerative colitis LP cells manifest increased secretion of IL-5. J Immunol, 1996. 157(3): p. 1261-70.
99. Strober, W. and I.J. Fuss, Proinflammatory cytokines in the pathogenesis of inflammatory bowel diseases. Gastroenterology, 2011. 140(6): p. 1756-1767.
100. Műzes, G., et al., Changes of the cytokine profile in inflammatory bowel diseases. World J Gastroenterol, 2012. 18(41): p. 5848-61.
101. Hirata, I., et al., Immunohistological characterization of intraepithelial and lamina propria lymphocytes in control ileum and colon and in inflammatory bowel disease. Dig Dis Sci, 1986. 31(6): p. 593-603.
102. Fu, S.H., et al., Interplay between Cytokine Circuitry and Transcriptional Regulation Shaping Helper T Cell Pathogenicity and Plasticity in Inflammatory Bowel Disease. Int J Mol Sci, 2020. 21(9).
103. Nakase, H., et al., The influence of cytokines on the complex pathology of ulcerative colitis. Autoimmun Rev, 2022. 21(3): p. 103017.
104. Bonneville, M., et al., Intestinal intraepithelial lymphocytes are a distinct set of gamma delta T cells. Nature, 1988. 336(6198): p. 479-81.
105. Cheroutre, H., F. Lambolez, and D. Mucida, The light and dark sides of intestinal intraepithelial lymphocytes. Nat Rev Immunol, 2011. 11(7): p. 445-56.
106. Olivares-Villagómez, D. and L. Van Kaer, Intestinal Intraepithelial Lymphocytes: Sentinels of the Mucosal Barrier. Trends Immunol, 2018. 39(4): p. 264-275.
107. Liu, Z., et al., The increased expression of IL-23 in inflammatory bowel disease promotes intraepithelial and lamina propria lymphocyte inflammatory responses and cytotoxicity. J Leukoc Biol, 2011. 89(4): p. 597-606.
108. Matsuzawa-Ishimoto, Y., et al., The γδ IEL effector API5 masks genetic susceptibility to Paneth cell death. Nature, 2022. 610(7932): p. 547-554.
109. Kotlarz, D., Identification of the γδ IEL-secreted Paneth cell protective factor API5 as a promising therapeutic target for ATG16L1-associated Crohn's disease. Gastroenterology, 2023.
110. Noronha, A.M., et al., Hyperactivated B cells in human inflammatory bowel disease. J Leukoc Biol, 2009. 86(4): p. 1007-16.
111. Uzzan, M., et al., Ulcerative colitis is characterized by a plasmablast-skewed humoral response associated with disease activity. Nat Med, 2022. 28(4): p. 766-779.

112. Timmermans, W.M., et al., B-Cell Dysregulation in Crohn's Disease Is Partially Restored with Infliximab Therapy. PLoS One, 2016. 11(7): p. e0160103.
113. Frede, A., et al., B cell expansion hinders the stroma-epithelium regenerative cross talk during mucosal healing. Immunity, 2022. 55(12): p. 2336-2351.e12.
114. Moller, F.T., et al., Familial risk of inflammatory bowel disease: a population-based cohort study 1977-2011. Am J Gastroenterol, 2015. 110(4): p. 564-71.
115. Hwang, S.W., et al., Influence of a Positive Family History on the Clinical Course of Inflammatory Bowel Disease. J Crohns Colitis, 2016. 10(9): p. 1024-32.
116. Santos, M.P.C., C. Gomes, and J. Torres, Familial and ethnic risk in inflammatory bowel disease. Ann Gastroenterol, 2018. 31(1): p. 14-23.
117. Halme, L., et al., Family and twin studies in inflammatory bowel disease. World J Gastroenterol, 2006. 12(23): p. 3668-72.
118. Halfvarson, J., et al., Age determines the risk of familial inflammatory bowel disease-A nationwide study. Aliment Pharmacol Ther, 2022. 56(3): p. 491-500.
119. Yang, H., et al., Familial empirical risks for inflammatory bowel disease: differences between Jews and non-Jews. Gut, 1993. 34(4): p. 517-24.
120. Rivas, M.A., et al., Insights into the genetic epidemiology of Crohn's and rare diseases in the Ashkenazi Jewish population. PLoS Genet, 2018. 14(5): p. e1007329.
121. Liu, J.Z., et al., Association analyses identify 38 susceptibility loci for inflammatory bowel disease and highlight shared genetic risk across populations. Nat Genet, 2015. 47(9): p. 979-986.
122. Sazonovs, A., et al., Large-scale sequencing identifies multiple genes and rare variants associated with Crohn's disease susceptibility. Nat Genet, 2022. 54(9): p. 1275-1283.
123. de Lange, K.M., et al., Genome-wide association study implicates immune activation of multiple integrin genes in inflammatory bowel disease. Nat Genet, 2017. 49(2): p. 256-261.
124. Szamosi, T., et al., The 3'UTR NFKBIA variant is associated with extensive colitis in Hungarian IBD patients. Dig Dis Sci, 2009. 54(2): p. 351-9.
125. Altaf-Ul-Amin, M., et al., Discovery of inflammatory bowel disease-associated miRNAs using a novel bipartite clustering approach. BMC Med Genomics, 2020. 13(Suppl 3): p. 10.

126. Hornschuh, M., et al., The role of epigenetic modifications for the pathogenesis of Crohn's disease. Clin Epigenetics, 2021. 13(1): p. 108.
127. Razali, N.N., et al., Targeted Sequencing of Cytokine-Induced PI3K-Related Genes in Ulcerative Colitis, Colorectal Cancer and Colitis-Associated Cancer. Int J Mol Sci, 2022. 23(19).
128. Fernandez, L., et al., IBD1 and IBD3 determine location of Crohn's disease in the Spanish population. Inflamm Bowel Dis, 2004. 10(6): p. 715-22.
129. Hugot, J.P., et al., Mapping of a susceptibility locus for Crohn's disease on chromosome 16. Nature, 1996. 379(6568): p. 821-3.
130. Cooney, R., et al., NOD2 stimulation induces autophagy in dendritic cells influencing bacterial handling and antigen presentation. Nat Med, 2010. 16(1): p. 90-7.
131. Parkes, M., et al., Sequence variants in the autophagy gene IRGM and multiple other replicating loci contribute to Crohn's disease susceptibility. Nat Genet, 2007. 39(7): p. 830-2.
132. Hampe, J., et al., A genome-wide association scan of nonsynonymous SNPs identifies a susceptibility variant for Crohn disease in ATG16L1. Nat Genet, 2007. 39(2): p. 207-11.
133. Duerr, R.H., et al., A genome-wide association study identifies IL23R as an inflammatory bowel disease gene. Science, 2006. 314(5804): p. 1461-3.
134. Fisher, S.A., et al., Genetic determinants of ulcerative colitis include the ECM1 locus and five loci implicated in Crohn's disease. Nat Genet, 2008. 40(6): p. 710-2.
135. Jostins, L., et al., Host-microbe interactions have shaped the genetic architecture of inflammatory bowel disease. Nature, 2012. 491(7422): p. 119-24.
136. Browning, B.L., et al., Association of DLG5 variants with inflammatory bowel disease in the New Zealand Caucasian population and meta-analysis of the DLG5 R30Q variant. Inflamm Bowel Dis, 2007. 13(9): p. 1069-76.
137. Kaser, A., et al., XBP1 links ER stress to intestinal inflammation and confers genetic risk for human inflammatory bowel disease. Cell, 2008. 134(5): p. 743-56.
138. Ek, W.E., M. D'Amato, and J. Halfvarson, The history of genetics in inflammatory bowel disease. Ann Gastroenterol, 2014. 27(4): p. 294-303.
139. McCole, D.F., IBD candidate genes and intestinal barrier regulation. Inflamm Bowel Dis, 2014. 20(10): p. 1829-49.

140. Anderson, C.A., et al., Meta-analysis identifies 29 additional ulcerative colitis risk loci, increasing the number of confirmed associations to 47. Nat Genet, 2011. 43(3): p. 246-52.
141. Huang, H., et al., Fine-mapping inflammatory bowel disease loci to single-variant resolution. Nature, 2017. 547(7662): p. 173-178.
142. Uhlig, H.H. and A.M. Muise, Clinical Genomics in Inflammatory Bowel Disease. Trends Genet, 2017. 33(9): p. 629-641.
143. Graham, D.B. and R.J. Xavier, Pathway paradigms revealed from the genetics of inflammatory bowel disease. Nature, 2020. 578(7796): p. 527-539.
144. Glocker, E.O., et al., Inflammatory bowel disease and mutations affecting the interleukin-10 receptor. N Engl J Med, 2009. 361(21): p. 2033-45.
145. Nambu, R., et al., A Systematic Review of Monogenic Inflammatory Bowel Disease. Clin Gastroenterol Hepatol, 2022. 20(4): p. e653-e663.
146. Crowley, E., et al., Prevalence and Clinical Features of Inflammatory Bowel Diseases Associated With Monogenic Variants, Identified by Whole-Exome Sequencing in 1000 Children at a Single Center. Gastroenterology, 2020. 158(8): p. 2208-2220.
147. Machida, H., et al., Association of polymorphic alleles of CTLA4 with inflammatory bowel disease in the Japanese. World J Gastroenterol, 2005. 11(27): p. 4188-93.
148. Bouzid, D., et al., Polymorphisms in the IL2RA and IL2RB genes in inflammatory bowel disease risk. Genet Test Mol Biomarkers, 2013. 17(11): p. 833-9.
149. Okou, D.T., et al., Exome sequencing identifies a novel FOXP3 mutation in a 2-generation family with inflammatory bowel disease. J Pediatr Gastroenterol Nutr, 2014. 58(5): p. 561-8.
150. Hedl, M., et al., STAT3 and STAT5 Signaling Thresholds Determine Distinct Regulation for Innate Receptor-Induced Inflammatory Cytokines, and STAT3/STAT5 Disease Variants Modulate These Outcomes. J Immunol, 2019. 203(12): p. 3325-3338.
151. Shouval, D.S., et al., Interleukin-10 receptor signaling in innate immune cells regulates mucosal immune tolerance and anti-inflammatory macrophage function. Immunity, 2014. 40(5): p. 706-19.
152. Winkelstein, J.A., et al., Chronic granulomatous disease. Report on a national registry of 368 patients. Medicine (Baltimore), 2000. 79(3): p. 155-69.

153. Muise, A.M., et al., NADPH oxidase complex and IBD candidate gene studies: identification of a rare variant in NCF2 that results in reduced binding to RAC2. Gut, 2012. 61(7): p. 1028-35.
154. Dhillon, S.S., et al., Variants in nicotinamide adenine dinucleotide phosphate oxidase complex components determine susceptibility to very early onset inflammatory bowel disease. Gastroenterology, 2014. 147(3): p. 680-689.e2.
155. Visser, G., et al., Neutropenia, neutrophil dysfunction, and inflammatory bowel disease in glycogen storage disease type Ib: results of the European Study on Glycogen Storage Disease type I. J Pediatr, 2000. 137(2): p. 187-91.
156. Lehle, A.S., et al., Intestinal Inflammation and Dysregulated Immunity in Patients With Inherited Caspase-8 Deficiency. Gastroenterology, 2019. 156(1): p. 275-278.
157. Li, Y., et al., Human RIPK1 deficiency causes combined immunodeficiency and inflammatory bowel diseases. Proc Natl Acad Sci U S A, 2019. 116(3): p. 970-975.
158. Parlato, M., et al., Human ALPI deficiency causes inflammatory bowel disease and highlights a key mechanism of gut homeostasis. EMBO Mol Med, 2018. 10(4).
159. Nenci, A., et al., Epithelial NEMO links innate immunity to chronic intestinal inflammation. Nature, 2007. 446(7135): p. 557-61.
160. Blaydon, D.C., et al., Inflammatory skin and bowel disease linked to ADAM17 deletion. N Engl J Med, 2011. 365(16): p. 1502-8.
161. Leung, G. and A.M. Muise, Monogenic Intestinal Epithelium Defects and the Development of Inflammatory Bowel Disease. Physiology (Bethesda), 2018. 33(5): p. 360-369.
162. Kammermeier, J., et al., Stem cell transplantation for tetratricopeptide repeat domain 7A deficiency: long-term follow-up. Blood, 2016. 128(9): p. 1306-8.
163. Lien, R., et al., Novel Mutations of the Tetratricopeptide Repeat Domain 7A Gene and Phenotype/Genotype Comparison. Front Immunol, 2017. 8: p. 1066.
164. Miot, C., et al., Hematopoietic stem cell transplantation in 29 patients hemizygous for hypomorphic IKBKG/NEMO mutations. Blood, 2017. 130(12): p. 1456-1467.
165. Verma, P., et al., Nanoparticle-mediated gene therapy strategies for mitigating inflammatory bowel disease. Biomater Sci, 2021. 9(5): p. 1481-1502.

166. Uhlig, H.H., et al., Precision medicine in monogenic inflammatory bowel disease: proposed mIBD REPORT standards. Nat Rev Gastroenterol Hepatol, 2023. 20(12): p. 810-828.
167. Ussar, S., et al., Loss of Kindlin-1 causes skin atrophy and lethal neonatal intestinal epithelial dysfunction. PLoS Genet, 2008. 4(12): p. e1000289.
168. Pathak, S.J., et al., EPCAM mutation update: Variants associated with congenital tufting enteropathy and Lynch syndrome. Hum Mutat, 2019. 40(2): p. 142-161.
169. Owen, K.A., et al., FAK regulates intestinal epithelial cell survival and proliferation during mucosal wound healing. PLoS One, 2011. 6(8): p. e23123.
170. Thomas, K.S., et al., Non-redundant functions of FAK and Pyk2 in intestinal epithelial repair. Sci Rep, 2019. 9(1): p. 4497.
171. Wozniak, M.A., et al., Focal adhesion regulation of cell behavior. Biochim Biophys Acta, 2004. 1692(2-3): p. 103-19.
172. Horton, E.R., et al., Definition of a consensus integrin adhesome and its dynamics during adhesion complex assembly and disassembly. Nat Cell Biol, 2015. 17(12): p. 1577-1587.
173. Nikolopoulou, P.A., M.A. Koufaki, and V. Kostourou, The Adhesome Network: Key Components Shaping the Tumour Stroma. Cancers (Basel), 2021. 13(3).
174. Case, L.B. and C.M. Waterman, Integration of actin dynamics and cell adhesion by a three-dimensional, mechanosensitive molecular clutch. Nat Cell Biol, 2015. 17(8): p. 955-63.
175. Crawford, A.W., J.W. Michelsen, and M.C. Beckerle, An interaction between zyxin and alpha-actinin. J Cell Biol, 1992. 116(6): p. 1381-93.
176. Reinhard, M., et al., The proline-rich focal adhesion and microfilament protein VASP is a ligand for profilins. Embo j, 1995. 14(8): p. 1583-9.
177. Beckerle, M.C., Zyxin: zinc fingers at sites of cell adhesion. Bioessays, 1997. 19(11): p. 949-57.
178. Hirota, T., et al., Zyxin, a regulator of actin filament assembly, targets the mitotic apparatus by interacting with h-warts/LATS1 tumor suppressor. J Cell Biol, 2000. 149(5): p. 1073-86.
179. Sadler, I., et al., Zyxin and cCRP: two interactive LIM domain proteins associated with the cytoskeleton. J Cell Biol, 1992. 119(6): p. 1573-87.

180. Reinhard, M., et al., The 46/50 kDa phosphoprotein VASP purified from human platelets is a novel protein associated with actin filaments and focal contacts. Embo j, 1992. 11(6): p. 2063-70.
181. Drees, B., et al., Characterization of the interaction between zyxin and members of the Ena/vasodilator-stimulated phosphoprotein family of proteins. J Biol Chem, 2000. 275(29): p. 22503-11.
182. Cattaruzza, M., C. Lattrich, and M. Hecker, Focal adhesion protein zyxin is a mechanosensitive modulator of gene expression in vascular smooth muscle cells. Hypertension, 2004. 43(4): p. 726-30.
183. Kouwaki, T., et al., Zyxin stabilizes RIG-I and MAVS interactions and promotes type I interferon response. Sci Rep, 2017. 7(1): p. 11905.
184. Yu, J., et al., High-throughput proteomics integrated with gene microarray for discovery of colorectal cancer potential biomarkers. Oncotarget, 2016. 7(46): p. 75279-75292.
185. Zhong, C., et al., Zyxin as a potential cancer prognostic marker promotes the proliferation and metastasis of colorectal cancer cells. J Cell Physiol, 2019. 234(9): p. 15775-15789.
186. Kotb, A., M.E. Hyndman, and T.R. Patel, The role of zyxin in regulation of malignancies. Heliyon, 2018. 4(7): p. e00695.
187. Dai, Y.C., et al., Single-cell RNA-sequencing combined with bulk RNA-sequencing analysis of peripheral blood reveals the characteristics and key immune cell genes of ulcerative colitis. World J Clin Cases, 2022. 10(33): p. 12116-12135.
188. Hoffman, L.M., et al., Genetic ablation of zyxin causes Mena/VASP mislocalization, increased motility, and deficits in actin remodeling. J Cell Biol, 2006. 172(5): p. 771-82.
189. Oldenburg, J., et al., VASP, zyxin and TES are tension-dependent members of Focal Adherens Junctions independent of the α-catenin-vinculin module. Sci Rep, 2015. 5: p. 17225.
190. Chow, J.C., et al., Toll-like receptor-4 mediates lipopolysaccharide-induced signal transduction. J Biol Chem, 1999. 274(16): p. 10689-92.
191. Bohannon, J.K., et al., The immunobiology of toll-like receptor 4 agonists: from endotoxin tolerance to immunoadjuvants. Shock, 2013. 40(6): p. 451-62.

192. Nagai, Y., et al., Essential role of MD-2 in LPS responsiveness and TLR4 distribution. Nat Immunol, 2002. 3(7): p. 667-72.
193. Dziarski, R., et al., MD-2 enables Toll-like receptor 2 (TLR2)-mediated responses to lipopolysaccharide and enhances TLR2-mediated responses to Gram-positive and Gram-negative bacteria and their cell wall components. J Immunol, 2001. 166(3): p. 1938-44.
194. Hornung, V., et al., Quantitative expression of toll-like receptor 1-10 mRNA in cellular subsets of human peripheral blood mononuclear cells and sensitivity to CpG oligodeoxynucleotides. J Immunol, 2002. 168(9): p. 4531-7.
195. Hoshino, K., et al., Cutting edge: Toll-like receptor 4 (TLR4)-deficient mice are hyporesponsive to lipopolysaccharide: evidence for TLR4 as the Lps gene product. J Immunol, 1999. 162(7): p. 3749-52.
196. Arbour, N.C., et al., TLR4 mutations are associated with endotoxin hyporesponsiveness in humans. Nat Genet, 2000. 25(2): p. 187-91.
197. Kelly, M.G., et al., TLR-4 signaling promotes tumor growth and paclitaxel chemoresistance in ovarian cancer. Cancer Res, 2006. 66(7): p. 3859-68.
198. Bhatelia, K., K. Singh, and R. Singh, TLRs: linking inflammation and breast cancer. Cell Signal, 2014. 26(11): p. 2350-7.
199. Ou, T., M. Lilly, and W. Jiang, The Pathologic Role of Toll-Like Receptor 4 in Prostate Cancer. Front Immunol, 2018. 9: p. 1188.
200. Zou, Y., et al., sTLR4/MD-2 complex inhibits colorectal cancer in vitro and in vivo by targeting LPS. Oncotarget, 2016. 7(32): p. 52032-52044.
201. Herrinton, L.J., et al., Incidence and mortality of colorectal adenocarcinoma in persons with inflammatory bowel disease from 1998 to 2010. Gastroenterology, 2012. 143(2): p. 382-9.
202. Guo, J., M. Liao, and J. Wang, TLR4 signaling in the development of colitis-associated cancer and its possible interplay with microRNA-155. Cell Commun Signal, 2021. 19(1): p. 90.
203. Gaidt, M.M., et al., Human Monocytes Engage an Alternative Inflammasome Pathway. Immunity, 2016. 44(4): p. 833-46.
204. Luo, M., et al., MD-2 regulates LPS-induced NLRP3 inflammasome activation and IL-1beta secretion by a MyD88/NF-κB-dependent pathway in alveolar macrophages cell line. Mol Immunol, 2017. 90: p. 1-10.

205. Yang, J., L. Wise, and K.I. Fukuchi, TLR4 Cross-Talk With NLRP3 Inflammasome and Complement Signaling Pathways in Alzheimer's Disease. Front Immunol, 2020. 11: p. 724.
206. Yu, B. and S.D. Wright, Catalytic properties of lipopolysaccharide (LPS) binding protein. Transfer of LPS to soluble CD14. J Biol Chem, 1996. 271(8): p. 4100-5.
207. Gioannini, T.L., et al., Monomeric endotoxin:protein complexes are essential for TLR4-dependent cell activation. J Endotoxin Res, 2005. 11(2): p. 117-23.
208. Lloyd, K.L. and P. Kubes, GPI-linked endothelial CD14 contributes to the detection of LPS. Am J Physiol Heart Circ Physiol, 2006. 291(1): p. H473-81.
209. Bonham, K.S., et al., A promiscuous lipid-binding protein diversifies the subcellular sites of toll-like receptor signal transduction. Cell, 2014. 156(4): p. 705-16.
210. Ciesielska, A., M. Matyjek, and K. Kwiatkowska, TLR4 and CD14 trafficking and its influence on LPS-induced pro-inflammatory signaling. Cell Mol Life Sci, 2021. 78(4): p. 1233-1261.
211. Xing, Y., et al., Cutting Edge: TRAF6 Mediates TLR/IL-1R Signaling-Induced Nontranscriptional Priming of the NLRP3 Inflammasome. J Immunol, 2017. 199(5): p. 1561-1566.
212. Guven-Maiorov, E., et al., The Architecture of the TIR Domain Signalosome in the Toll-like Receptor-4 Signaling Pathway. Sci Rep, 2015. 5: p. 13128.
213. Yamamoto, M., et al., TRAM is specifically involved in the Toll-like receptor 4-mediated MyD88-independent signaling pathway. Nat Immunol, 2003. 4(11): p. 1144-50.
214. Buttmann, M., et al., Interferon-beta is a potent inducer of interferon regulatory factor-1/2-dependent IP-10/CXCL10 expression in primary human endothelial cells. J Vasc Res, 2007. 44(1): p. 51-60.
215. Nakano, M., et al., Type I interferon induces CX3CL1 (fractalkine) and CCL5 (RANTES) production in human pulmonary vascular endothelial cells. Clin Exp Immunol, 2012. 170(1): p. 94-100.
216. Kawai, T., et al., Lipopolysaccharide stimulates the MyD88-independent pathway and results in activation of IFN-regulatory factor 3 and the expression of a subset of lipopolysaccharide-inducible genes. J Immunol, 2001. 167(10): p. 5887-94.
217. Needham, B.D. and M.S. Trent, Fortifying the barrier: the impact of lipid A remodelling on bacterial pathogenesis. Nat Rev Microbiol, 2013. 11(7): p. 467-81.

218. Yanagimachi, M.D., et al., Robust and highly-efficient differentiation of functional monocytic cells from human pluripotent stem cells under serum- and feeder cell-free conditions. PLoS One, 2013. 8(4): p. e59243.
219. Fan, Y., et al., Analyzing mitochondrial respiration of human induced pluripotent stem cell-derived myeloid progenitors using Seahorse technology. STAR Protoc, 2023. 4(1): p. 102073.
220. Ng, P.C. and S. Henikoff, SIFT: Predicting amino acid changes that affect protein function. Nucleic Acids Res, 2003. 31(13): p. 3812-4.
221. Flanagan, S.E., A.M. Patch, and S. Ellard, Using SIFT and PolyPhen to predict loss-of-function and gain-of-function mutations. Genet Test Mol Biomarkers, 2010. 14(4): p. 533-7.
222. Karczewski, K.J., et al., The mutational constraint spectrum quantified from variation in 141,456 humans. Nature, 2020. 581(7809): p. 434-443.
223. Jumper, J., et al., Highly accurate protein structure prediction with AlphaFold. Nature, 2021. 596(7873): p. 583-589.
224. Varadi, M., et al., AlphaFold Protein Structure Database: massively expanding the structural coverage of protein-sequence space with high-accuracy models. Nucleic Acids Res, 2022. 50(D1): p. D439-d444.
225. Mise, N., et al., Zyxin is a transforming growth factor-β (TGF-β)/Smad3 target gene that regulates lung cancer cell motility via integrin α5β1. J Biol Chem, 2012. 287(37): p. 31393-405.
226. Nguyen, T.N., et al., Zyxin-mediated actin assembly is required for efficient wound closure. J Biol Chem, 2010. 285(46): p. 35439-45.
227. Yamamura, M., et al., Functional analysis of Zyxin in cell migration and invasive potential of oral squamous cell carcinoma cells. Int J Oncol, 2013. 42(3): p. 873-80.
228. Kelley, N., et al., The NLRP3 Inflammasome: An Overview of Mechanisms of Activation and Regulation. Int J Mol Sci, 2019. 20(13).
229. Ohto, U., et al., Crystal structures of human MD-2 and its complex with antiendotoxic lipid IVa. Science, 2007. 316(5831): p. 1632-4.
230. Zughaier, S.M., et al., Differential induction of the toll-like receptor 4-MyD88-dependent and -independent signaling pathways by endotoxins. Infect Immun, 2005. 73(5): p. 2940-50.

231. Fukata, M., et al., Toll-like receptor-4 is required for intestinal response to epithelial injury and limiting bacterial translocation in a murine model of acute colitis. Am J Physiol Gastrointest Liver Physiol, 2005. 288(5): p. G1055-65.
232. Park, B.S. and J.O. Lee, Recognition of lipopolysaccharide pattern by TLR4 complexes. Exp Mol Med, 2013. 45(12): p. e66.
233. Yang, H., et al., MD-2 is required for disulfide HMGB1-dependent TLR4 signaling. J Exp Med, 2015. 212(1): p. 5-14.
234. Ohnishi, T., M. Muroi, and K. Tanamoto, MD-2 is necessary for the toll-like receptor 4 protein to undergo glycosylation essential for its translocation to the cell surface. Clin Diagn Lab Immunol, 2003. 10(3): p. 405-10.
235. Yu, Y., et al., Macrophages play a key role in tissue repair and regeneration. PeerJ, 2022. 10: p. e14053.
236. Benchimol, E.I., et al., Incidence, outcomes, and health services burden of very early onset inflammatory bowel disease. Gastroenterology, 2014. 147(4): p. 803-813.e7; quiz e14-5.
237. Kelsen, J.R., et al., The Unique Disease Course of Children with Very Early onset-Inflammatory Bowel Disease. Inflamm Bowel Dis, 2020. 26(6): p. 909-918.
238. Odenwald, M.A. and J.R. Turner, The intestinal epithelial barrier: a therapeutic target? Nat Rev Gastroenterol Hepatol, 2017. 14(1): p. 9-21.
239. Muise, A.M., et al., Polymorphisms in E-cadherin (CDH1) result in a mis-localised cytoplasmic protein that is associated with Crohn's disease. Gut, 2009. 58(8): p. 1121-7.
240. Avitzur, Y., et al., Mutations in tetratricopeptide repeat domain 7A result in a severe form of very early onset inflammatory bowel disease. Gastroenterology, 2014. 146(4): p. 1028-39.
241. Salomon, J., et al., Genetic characterization of congenital tufting enteropathy: epcam associated phenotype and involvement of SPINT2 in the syndromic form. Hum Genet, 2014. 133(3): p. 299-310.
242. Xavier, R.J. and D.K. Podolsky, Unravelling the pathogenesis of inflammatory bowel disease. Nature, 2007. 448(7152): p. 427-34.
243. Bruewer, M., et al., Proinflammatory cytokines disrupt epithelial barrier function by apoptosis-independent mechanisms. J Immunol, 2003. 171(11): p. 6164-72.

244. Kucharzik, T., et al., Neutrophil transmigration in inflammatory bowel disease is associated with differential expression of epithelial intercellular junction proteins. Am J Pathol, 2001. 159(6): p. 2001-9.
245. Farquhar, M.G. and G.E. Palade, Junctional complexes in various epithelia. J Cell Biol, 1963. 17(2): p. 375-412.
246. Hirata, H., H. Tatsumi, and M. Sokabe, Zyxin emerges as a key player in the mechanotransduction at cell adhesive structures. Commun Integr Biol, 2008. 1(2): p. 192-5.
247. Uhlén, M., et al., Proteomics. Tissue-based map of the human proteome. Science, 2015. 347(6220): p. 1260419.
248. Karlsson, M., et al., A single-cell type transcriptomics map of human tissues. Sci Adv, 2021. 7(31).
249. Schmeichel, K.L. and M.C. Beckerle, The LIM domain is a modular protein-binding interface. Cell, 1994. 79(2): p. 211-9.
250. Hansen, M.D. and M.C. Beckerle, Opposing roles of zyxin/LPP ACTA repeats and the LIM domain region in cell-cell adhesion. J Biol Chem, 2006. 281(23): p. 16178-88.
251. Legerstee, K., et al., Dynamics and distribution of paxillin, vinculin, zyxin and VASP depend on focal adhesion location and orientation. Sci Rep, 2019. 9(1): p. 10460.
252. Li, G., et al., Zyxin-involved actin regulation is essential in the maintenance of vinculin focal adhesion and chondrocyte differentiation status. Cell Prolif, 2019. 52(1): p. e12532.
253. Kato, T., et al., Atrial natriuretic peptide promotes cardiomyocyte survival by cGMP-dependent nuclear accumulation of zyxin and Akt. J Clin Invest, 2005. 115(10): p. 2716-30.
254. Hervy, M., et al., The LIM Protein Zyxin Binds CARP-1 and Promotes Apoptosis. Genes Cancer, 2010. 1(5): p. 506-515.
255. Fujita, Y., et al., Zyxin is a novel interacting partner for SIRT1. BMC Cell Biol, 2009. 10: p. 6.
256. Schmitz, H., et al., Altered tight junction structure contributes to the impaired epithelial barrier function in ulcerative colitis. Gastroenterology, 1999. 116(2): p. 301-9.

257. Breslin, N.P., et al., Intestinal permeability is increased in a proportion of spouses of patients with Crohn's disease. Am J Gastroenterol, 2001. 96(10): p. 2934-8.
258. Wu, C.J., et al., Epithelial cell adhesion molecule (EpCAM) regulates claudin dynamics and tight junctions. J Biol Chem, 2013. 288(17): p. 12253-68.
259. Sy, S.M., et al., Novel identification of zyxin upregulations in the motile phenotype of hepatocellular carcinoma. Mod Pathol, 2006. 19(8): p. 1108-16.
260. Gianazza, E., et al., Alterations of the serum peptidome in renal cell carcinoma discriminating benign and malignant kidney tumors. J Proteomics, 2012. 76 Spec No.: p. 125-40.
261. Ma, B., et al., Zyxin-Siah2-Lats2 axis mediates cooperation between Hippo and TGF-β signalling pathways. Nat Commun, 2016. 7: p. 11123.
262. Zhou, J., et al., Zyxin promotes colon cancer tumorigenesis in a mitotic phosphorylation-dependent manner and through CDK8-mediated YAP activation. Proc Natl Acad Sci U S A, 2018. 115(29): p. E6760-e6769.
263. Nix, D.A. and M.C. Beckerle, Nuclear-cytoplasmic shuttling of the focal contact protein, zyxin: a potential mechanism for communication between sites of cell adhesion and the nucleus. J Cell Biol, 1997. 138(5): p. 1139-47.
264. Kang, X., et al., Zyxin Mediates Vascular Repair via Endothelial Migration Promoted by Forskolin in Mice. Front Physiol, 2021. 12: p. 741699.
265. Ghosh, S., et al., Loss of the mechanotransducer zyxin promotes a synthetic phenotype of vascular smooth muscle cells. J Am Heart Assoc, 2015. 4(6): p. e001712.
266. Han, X., et al., Zyxin regulates endothelial von Willebrand factor secretion by reorganizing actin filaments around exocytic granules. Nat Commun, 2017. 8: p. 14639.
267. Alexopoulou, L., et al., Recognition of double-stranded RNA and activation of NF-kappaB by Toll-like receptor 3. Nature, 2001. 413(6857): p. 732-8.
268. Chen, Y., et al., Toll-like receptor 3 (TLR3) regulation mechanisms and roles in antiviral innate immune responses. J Zhejiang Univ Sci B, 2021. 22(8): p. 609-632.
269. Kumagai, Y. and S. Akira, Identification and functions of pattern-recognition receptors. J Allergy Clin Immunol, 2010. 125(5): p. 985-92.

270. Ostvik, A.E., et al., Enhanced expression of CXCL10 in inflammatory bowel disease: potential role of mucosal Toll-like receptor 3 stimulation. Inflamm Bowel Dis, 2013. 19(2): p. 265-74.
271. Wen, S.M., W.C. Wen, and P.G. Chao, Zyxin and actin structure confer anisotropic YAP mechanotransduction. Acta Biomater, 2022. 152: p. 313-320.
272. Bozym, R.A., et al., Focal adhesion kinase is a component of antiviral RIG-I-like receptor signaling. Cell Host Microbe, 2012. 11(2): p. 153-66.
273. Ohman, T., et al., Actin and RIG-I/MAVS signaling components translocate to mitochondria upon influenza A virus infection of human primary macrophages. J Immunol, 2009. 182(9): p. 5682-92.
274. Hoffman, L.M., et al., Targeted disruption of the murine zyxin gene. Mol Cell Biol, 2003. 23(1): p. 70-9.
275. Hansen, M.C., T. Haferlach, and C.G. Nyvold, A decade with whole exome sequencing in haematology. Br J Haematol, 2020. 188(3): p. 367-382.
276. Sender, R., S. Fuchs, and R. Milo, Revised Estimates for the Number of Human and Bacteria Cells in the Body. PLoS Biol, 2016. 14(8): p. e1002533.
277. Ott, S.J., et al., Reduction in diversity of the colonic mucosa associated bacterial microflora in patients with active inflammatory bowel disease. Gut, 2004. 53(5): p. 685-93.
278. Miyoshi, J., et al., Peripartum Antibiotics Promote Gut Dysbiosis, Loss of Immune Tolerance, and Inflammatory Bowel Disease in Genetically Prone Offspring. Cell Rep, 2017. 20(2): p. 491-504.
279. Matsuno, H., et al., CD103+ Dendritic Cell Function Is Altered in the Colons of Patients with Ulcerative Colitis. Inflamm Bowel Dis, 2017. 23(9): p. 1524-1534.
280. Gevers, D., et al., The treatment-naive microbiome in new-onset Crohn's disease. Cell Host Microbe, 2014. 15(3): p. 382-392.
281. Mitsialis, V., et al., Single-Cell Analyses of Colon and Blood Reveal Distinct Immune Cell Signatures of Ulcerative Colitis and Crohn's Disease. Gastroenterology, 2020. 159(2): p. 591-608.e10.
282. Hug, H., M.H. Mohajeri, and G. La Fata, Toll-Like Receptors: Regulators of the Immune Response in the Human Gut. Nutrients, 2018. 10(2).
283. Szebeni, B., et al., Increased expression of Toll-like receptor (TLR) 2 and TLR4 in the colonic mucosa of children with inflammatory bowel disease. Clin Exp Immunol, 2008. 151(1): p. 34-41.

284. Frolova, L., et al., Expression of Toll-like receptor 2 (TLR2), TLR4, and CD14 in biopsy samples of patients with inflammatory bowel diseases: upregulated expression of TLR2 in terminal ileum of patients with ulcerative colitis. J Histochem Cytochem, 2008. 56(3): p. 267-74.
285. Vamadevan, A.S., et al., Regulation of Toll-like receptor 4-associated MD-2 in intestinal epithelial cells: a comprehensive analysis. Innate Immun, 2010. 16(2): p. 93-103.
286. Tan, Y., et al., Expression and implication of toll-like receptors TLR2, TLR4 and TLR9 in colonic mucosa of patients with ulcerative colitis. J Huazhong Univ Sci Technolog Med Sci, 2014. 34(5): p. 785-790.
287. Franchimont, D., et al., Deficient host-bacteria interactions in inflammatory bowel disease? The toll-like receptor (TLR)-4 Asp299gly polymorphism is associated with Crohn's disease and ulcerative colitis. Gut, 2004. 53(7): p. 987-92.
288. Shen, X., et al., The Toll-like receptor 4 D299G and T399I polymorphisms are associated with Crohn's disease and ulcerative colitis: a meta-analysis. Digestion, 2010. 81(2): p. 69-77.
289. Capitani, M., et al., Biallelic TLR4 deficiency in humans. J Allergy Clin Immunol, 2023. 151(3): p. 783-790.e5.
290. Araki, A., et al., MyD88-deficient mice develop severe intestinal inflammation in dextran sodium sulfate colitis. J Gastroenterol, 2005. 40(1): p. 16-23.
291. Dinarello, C.A., Biologic basis for interleukin-1 in disease. Blood, 1996. 87(6): p. 2095-147.
292. Wilson, S.P. and S.L. Cassel, Inflammasome-mediated autoinflammatory disorders. Postgrad Med, 2010. 122(5): p. 125-33.
293. Zheng, D., T. Liwinski, and E. Elinav, Inflammasome activation and regulation: toward a better understanding of complex mechanisms. Cell Discov, 2020. 6: p. 36.
294. Schroder, K. and J. Tschopp, The inflammasomes. Cell, 2010. 140(6): p. 821-32.
295. Bauernfeind, F.G., et al., Cutting edge: NF-kappaB activating pattern recognition and cytokine receptors license NLRP3 inflammasome activation by regulating NLRP3 expression. J Immunol, 2009. 183(2): p. 787-91.
296. Thiesen, S., et al., CD14(hi)HLA-DR(dim) macrophages, with a resemblance to classical blood monocytes, dominate inflamed mucosa in Crohn's disease. J Leukoc Biol, 2014. 95(3): p. 531-41.

297. Gren, S.T. and O. Grip, Role of Monocytes and Intestinal Macrophages in Crohn's Disease and Ulcerative Colitis. Inflamm Bowel Dis, 2016. 22(8): p. 1992-8.
298. Schromm, A.B., et al., Molecular genetic analysis of an endotoxin nonresponder mutant cell line: a point mutation in a conserved region of MD-2 abolishes endotoxin-induced signaling. J Exp Med, 2001. 194(1): p. 79-88.
299. Bauer, C., et al., Colitis induced in mice with dextran sulfate sodium (DSS) is mediated by the NLRP3 inflammasome. Gut, 2010. 59(9): p. 1192-9.
300. Bauer, C., et al., Protective and aggravating effects of Nlrp3 inflammasome activation in IBD models: influence of genetic and environmental factors. Dig Dis, 2012. 30 Suppl 1: p. 82-90.
301. Zaki, M.H., et al., The NLRP3 inflammasome protects against loss of epithelial integrity and mortality during experimental colitis. Immunity, 2010. 32(3): p. 379-91.
302. Demel, U.M., et al., A complex proinflammatory cascade mediates the activation of HSCs upon LPS exposure in vivo. Blood Adv, 2022. 6(11): p. 3513-3528.
303. Li, Y., et al., Human MD2 deficiency-an inborn error of immunity with pleiotropic features. J Allergy Clin Immunol, 2022.
304. Zanoni, I., et al., CD14 controls the LPS-induced endocytosis of Toll-like receptor 4. Cell, 2011. 147(4): p. 868-80.
305. Tan, Y., et al., Mechanisms of Toll-like Receptor 4 Endocytosis Reveal a Common Immune-Evasion Strategy Used by Pathogenic and Commensal Bacteria. Immunity, 2015. 43(5): p. 909-22.
306. da Silva Correia, J. and R.J. Ulevitch, MD-2 and TLR4 N-linked glycosylations are important for a functional lipopolysaccharide receptor. J Biol Chem, 2002. 277(3): p. 1845-54.
307. Darie, A.M., et al., BSG 2024 IBD guidelines protocol (standard operating procedures). BMJ Open Gastroenterol, 2023. 10(1).
308. Xu, W., et al., Reversible differentiation of pro- and anti-inflammatory macrophages. Mol Immunol, 2013. 53(3): p. 179-86.
309. Martinez, F.O. and S. Gordon, The M1 and M2 paradigm of macrophage activation: time for reassessment. F1000Prime Rep, 2014. 6: p. 13.
310. Mills, C.D. and K. Ley, M1 and M2 macrophages: the chicken and the egg of immunity. J Innate Immun, 2014. 6(6): p. 716-26.

311. Liu, Y.C., et al., Macrophage polarization in inflammatory diseases. Int J Biol Sci, 2014. 10(5): p. 520-9.
312. Zhu, W., et al., Disequilibrium of M1 and M2 macrophages correlates with the development of experimental inflammatory bowel diseases. Immunol Invest, 2014. 43(7): p. 638-52.
313. Lim, T.S., et al., CD80 and CD86 differentially regulate mechanical interactions of T-cells with antigen-presenting dendritic cells and B-cells. PLoS One, 2012. 7(9): p. e45185.
314. Parry, R.V., et al., CTLA-4 and PD-1 receptors inhibit T-cell activation by distinct mechanisms. Mol Cell Biol, 2005. 25(21): p. 9543-53.
315. Miyake, K., et al., Essential role of MD-2 in B-cell responses to lipopolysaccharide and Toll-like receptor 4 distribution. J Endotoxin Res, 2002. 8(6): p. 449-52.
316. Sri-Ngern-Ngam, K., et al., Upregulation of programmed cell death 1 by interferon gamma and its biological functions in human monocytes. Biochem Biophys Rep, 2022. 32: p. 101369.
317. Koeffler, H.P., et al., Gamma-interferon induces expression of the HLA-D antigens on normal and leukemic human myeloid cells. Proc Natl Acad Sci U S A, 1984. 81(13): p. 4080-4.
318. Luque-Martin, R., et al., IFN-γ Drives Human Monocyte Differentiation into Highly Proinflammatory Macrophages That Resemble a Phenotype Relevant to Psoriasis. J Immunol, 2021. 207(2): p. 555-568.
319. Pfeifer, J.D., et al., Phagocytic processing of bacterial antigens for class I MHC presentation to T cells. Nature, 1993. 361(6410): p. 359-62.
320. Martín-Orozco, N., A. Isibasi, and V. Ortiz-Navarrete, Macrophages present exogenous antigens by class I major histocompatibility complex molecules via a secretory pathway as a consequence of interferon-gamma activation. Immunology, 2001. 103(1): p. 41-8.
321. Schmeck, B., et al., Pneumococci induced TLR- and Rac1-dependent NF-kappaB-recruitment to the IL-8 promoter in lung epithelial cells. Am J Physiol Lung Cell Mol Physiol, 2006. 290(4): p. L730-l737.
322. Sánchez-Tarjuelo, R., et al., The TLR4-MyD88 Signaling Axis Regulates Lung Monocyte Differentiation Pathways in Response to Streptococcus pneumoniae. Front Immunol, 2020. 11: p. 2120.

323. Liu, L., et al., Global, regional, and national causes of child mortality in 2000-13, with projections to inform post-2015 priorities: an updated systematic analysis. Lancet, 2015. 385(9966): p. 430-40.
324. Huang, Y., et al., TLR2 promotes macrophage recruitment and Streptococcus pneumoniae clearance during mouse otitis media. Pediatr Res, 2016. 80(6): p. 886-893.
325. Hu, K.A. and J. Gubatan, Gut microbiome–based therapeutics in inflammatory bowel disease. Clinical and Translational Discovery, 2023. 3(2): p. e182.
326. Frenz-Wiessner, S., et al., Generation of complex bone marrow organoids from human induced pluripotent stem cells. Nat Methods, 2024.